Prantik Mukhopadhyay

Simulation of Primary Static Recrystallization with Cellular Operator Model

Simulation of Primary Static Recrystallization with Cellular Operator Model

Von der Fakultät für Georessourcen und Materialtechnik der

Rheinisch -Westfälischen Technischen Hochschule Aachen

zur Erlangung des akademischen Grades eines

Doktors der Ingenieurwissenschaften

genehmigte Dissertation

vorgelegt von **M. Tech**

Prantik Mukhopadhyay

aus Bishnupur, West Bengal, India

Berichter: Univ.-Prof. Dr. rer. nat. Günter Gottstein
Prof. Dr. –Ing. Dierk Raabe

Tag der mündlichen Prüfung: 28. September 2005

Diese Dissertation ist auf den Internetseiten der Hochschulbibliothek online verfügbar

Contents:

Acknowledgement

I would like to thank my academic advisor University-Prof. Dr. rer. nat. Günter Gottstein, Guest Prof. Dr. Lasar Shvindlerman, Prof. Dr. Dierk Raabe and Prof. Dr. Oalf Engler for their inspiration, encouragement during the course of this project.

I am indebted to my colleagues Dipl. Ing. Manfred Schneider, Dipl. Ing. Matthias Goerdeler, Dipl. Ing. Mischa Crumbach, Dipl. Ing. Dirk Kirch, Dipl. Ing. H. Artz and Dipl. Ing. Luc Neumann for their valuable comments, suggestions and association on the simulation work and FEM calculations.

I would like to express thanks to system administrator Matthias Loeck and to Dipl. Math Gerda Pomana for necessary discussions and programming.

I must take opportunity to thank all colleagues form the vir[FAB] project work for supplying me the aluminium alloys used in that project and necessary experimental data for validation of the simulation results and all the laboratory staffs and the members of IMM-Aachen, who have helped me a lot.

Finally I gratefully acknowledge the support by the vir[FAB] consortium for their collaborative support, the funding by the European Community and the Deutsche Forschungsgemeinschaft (DFG) through the Collaborative Research Centre 370.

1. Introduction.

A deformed material, e.g. a rolled sheet, is liable to softening by recrystallization during an annealing treatment. Recrystallization proceeds by nucleation of strain free grains and their growth by consumption of the deformed microstructure. A competing process to recrystallization is recovery which consists of a rearrangement of deformation induced dislocations in energetically more favourable patterns, in particular in low angle grain boundaries.

A recrystallized microstructure is in first order defined by the distribution of its grain diameters (grain size distribution) and the distribution of their crystallographic orientations (crystallographic texture). Both recrystallization grain size and texture, for instance obtained after hot rolling or by batch annealing after cold rolling depend on the respective processing parameters. Texture is the cause of mechanical anisotropy. Therefore, a textured sheet deforms inhomogeneously during a sheet forming process and gives rise to earing, which is undesired since it can cause serious losses of production time. A profound understanding of the development of texture during the fabrication process of a sheet metal is prerequisite for enhanced productivity and efficient quality improvement of the finished product.

The recrystallization during thermomechanical treatment of a material generates textures which are characteristic of the material and the process parameters. In turn they will have a strong influence on the plastic behavior and the development of deformation texture during subsequent forming. Therefore, it is the ultimate goal of recrystallization research to predict the recrystallization texture development during processing of a material, which requires a reliable model that takes into account the physics and mechanisms of recrytallization. The validation of a model requires at the same time reliable experimental data that can be compared with model predictions. On the other hand modelling can provide the rare opportunity to reveal so far unknown features of recrystallization, which can not be realized by the simple experimental means.

There have been many attempts to model recrystallization, in particular its kinetics, the recrystallized grain size and recrystallization texture. The kinetics of homogeneous recrystallization was first modelled by Avrami [1], Kolmogorov [2], Johnson and Mehl [3], who considered the nucleation and growth of spherical grains and solved in particular the problem of impingement of grains, which locally terminates the growth of

the recrystallization nuclei. While the general features of nucleation and growth are elemental essentials of the recrystallization process, models those assume homogeneous nucleation and isotropic nuclei growth in homogeneously deformed matrix suffer from their distance to reality. In fact, it is the departure from homogeneity that sets off and controls recrystallization. The microstructure prior to recrystallization is introduced by deformation and contains inhomogeneities in terms of a deformation substructure with grain boundaries, local deformation zones around large particles and bandlike structure like shear band or transition bands. At the same time the material is usually not a pure metallic element but an alloy with spatial fluctuations of solute content and second phase particles. An appropriate approach of recrystallization has to take these microstructural features into account to properly reflect the evolution of recrystallized microstructure and texture. To account for spatial heterogeneity requires discretization of space into 3D grid, where each element of the grid will contain the actual microstructure information, i.e. chemistry, defect density, orientation, etc. besides local processing variables like temperature and all parameters can change with time owing to thermal fluctuations.

Simulation of recrystallization on a spatial and temporal grid has been attempted before by the Monte-Carlo method or cellular automata approaches. These attempts, however, do not make use of microstructural details and their temporal changes. Also the problem of nucleation of recrystallized grains, which strongly influences the recrystallization texture, has been circumvented by assuming homogeneous nucleation, which is very far from reality.

In this study it is attempted to improve existing cellular automata codes by integration of microstructural and temporal information in terms of deformation texture, stored energy distribution, nucleation mechanism and anisotropic growth of nuclei. This new model is referred to as cellular operator approach and will be discussed in the following with regard to both predictive strength and computational efficiency.

2. Recrystallization texture, microstructure and kinetics.

2.1 Phenomenon, definitions and energies: The formation of new strain free grains from deformed materials is called recrystallization. The plastic deformation of materials induces dislocations, which increases the free energy and takes material to a state, which is not thermodynamically stable. The inert desire of deformed materials continues its effort to be strain free so that it can lowers its free energy. The driving force for new strain free grain formation is the lowering of free energy of materials. The lowering of free energy because of dx distance movement of a segment of grain boundary with surface area dS is expressed as dG = pdSdx. The term p (p=dG/dSdx or p=dG/dV, where dV is the volume swept by the surface segment) is referred to as driving force on the grain boundary per unit area.

In earlier days, due to lack of efficient experimental means, the common notion about the deformation of metallic materials was the loss of crystallinity. There was a firm belief that the crystal structure of metal destroyed after deformation but reappeared after annealing. The reappearance of metallic crystallinity after annealing was termed as recrystallization.

The knowledge obtained from several investigations, which build the modern concepts of this phenomenon in terms of texture, microstructure and kinetics is included in this review on recrystallization.

The earlier mentioned definition of recrystallization i.e. formation of new strain free grains from deformed matrix is suitable for both dynamic and static recrystallization. The dynamic recrystallization occurs during deformation while the static recrystallization occurs after deformation during subsequent annealing. The formation of strain free grains can happen also continuously or discontinuously. The discontinuous recrystallization occurs through nucleation and nuclei growth where the dislocation density of the deformed matrix gradually disappears because of time dependent growth of nuclei by fast moving high angle grain boundary. In continuous recrystallization the microstructural change happens uniformly without the migration of grain boundary. It occurs through local rearrangements of low angle boundaries and resembles a recovery of dislocation. This homogeneous change in microstructure is also termed as

recrystallization in situ. The recrystallization develops certain textures in metals and alloys. The basic knowledge about texture is shortly described in the following paragraph.

2.2 **Recrystallization texture:**

2.2.1 Definition and measurement of texture: In a polycrystalline metallic material the individual crystal can have a reference system defined by three axes in three directions x, y and z. A piece of that metal, which consists of several such crystals, can have another reference system (X, Y, Z) at the macroscopic level. The angular deviation between these two reference systems is termed as orientation of the crystal. The orientation distribution of crystals in metallic material is known as texture. The orientation distribution is greatly influenced by production parameters defined by forming, heat treatments etc. A preference in orientations or the texture of the product inherits its production history. Since the orientation distribution depends on the type of metals or alloy and the condition imposed by the production parameters, no preference of a particular orientation in the orientation distribution can also be obtained. This is known as random texture, which emerges because of an arrangement of crystals in the metallic material, where orientations of crystals are mutually different. This is called random texture, which is generally found in powder aggregate. The texture goniometer is used for experimental measurement of texture. The diffracted monochromatic X-ray beam from planes, which satisfy the condition of Bragg's law, is captured in counter and the intensity distributions obtained from several such diffractions from different planes represent pole figures. A continuous orientation distribution is calculated from several such measurements, represents the texture in a three dimensional frame, which is known as Euler room. Three angular rotations (φ_1 ϕ φ_2) are used to merge the crystal axis on macroscopic reference axis and the crystal orientation is defined by these three angles i.e. Euler angles. This three dimensional function of orientation distribution is typically shown in two dimension with sections which are parallel to the angle φ_2 and 5° apart in the Euler room for face centred cubic metals.

2.2.2 **Development of recrystallization texture:** The recrystallization texture development during annealing strongly depends on many factors like the initial microstructure before deformation, severity of straining during deformation, chemistry of the material and on the type of annealing process [4-15]. Improper control over

annealing process may lead to other related processes like recovery and grain growth to occur and may change the recrystallization texture significantly.

The origin of recrystallization texture of aluminium during recrystallization has been studied extensively [16-20]. The recrystallization texture of aluminium generally produces its characteristic cube texture. The recrystallization texture is found to be governed by deformation microstructure, degree of deformation, time and temperature of annealing. The effects of some of these factors on recrystallization of aluminium alloy will also be discussed in this work. The well-known theories available in order to explain the recrystallization behavior of the material are shortly explained below.

The Oriented nucleation theory tells that certain orientations are favored during recrystallization and the resulting recrystallization texture is the out come of selection of some specific orientations as nucleus. Important findings, which strengthen this view, was that certain orientations form transition band due to anisotropic rotations path followed by nearly oriented crystallines, give strong divergence in orientation with deformation, starting from more or less same orientations [21,22]. The resulting steep disorientation gradient connects rotated and not rotated parts of grains are related to certain crystallographic direction and susceptible to give nucleation during subsequent annealing process. Availability of this type of transition in deformed structure was also reported to occur in fcc material as well [23-25]. Other investigations of present time added with more sophisticated experimental means [26-30] tells that a grain as a whole does not rotate but different parts of a grain rotate in different directions, which makes the understanding of deformation behavior of grain a very difficult problem.

The theory of oriented growth is based on the observation that some grain boundaries move faster than others and orientations associated with those boundaries consume the deformation microstructure during recrystallization [31,32]. They found that a specific rotation relation $40°<111>$ is important to determine the recrystallization texture of the face centred cubic (fcc) material. According to this theory the strength of cube texture component improves after recrystallization because it satisfies the disorientation relationship with certain major texture components like S components of deformed microstructure. A faster growth because of this orientation favour helps cube texture component to remove other texture components in recrystallized material.

With the help of sophisticated experimental techniques of precise micro texture measurement and selected area diffraction pattern analysis, the deformed microstructure and the incipient stage of nucleation during recrystallization of material are easier to

examine nowadays. Developments may still be required to improve the poor pattern quality of highly deformed microstructure so that a better understanding about an exact orientation and location could be possible but information available from present experimental techniques can also reveal that nucleation of recrystallization in deformed microstructure is heterogeneous. It takes place at certain locations like along grain boundary, from deformation band and in the deformation zone of precipitate bearing alloys. At the same time experimental and simulation evidence show recrystallized nuclei do not grow isotropically [33]. The growth of nuclei strongly depends on the orientation relationship between the growing grain and the deformed matrix environment [34]. The initially uniform grain breaks with deformation and creates a deformed orientation spread around the original orientation. A very high deformation can be responsible for generating a very strong gradient of disorientation where a sharp orientation change is found in a micron length. Naturally for a growing nucleus is it difficult to restore a specific orientation relationship in all three directions through out its growth. A wide scatter around above-mentioned rotational relationship is quite reasonable to assume for the growth simulation of recrystallization [35, 36].

2.3   Microstructure evolution during recrystallization: The new strain free grain develops in a time dependent fashion. The resulting granular structure is called microstructure, which consists of grains. A wide range of experimental work carried out, provides qualitative overview over this phenomenon [9, 10]. These were referred as laws of recrystallization, which dealt with the minimum deformation energy, and critical strain, time and temperature dependent criteria of recrystallization in a qualitative fashion. Since an exact knowledge of recrystallization needed a better qualitative and quantitative description of this phenomenon extensive research work performed even after that.

The microstructure development during recrystallization depends on two factors namely the nucleation kinetics, which is not necessarily always constant and the growth kinetics of nuclei. Depending on the characteristic of materials and process both factors show huge scatter in their behaviour and not a fixed rule may be suitable for explaining the nucleation process of all materials. The growth of nuclei during recrystallization is accepted as a product of mobility of the grain boundary and driving pressure for recrystallization arises from the high dislocation density of deformed structure. The

curvature of growing nuclei may also retard the movement of recrystallization front but the effect is found to be very small. Since both processes strongly depend on characteristics of the deformation microstructure an exact knowledge about deformation behaviour depending on the grain properties, chemistry, type of substructure evolution and the dislocation dynamics under the effect of strain rate and temperature are required apart from the rotational relationship between the nuclei and the environment of growth. The growth or the velocity of the recrystallization front depends not only on the thermodynamic driving force (p) but also the mobility (m) of the grain boundary along the recrystallization front. The first term (p) bears the energetics and consists of the total strain energy of deformed metals because of the presence of dislocation density. The strain energy of the dislocation per unit length is approximately expressed as $0.5Gb^2$, where G is the shear modulus and b is the direction vector of dislocation. The total strain energy of per unit volume of deformed metals with dislocation density ρ (length/length^3) can be expressed as $0.5Gb^2\rho$. It would be more appropriate to call $0.5Gb^2\rho$ a driving pressure for recrystallization instead of a driving force.

Whatever be the magnitude of this driving pressure of a deformed material the recrystallization does not occur without the help of grain boundary mobility which bears the temperature dependency of growth of recrystallization front or the involved grain boundary. The kinetic aspects of grain boundary motion are included in the recrystallization through the mobility term. The basic expression for the mobility is given by the $m=m_0\exp(-Q/kT)$, where Q is the activation energy for grain boundary mobility, k is the Boltzmann constant and m_0 is the pre-exponential mobility factor. In certain metals the presence of subgrains after deformation may introduce a different velocity of recrystallization, which is dominated by the energy and the mobility of small angle grain boundaries but basic two factors remain preserved the driving pressure and mobility. The driving pressure and the mobility both vary in deformed metal locally and hence the velocity of the recrystallization grain boundary also changes during the course of recrystallization. This local variation in driving pressure and mobility should have certain effect on the recrystallized volume fraction at a particular time. There are different experimental techniques by which the time dependent recrystallized volume fractions of recrystallizing metals can be measured. All experimental techniques i.e. optical microscopy, orientation image mapping, calorimetric method, X-ray texture and peak intensity, hardness measurement etc. are based on certain considerations which directly or indirectly result in the recrystallization volume fractions of metals. The time

vs. recrystallization volume fractions can also be obtained from different mathematical and location discrete models, which will be discussed in the following chapter [1-3, 37-39].

2.4 Quantitative description of microstructure:
The recrystallization microstructure, defined earlier, is quantitatively described in general by grain distribution. The recrystallized grain shape and diameter can give two types of distribution. The shape and diameter variables are considered to be independent to each other. Hence, a quantitative description of grain geometry needs two separate mathematical expressions. It should be worthy to mention that the currently used models for polycrystal properties pay more attention to the size than the shape distribution. A better quantitative description of recrystallization microstructure would be the distribution of grains than the average property of grains. This grain distribution can be based on volume, on area or on diameter. This distribution can be a continuous or a discrete function. In two-phase alloys the precipitate or particles distribution can also be necessary apart from the grain distribution. Any discrete distribution function f(V), which represents the number of grains or particles of volume V in total number of grains or particles N, is expressed as

$$f(V) = N(V)/N \qquad (2.1)$$

In case of a continuous function the number of grains or particles N(V1, V2) in the range of V1 and V2 can be expressed in the following equation

$$N(V1,V2) = \frac{1}{V} \int_{V1}^{V2} f(V)\,dV. \qquad (2.2)$$

The continuous functions should fulfill the non-negative condition and can be normalized to unity. Normal and log normal distribution are generally used widely in material science. A measured grain diameter distribution is not symmetrical with regard to the average value, i.e., the most frequent value (median value) or the grain diameter D_{mean} where the grain distribution has its maximum, is not indicated with the average value D_o. Therefore, the grain diameter distributions are not represented by a normal distribution (Gauss Distribution or the bell curve) in statistics, which can be expressed mathematically for a single observable x.

$$w(x)dx = \frac{1}{\sqrt{2\pi}\sigma} \exp\left(-\frac{1}{2}\left(\frac{x - x_0}{\sigma}\right)^2\right)dx \qquad (2.3)$$

Here, w (x) dx is the probability of findings the measured value in the interval [x, x+dx]; x_0 is the average and σ the standard deviation, which is a measure of the width of the distribution. Grain distribution can be converted to a symmetrical shape, if the frequency is plotted against the logarithm of the grain size, lnD. Such a distribution is termed as a lognormal distribution and can be mathematically represented for a single observable x applied to the grain diameter, i.e. x = D, the average value of the lognormal grain distribution is not known and all attempts to derive the lognormal distribution from first principles have been dissatisfactory so far. For lognormal distribution there is a difference between the average Xo and the most frequent X_1.

$$X_1 = \exp (\ln Xo - \sigma^2) \tag{2.4}$$

Obviously, besides the average value of a distribution also its width (scattering width) is important. It is represented by the standard deviation. For very broad distribution it is not always obvious whether they consist of a single distribution or of the super position of several distributions. Deviations from a straight line like curved segments indicate the superposition of several distributions, which, however can be deconvoluted by appropriate mathematical procedure [40,41].

3. Review of existing recrystallization models.

During plastic deformation of crystalline materials, dislocations are generated and stored in the crystals. They raise the free energy of the solid and provide the driving force for their removal.

Static primary Recrystallization comprises all phenomena associated with the formation of the strain free microstructure during annealing of cold deformed crystalline solids. It proceeds by nucleation of strain free grains and their subsequent growth until impingement and completely replaces the deformed microstructure. Since the most stringent requirement for a viable nucleus is the formation of a mobile grain boundary, the process of RX can be essentially reduced to the generation and motion of high angle boundaries in a deformed microstructure [33,42].

There are three major factors of significance with regard to recrystallization, namely kinetics, microstructure and texture. For each topic (phenomenological) theories have been developed to account for the observed phenomena and to allow predictions. Only recently, space and time resolved models and simulation tools have become available that reflect the recrystallization phenomenon on a physical basis.

3.1 **Phenomenological models:** The prototype of the analytical treatment of the recrystallization (or more general, phase transformation) kinetics was due to Johnson, Mehl, Avrami and Kolmogorov (JMAK) [1-3]. The following assumptions were made

i)   The grains grew as spheres as long as not in touch with each other,

ii)   Nucleation occurred statistically without preference of sites,

iii)   Growth velocity, v and number of nuclei, N remained constant.

iv)   Growth ceased after impingement.

This was taken care of by a reduced increment of the true transformed volume dX, as expressed by the product of the unrecrystallized volume fraction (1 - X) and the extended transformed volume dX_e, which would be obtained without impingement (Fig.1) The kinetics of recrystallization i.e. the variation of volume fraction recrystallized, X (t) with time was calculated according to Johnson & Mehl, on the basis of two phenomena nucleation and nuclei growth in following way:

a) Nucleation kinetics N: Number of nuclei dn per unit volume generated per time interval dt within the unrecrystallized volume (1-X).

$$N = dn/dt \cdot 1/(1-X) \tag{3.1}$$

b) Growth velocity v: Grain boundary migration velocity, i.e. the displacement dR of a grain boundary element parallel to its normal direction per time interval dt

$$v = dR/dt \tag{3.2}$$

If the shape of the grain was a sphere, dR was the radial increment.

Kinetics for Site Saturation Nucleation: For site saturation nucleation (all nuclei generated at t=0) the volume of a nucleus at any instant of time t was given by

$$V' = \frac{4}{3}\pi[tv]^3 \tag{3.3}$$

and the growth of that nucleus in the interval (t, t + dt) incorporated the volume change

$$dV'_N = 4\pi t^2 v^3 dt \tag{3.4}$$

The volume fraction recrystallized, X (t) at any time instant t the unrecrystallized volume fraction was 1-X (t). Hence the decrease of unrecrystallized volume in the above mentioned time frame given by

$$dV_N(t) = \{1 - X(t)\}dV'_N(t) = 4\pi v^3 t^2 \{1 - X(t)\}dt \tag{3.5}$$

If the total number of nuclei generated is N which was not a function of time for site saturation condition, the change of recrystallized volume fraction was written as

$$dX(t) = 4\pi v^3 t^2 N\{1 - X(t)\}dt \tag{3.6}$$

Because of

$$dX = (1 - X)dX_e \tag{3.7}$$

and

$$dX_e = N.4\pi v^3 t^2 dt \tag{3.8}$$

Integration of Eq.(3.6) yielded

$$X = 1 - \exp(-X_e) = 1 - \exp\left(-\frac{4}{3}\pi N v^3 t^3\right) \tag{3.9}$$

Kinetics for Constant Nucleation with time: At time t >0, a nucleus produced at time τ< t, had the volume

$$V'_N = \frac{4}{3}\left[(t - \tau).v\right]^3 \tag{3.10}$$

and grew in the interval (t, t + dt)

$$dV_N' = 4\pi \left[(t-\tau)^2 v^3 \right] dt \tag{3.11}$$

Because of the impingement the decrease of the unrecrystallized volume in the considered time interval was given by

$$dV_N(t) = \{1 - X(t)\}dV_N'(t) = 4\pi v^3 (t-\tau)^2 \{1 - X(t)\}dt \tag{3.12}$$

The number of nuclei generated at τ, i.e. in the interval (τ, $\tau + d\tau$) is $N(\tau)$ dτ.

Therefore, the increase in recrystallized volume fraction increased in the time interval (t, t + dt) due to nuclei generation at (τ, $\tau + d\tau$) with $\tau < t$

$$dX_\tau = 4\pi v^3 (t-\tau)^2 \{1 - X(t)\}dt.N(\tau)d\tau \tag{3.13}$$

The total increment of the recrystallized volume fraction in (t, t+dt) was given by the sum of all nuclei produced at all times $\tau < t$

$$dX = \int_0^t dX_\tau d\tau = 4\pi v^3 t^2 N\{1 - X(t)\}dt \tag{3.14}$$

with N constant. Finally the recrystallized volume fraction at time t was given by the summation over all increments dX until time t.

$$X(t) = \int_0^t dX(t')dt' = 1 - \exp(-\frac{\pi}{3}Nv^3 t^4) \tag{3.15}$$

In general terms the JMAK equation read

$$X = 1 - \exp\left(-\left(\frac{t}{\tau}\right)^q\right) \tag{3.16}$$

where τ was a characteristic time for recrystallization (in short, recrystallization time $X(\tau) = 1 - e^{-1}$) and q was the Avrami exponent (Fig. 2). For site saturation q = 3, for constant nucleation rate, q = 4, but experimentally typically $1 < q < 3$.
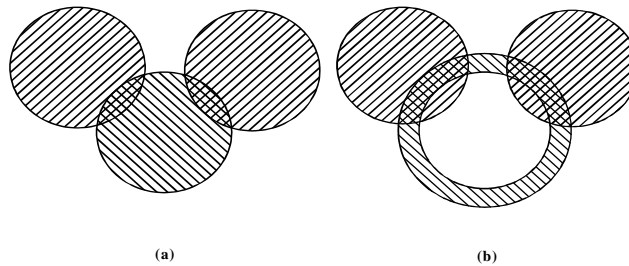

(a)   (b)

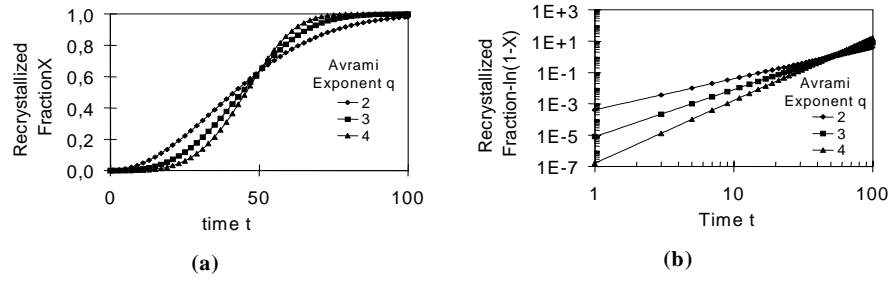Fig. 1 True (hatched) and extended (hatched + cross hatched) recrystallized volume.

Fig 2 Recrystallization kinetics for different Avrami exponents a) Recrystallized volume fraction X vs. annealing time t, b) Avrami plot: log (-ln (1-X)) vs. log t.

The main reason for the deviation of the experimental resulted from the predictions of the JMAK model was the violation of the homogeneity assumption. In reality there is no homogeneous nucleation and spatially and temporally constant growth rate. Statistical approaches like the JMAK theory can hardly overcome this problem. This was extensively treated by Vandermeer and co-workers, who used experimental data on the unconstrainedly growing nuclei to define a "microstructural path" which effectively incorporated the inhomogeneity of microstructure and its impact on recrystallization kinetics [38,43].

Owing to the statistical nature of the JMAK approach, it is essentially restricted to describe recrystallization kinetics and related phenomena, while microstructure and texture predictions require more substantial input. Nevertheless, the development of recrystallized grain diameter can be assessed from the JMAK approach, since

$$d_{rx} \approx 2v\tau \approx 2\sqrt[n]{\frac{v}{N}} \tag{3.17}$$

and the orientation dependence of N and v will also affect texture evolution. Since the growth velocity enters Eq. (3.9) with a power $q > 1$, a pronounced orientation dependence of v will severely influence texture development. This has been treated in time resolved simulations as will be addressed below.

3.2 Geometrical microstructure models:
The first computer simulation of primary recrystallization, which also generated microstructures, was due to Malin, Hanson and Morris (1976) [44]. They generated nuclei by a random generator, calculated the shape of the isotropically growing and impinging 3 dimensional grains and generated 2 dimensional sections of the microstructure (Fig.3). A refinement of the model took into account a time dependence of nucleation kinetics and growth kinetics,

which affected the morphology of the recrystallized grains. Marthinsen, Lohne and Nes extended the model to differentiate nucleus species with different growth kinetics [45]. With increasing nucleation kinetics and decreasing growth kinetics, good agreement with the predictions of the JMAK theory and similarity of the grain size distribution with a lognormal distribution - as generally observed in experiments - was obtained. It was shown that an Avrami exponent q > 3 could be obtained for site saturation nucleation but a non-stationary growth kinetics. Furu and Marthinsen investigated with this approach the effect of spatial variation of influence factors on recrystallization like nucleation, growth,
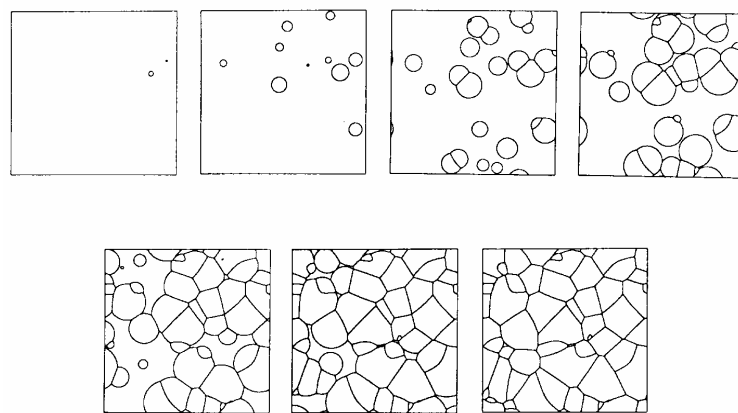
Fig. 3 Microstructure evolution according to the „Avrami machine" with constant nucleation kinetics.
(Courtesy: Trondheim Avrami machine)

drag effects and recovery [46-47]. On the basis of the so-called 'Trondheim Avrami machine' J. Jensen developed the RIS∅ -component model [48]. It was defined on a fixed 3 dimensional grid with up to four texture components. The growth could be anisotropic in terms of the global co-ordinate system. The input required

- the average recrystallized grain size.
- the number of texture components.
- the nucleation rate and its spatial distribution.
- the spatial and temporal dependency of the growth rate.

Frost and Thompson pursued a similar approach like the Avrami machine for microstructure development in thin films [49]. However, while the Avrami machine discretizes space and solves a system of equations for any point in space to obtain a 2D microstructure, Frost's model determined the triple junctions and then derived the grain boundaries as circular connecting curves in space (Fig. 4).
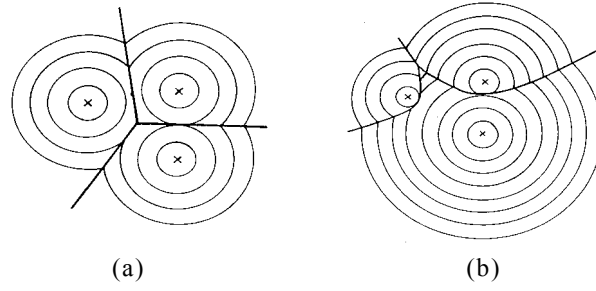
Fig. 4 Grain boundary geometry according to the Frost model, a) Site saturation, b) Continuous nucleation. (Courtesy: Frost)

Deficiencies were grain distributions far from a lognormal one and non-equilibrium contact angles at triple junctions. This caused a need for incorporation of grain boundary surface tensions to revive equilibrium at junctions. Frost investigated extensively normal and abnormal grain growth.

3.3. Vertex models:
If the deformed structure can be idealized as a perfect cellular structure, all microstructural changes are due to the force equilibrium at grain boundary junctions. Any junction moves in proportion to the resulting force acting on it, while the kinetics are determined by the grain boundary mobility and the grain boundary surface tension.

$$\sum_{j}^{(i)} D_{ij} \cdot \left(v_i + \frac{1}{2} v_j \right) = -\sum_{j}^{(i)} \gamma_{ij} \frac{r_{ij}}{|r_{ij}|} \qquad (3.18a)$$

$$D_{ij} = \frac{1}{3 m_{ij} |r_{ij}|} \begin{bmatrix} y_{ij}^2 & -x_{ij} y_{ij} \\ -x_{ij} y_{ij} & x_{ij}^2 \end{bmatrix} \qquad (3.18b)$$

Where mij is the mobility and r_{ij} = (xij, yij) is the line vector of the boundary connecting vertices i and j. The surface tension is the specific grain boundary energy, which is determined by the disorientation according to the Read-Shockley equation for the energy of a perfect small angle grain boundary of deformed microstructure. The grain boundary curvature is constant along a boundary and determined by the equilibrium at nearest neighbour junctions. Actually the model is a grain growth model for subgrain structures. Humphreys considered a large variety of 2 dimensional microstructures with regard to their stability and found arrangements that would produce discontinuous subgrain growth, which could be considered to be equivalent to a nucleation event in recrystallization (Fig. 5) [50,51].Correspondingly, he proposed a unified model of
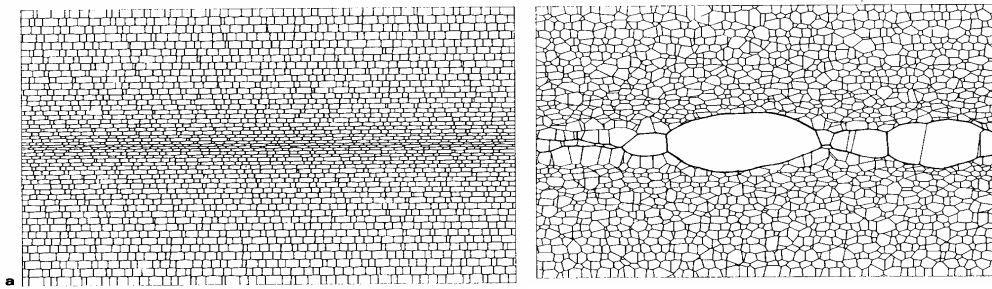
Fig. 5 Microstructure evolution according to a 2D-vertex model with in grain gradient. (Courtesy: Humphreys)

recrystallization and grain growth [52]. Weigand et al. were able to reproduce experimental results on tricrystals with a 2D vertex model by implementing limited triple junction mobility. The 2D vertex approach was recently extended to 3D networks of grain boundaries by Maurice [53].

3.4 Discrete models: The heterogeneity of the deformed microstructure requires a local and temporal variation of the physical phenomena to be taken into account. This can be obtained discretizing of the microstructure in space and time. It requires high computer power and large storage capacity, which can be met by high performance computers nowadays available. To tackle space and time resolved emergence of microstructure two principally different discrete approaches have been developed, an energetic and a kinetic approach. In the energetic approach the system searches for a trajectory to the lowest energy state and in the kinetic approach it anticipates such trajectory and utilizes the respective kinetic relations. The well-known method for the former is the Monte Carlo (MC) method and for the latter is the cellular automaton (CA). Srolovitz et al. used extensively the MC method to predict microstructure evolution during grain growth and also during recrystallization [54,55]. The cellular automaton approach for predicting recrystallization microstructures was first proposed by Göbel and Hesselbarth [56]. In both cases for each discrete cell in space at any given time steps a transformation rule was applied to change the state of a cell from deformed to recrystallize or to leave it unchanged.

a) The Monte-Carlo Technique: The Monte-Carlo (MC) technique is usually applied in terms of the Metropolis algorithm, which defines the transformation probability P by

$$P = \begin{cases} \exp\left(-\dfrac{\Delta E}{kT}\right) & \Delta E \geq 0 \\ 1 & \Delta E \leq 0 \end{cases} \qquad (3.19)$$

Since recrystallization is an irreversible phenomenon, there is no return from the recrystallized to the deformed state, which requires T = 0 in this algorithm.

A random number generator picks a cell, changes the state of the cell, and the total energy change ΔE is calculated. According to the transformation rule given by eq. (3.19) the state is either changed or kept in the unchanged state. For domain growth in periodic lattices Potts-models are used as described by Holm and Glazier, which discriminated Q different states of a cell, e.g. different orientations, deformed, recrystallized etc [57,58]. Srolovitz showed that for Q > 48 the microstructure evolution
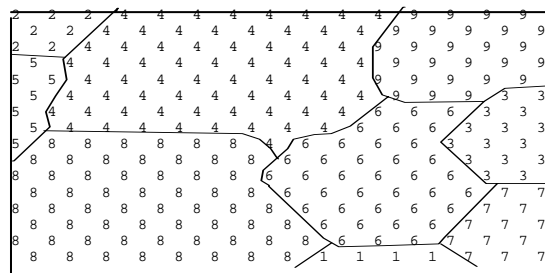
Fig. 6 Microstructural set up of a MC simulation. (Courtesy: Srolovitz)

of a metal was sensibly reflected. The larger Q, the larger the computational requirements and hence, usually Q = 48 was a reasonable compromise for recrystallization.

In 1985 Srolovitz et al. proposed their first MC recrystallization model. It was a Q = 48, 2D Potts model, which considered volume and surface energy terms. The MC simulation successfully reproduced nucleus growth and grain coarsening (Fig.7). The surface and volume energies strongly influenced kinetics and morphology of microstructure. The influence of the surface was usually very high.

The same model extended to take into account the effect of particles in recrystallization incorporating Zener drag energy in the total energy (E) for recrystallization [59]. The particles were introduced in to the simulation as sites, which had an orientation different from any of the grains. This assumption resulted in an inequality of the particle-matrix interfacial energy and the grain boundary energy, which was reasonable for incoherent particles. The particles were not allowed to move through the lattice.
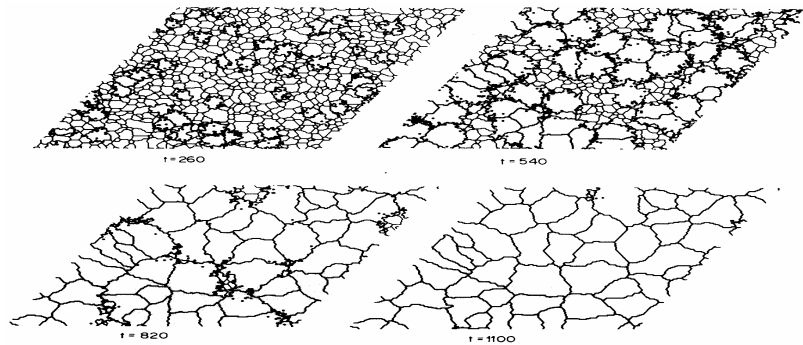
Fig 7 Microstructural evolution according to a MC simulation. (Courtesy: Srolovitz)

b) The Cellular Automaton Approach: CA-approaches also discretize space and time like MC models except that the transformation rule of a cell is different. CA changes its state in a deterministic way, which is determined by the state of its neighbours (Fig. 8) [60]. It makes the assumption that the decrease in free energy is automatically taken care of, which is certainly true for recrystallization where growth of nuclei always follows a trajectory to a more stable state, i.e. of lower free energy state. The transition rule determines the state of a cell, which only belongs to the recrystallization front. The transformation of a cell was made dependent on its stored energy, disorientation, local temperature and pressure etc.

$$P = P\left(\Delta g, \rho, T\right) \qquad (3.20)$$

where Δg: the disorientation, ρ: the dislocation density or local stored energy and T: the annealing temperature. This was the modified cellular automata approach [61]. Also, these state parameters may change during time, for instance to account for recovery.
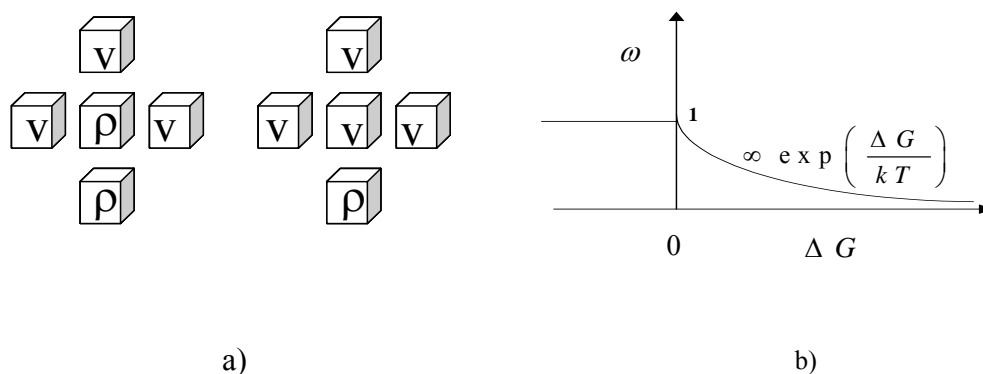

a)   b)

Fig. 8 a) The CA uses a deterministic transformation rule which depends on the state of the environment. b) The transformation probability in the MC approach depends on the respective free energy change.

Earlier investigation showed that the shape of the growing grains will reflect the geometry of the spatial grid if an environment of only nearest or second next neighbors

was used. This is less desirable but uncritical and can be prevented by a proper choice of neighbors [61].

There is a principal problem with both the MC and CA approach. The transformation rule, i.e. the growth of the nucleus, is not affected at all by any physical condition, like temperature, stored energy, disorientation etc. Consequently, such approach can only model homogeneous systems, which are less likely to meet the conditions set by deformation microstructures. Only the 3 dimensional CA model, which follows kinetics and energies in a local fashion, can only highlight the effect of local grain boundary properties, local driving force and local crystallographic texture on recrystallization process of heterogeneous materials, which are of industrial interest. Raabe used the 3 dimensional CA model with probabilistic switching rule where Turnbull's equation for grain boundary motion under the driving force of reduction of Gibbs free energy separated in to two parts, one deterministic part ($\dot{x}_0$) which depended weakly on temperature and a probabilistic part (w), which depended strongly on temperature

$$ x = \dot{x}_0 w = n \frac{k_B T m_0}{V} \frac{pV}{k_B T} \exp\left(-\frac{Q_{gb}}{k_B T} \right) \tag{3.21} $$

w was the product of a linear part $pV/(k_B T)$ and the nonlinear part $\exp(-Q_{gb}/(k_B T))$ of the original Boltzmann terms [62,63]. According to this model transformation (switching) of the state of a grid point was not performed in a deterministic way but with certain probability.
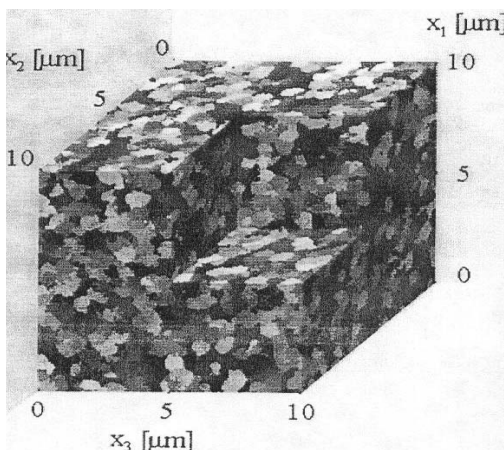

Fig. 9 a. Simulated rex microstructure of Al single crystal 1.41s, 78.1 vol% recrystallized at T =800K (Courtesy: Raabe)
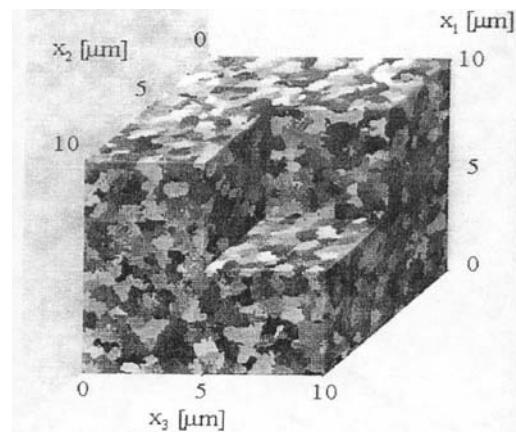
Fig. 9 b. Simulated Rex microstructure of Al single Crystal 2.11s, 99.9 vol% recrystallized at T=800K. (Courtesy: Raabe)

According to the above equation Eqn. (3.21) the local switching probability for each grid point was calculated using local and maximum driving force and mobility of boundary. The normalized form of local switching probability was given by

$$\hat{w}^{Local} = \left(\frac{m^{local} p^{local}}{m^{max} p^{max}} \right) = \left(\frac{\dot{x}^{local}}{\dot{x}^{max}} \right) = \left(\frac{t^{max}}{t^{local}} \right) \qquad (3.22)$$

Since boundaries with different mobilities and driving forces could not equally switch the state of the automaton in a given time step, either the time step were chosen such that boundaries with minimum probabilities crossed the cell or the condition was selected where the boundaries with the maximum velocity crossed the cell during one time step [64]. The advantage of the former method is an increased simulation speed. The disadvantage is a less smooth grain boundary shape.

The use of Metropolis Monte Carlo algorithm in CA model for defining the transformation rules of a particular cell was based on the selection of a random number R{0, 1}[64]. Transformation was accepted if: $R \le \hat{w}^{local}$ and it was rejected if $R > \hat{w}^{local}$. Use of the Eqn. (3.20) made CA temperature dependent and the use of local switching probability incorporated the effect of local disorientations and stored energy.
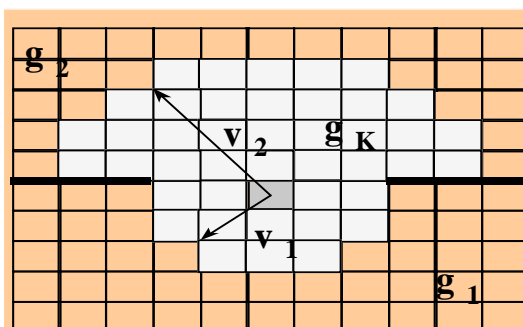

Fig.10 Growth of a nucleus (origin of growth v1 and v2) formed at a pre-existing grain boundary in the modified cellular automaton model. (White = recrystallized grain) (Courtesy: Reher, Marx)

c) **Hybrid CA-MC Model:** The standard form of the Monte Carlo (MC) model does not result in a linear relationship between migration velocity and stored energy. On the other hand, the standard form of the CA model used for recrystallization does not consider the grain boundary curvature as a driving force for migration. An MC-CA hybrid approach used two different methods for determining orientation change of each site in a lattice, which should be strictly suitable for simulation of recrystallization of certain category material, which forms sharp subgrains only [65]. In MC-CA model at any point of time the choice of a particular method were determined weighing

probabilities for each type according to the available knowledge of driving forces. A ratio R, between the frequency of the CA and MC reorientation attempts determined the magnitudes of the grain boundary energy compared with the stored energy. Only the configurational energy was used to determine the MC reorientations. The effect of stored energy was incorporated in CA model. A random number N in the interval (0, 1) determined the possibility of application of MC or CA for any given reorientation attempt in terms of the earlier mentioned ratio R.

The use of high-resolution FE computations was to predict microstructural dependence of nucleation, but success was rather limited so far [66,67]. The major reason is that the FE codes remain continuum approaches and do not account for microstructure in terms of dislocation arrangements. Owing to their lack of predictive power we will not further pursue these approaches in our consideration. It is more appropriate to choose nucleation criteria based on location, e.g. grain boundaries, or second phase particles (random nucleation), or physical conditions, e.g. stored energy etc. as proposed by Vatne et al. [68].
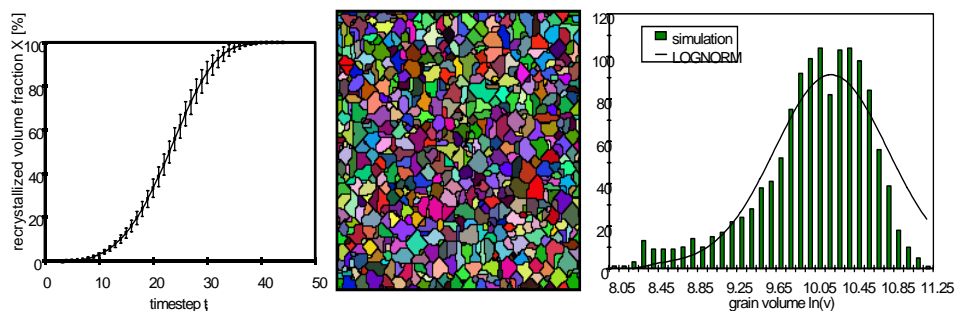

Fig. 11 Results of a CA-simulation: kinetics, microstructure, and grain size distribution.

(Courtesy: Marx)

3.5   Texture models: The critical challenge for all discrete models, however, is texture evolution. For given nucleation conditions and growth competition the mCA approach gave good agreement with experimental results [69] (Fig. 12). The accuracy of texture prediction, however, strongly depends on the local distribution of stored energy, disorientation and nucleus orientation. The local variations of stored energy and discrete texture orientations have to be fed into the program. The most convenient and adequate way to do this was by a combination of mCA (modified cellular automata)
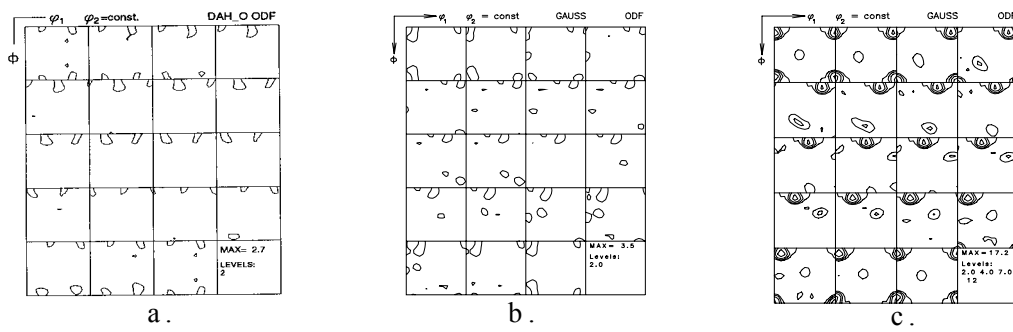
Fig.12 a) Measured annealing texture of a rolled particle containing Al-alloy; (b) Simulated texture under assumption of particle stimulated nucleation; (c) Simulated texture under assumption of nucleation at cube bands. (Courtesy: Marx)
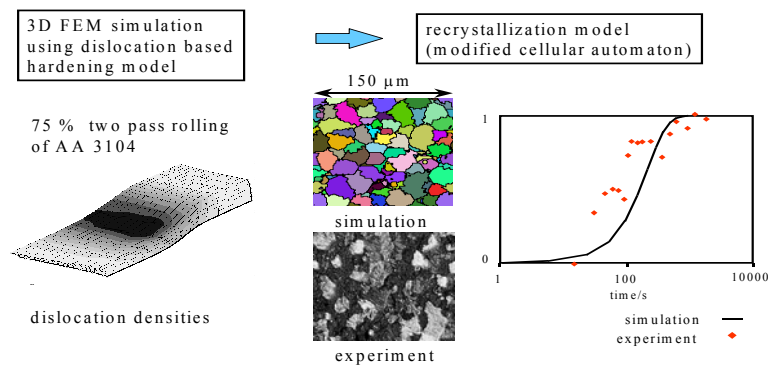

Fig.13 Integral recrystallization modeling of a two pass hot rolling process of AA 3104 (AlMg1Mn1): dislocation density in rolling gap (left), simulated (centre top) and measured (centre bottom) microstructure, simulated and measured (right) recrystallized volume fraction vs. annealing time. (Courtesy: Marx)

with FE codes and Taylor simulations. This was referred to as integral modelling [70-72]. A superposition of a finer mCA grid on the FE grid allowed to account for gradients of stored energy and texture as a local small volume average. This way, though thickness variation of texture and strain condition can be input for recrystallization texture modelling. Such mCA code was successfully applied to multi-step hot rolling of Al-alloys to predict grain size, kinetics and texture. If only texture is of interest there are special models, which consider this aspect only. These models require much less computer performance, because there is no need to determine the microstructure. In advanced concepts the volume fraction of the recrystallization texture components is determined by the nucleation and their growth probability. Jonas et al. formulated nucleation and growth probabilities for bcc materials [73]. Engler used a similar approach for Al alloys with more sophisticated criteria for nucleation phenomena based on proposals by Vatne, Nes et al. [74-79]. It was assumed that the recrystallization textures of Al-alloys can be explained by a growth selection of grains

with an approximate 40°<111> orientation relationship out of a limited spectrum of preferentially formed nucleus orientations. Accordingly, the probability of a given orientation to form during recrystallization was given by the probability of its nucleation and the probability of its subsequent growth. With this basic premise, recrystallization textures were modeled multiplying a function $f(g)^{nucl}$ representing the probability of the nucleation of the new grains with their growth probability function $f(g)^{grow}$ [74]:

$$f(g)^{sim} = f(g)^{nucl} \cdot f(g)^{grow} \qquad (3.23)$$

weak oriented growth
($m_{av}=0.2\ m_{max}$)

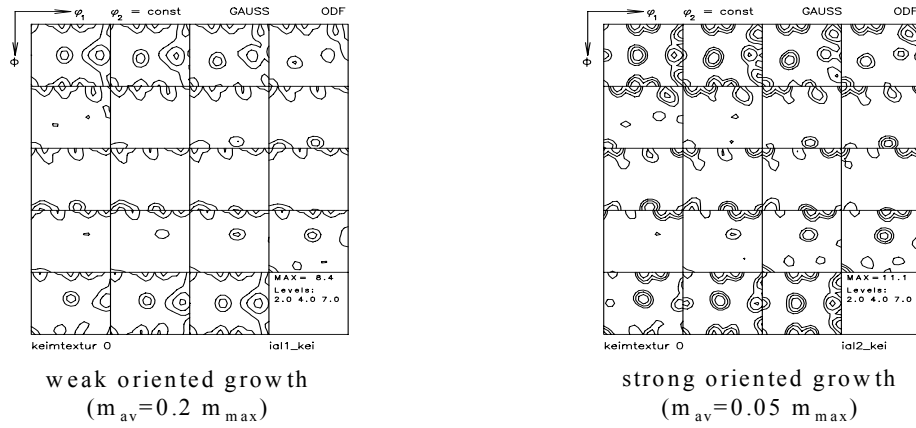strong oriented growth
($m_{av}=0.05\ m_{max}$)

Fig. 14 Nucleation texture under the assumption of weak oriented growth (left), and strong oriented growth. (Courtesy: Sebald)

The orientation distribution function (ODF) is defined as the function describing the intensity or *probability* with which a given orientation appears in the corresponding texture. Therefore, the probability of nucleation can be derived from the orientation distribution of the potential nuclei, which can e.g. be obtained by electron back scattered diffraction (EBSD)-local texture measurements at the potential nucleation sites. However, detailed EBSD-analysis of the potential nucleus orientations is an extremely time-consuming procedure, which is certainly not suitable for large-scale texture simulations. Therefore, based on the current understanding on the mechanisms of recrystallization nucleation in Al-alloys, for either nucleation site generic nucleus orientation distributions $f(g)^{nucl}_{Cube}$, $f(g)^{nucl}_{GB}$ and $f(g)^{nucl}_{PSN}$ were generated, where the functions $f(g)^{nucl}_{Cube}$, $f(g)^{nucl}_{GB}$ and $f(g)^{nucl}_{PSN}$ respectively denote the characteristic orientation spectra of the cube-bands, grain boundaries and large second-phase particles [75, 78].

In order to take the simultaneous nucleation at different nucleation sites into account, the nucleation distribution function $f(g)^{nucl}$ was derived by weighting the contributions of the different nucleation sites:

$$f(g)^{nucl} = x_{Cube} \cdot f(g)^{nucl}_{Cube} + x_{GB} \cdot f(g)^{nucl}_{GB} + x_{PSN} \cdot f(g)^{nucl}_{PSN} \qquad (3.24)$$

The weight factors x_i denoted the probability or efficiency of nucleation at the corresponding nucleation sites. The derivation of these parameters was based on experimental investigations about the nature and particularly on the evolution of the various nucleation sites during the preceding deformation [79]. The growth probability function $f(g)^{grow}$ considered the preference of nuclei with a 40°<111> orientation relationship to the deformed matrix.

Finally, the nucleation and the growth probabilities were multiplied to yield the simulated recrystallization texture $f(g)^{sim}$. This approach was successfully applied to simulate the recrystallization textures of a variety of Al-alloys with different microstructural characteristics processed under different processing parameters, *viz.* strain, strain rate and deformation temperature [77-79].

A more flexible treatment was given by Sebald et al. [80] who introduced temporal resolution in terms of an Avrami approach which allowed to take a time dependence of nucleation and growth rate into account as well as new processes like twinning etc [80]. The model was based on both nucleation and nucleus growth. The nuclei were assumed to be distributed at random in space. The crystallographic texture as given by the orientation distribution function (ODF) was discretized randomly oriented components.

Various nucleation conditions could be accounted for. For pure oriented growth a random nucleation texture was used where the number of nuclei was equal for all orientations. Nucleation was assumed to be site saturated, i.e. all nuclei are created at $t = 0$. The growth of nuclei corresponds to their grain boundary velocities v_{GB}, which was given by the product of the grain boundary mobility m and the local driving force p:

$$v_{GB} = mp \qquad (3.25)$$

The mobility of a grain boundary depended on the disorientation between the two adjacent grains. Three different categories of grain boundaries were discriminated, small angle, large angle and special boundaries. Small angle grain boundaries were

assumed to be immobile. In the case of aluminum it is generally accepted that grain boundaries with 40°<111> disorientation exhibit the highest mobility.

The driving force for primary static recrystallization is the difference between the specific stored energy of the deformed matrix and the nucleus, which is usually unknown for a given location. The Taylor factor of the deformed matrix components as derived from a simulation of the deformation texture was taken as first order approximation for this energy, as supported by X-ray line broadening measurements. Growth was assumed to be isotropic, but it ceased locally whenever two nuclei impinge, i.e. a growing nucleus can only grow into the non-recrystallized volume fraction (1-X). An Avrami approach as introduced in earlier was used. The non-recrystallized volume fraction (1-X) of a deformed component with orientation g_d was the ratio of the actual volume fraction of the deformed component V_d (g_d) and its volume fraction before recrystallization $V_{d0}(g_d)$. The change of the volume fraction of the component g_{rx}, which grew into g_d in a short time interval $t_1 < t < t_2$ read:

$$\Delta V\left(g_d, g_{rx}\right) = \frac{V_{d(g_d)}}{V_{d0(g_d)}} \cdot N\left(g_d, g_{rx}\right) \cdot \sigma \cdot v_{GB}\left(g_d, g_{rx}\right)^3 \cdot \left(t_2^3 - t_1^3\right) \qquad (3.26)$$

N (g_d, g_{rx}) denoted the number of nuclei, σ was a shape factor describing the nucleus geometry and $V_d(g_d)$ was the actual volume fraction of the deformed component with orientation g_d. Equation (3.26) shows that the volume increase is proportional to the local recrystallized fraction, the number of nuclei and the growth rate of the nuclei. During a time step the volume fraction of the deformed matrix was reduced by ΔV while the recrystallized volume was increased by the same amount. This procedure was performed at every time step for all possible combinations of g_d and g_{rx}.

These models provided a flexible and generic tool when fed with respective information on the deformed structure and its properties. Temporal resolution also allowed to invert the time vector and thus, to reveal the nucleation texture for a given recrystallization texture. This information could be utilized to assess the importance and occurrence of the actual nucleation mechanisms.

4. Cellular operator model for primary static recrystallization.

4.1 Necessity of this model: The present approach of modelling dynamic physical phenomenon like recrystallization of metallic materials is to avoid mathematical difficulties for describing the time and space dependent phenomenon, but to address the physical phenomenon cumulating different time dependent simple interactions, built on physical basis, among representatives of the real space.

It is a sophisticated three-dimensional Cellular Automata (CA) modelling approach to simulate primary static recrystallization of materials in terms of its kinetics, texture and microstructure in a deterministic way. As in every CA model, space and time are discrete; here we use a CA lattice where each cell has specific reference to a list of orientations, which contains the information of the deformed microstructure with respect to texture volume fractions and deformation energies. The status of a cell is fully resolved in terms of not recrystallized, partially recrystallized and fully recrystallized and is put in bit vectors. The gradual growth of recrystallized grains is governed by the collective information about the status of cells.

The recrystallization microstructure starts evolving in certain cells with certain deformation microstructure properties. Depending on the velocity of the recrystallization front, in one time step a cell may either be fully or partially crossed. The recrystallization front is considered to cross one cell with its maximum velocity in one time step. The front movement inside one cell when the front velocity is less than the maximum velocity is minutely scaled up with a number of microsteps. In the present calculations one cell is divided up to 65000 microsteps. Information on partially recrystallized cells includes the possibility of monitoring more than a single front movement inside one cell. The employment of partially recrystallized cells provides a high local resolution of microstructure in comparison with conventional models, which consider only fully recrystallized sets of cells. This high local resolution is very much required to follow the variations in kinetics and energies during recrystallization of deformed microstructure and to obtain a good number of recrystallized grains for a better statistics of recrystallization texture.
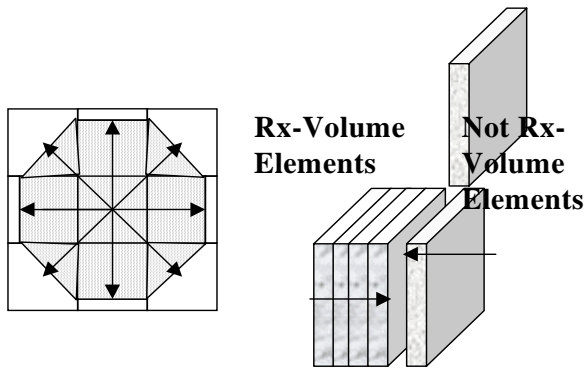
Fig. 15 a) Recrystallization growth from original to neighbouring cells in this model.
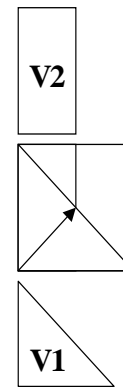
Fig. 15 b) The direction vector transforms the recrystallized fraction V1 to scalable fraction V2.

4.2 Sources and depiction of space variables: Since from the very beginning to the end the recrystallization process undergoes continuous interaction with the deformed microstructure the first step for simulation of the recrystallization process on the CA grid is the careful depiction of the deformed microstructure. Apart from the thermodynamical and kinetic instability criteria for formation of a viable nucleus, the the deformed grain shape and orientation spread in the deformed structure have direct impact on recrystallized microstructure evolution through the growth process. These long range and short range disorientation distributions can be successfully taken into account either by a statistical distribution of deformed orientations inside the created virtual deformed grains or by direct superposition of OIM (Orientation Image Maps) obtained from local texture measurements, on the CA grid. Since the former technique has the advantage to address better statistics, which is essential for explaining a proper recrystallization texture and a grain size distribution, the present modelling activity deals with space discrete variables, which are obtained from other associated model output.

Among the input parameters required for recrystallization simulation the deformed orientations and deformed grain size are obtained from the grain interaction model (GIA) through the 8 grain cluster depiction in cellular grid in 3 dimensions, the orientation discrete dislocation density or the summed up slip are obtained from the combined GIA and 3 internal variable (3IVM) model and the average precipitate number, size and solute content are obtained from the Classical nucleation and growth (ClaNG) model. The following table describes the input variables and their source.

Input	Source
Deformed Orientations, Size :	**Depiction of GIA 8 Grain Cluster in 3 Dimensional Cellular Operator. Real Length Scaling of Cells**
Deformation Energy:	**Summed up Slip from GIA or Dislocation Density from Dislocation Based Flow Stress Model (3IVM).**
Precipitate Number, Size, Solutes :	**Classical Nucleation and Growth .**

Deformation texture from GIA model: The initial deformation texture of the aluminium alloy, which is a prerequisite for recrystallization modelling, is obtained from a Taylor type deformation texture model (GIA), which considers the interaction of next neighbouring grains. GIA model assumes an 8-grain aggregate, embedded in a homogeneous surrounding. The homogeneous surrounding has been assumed to be deformed according to the prescription of FC Taylor model. From the very basic assumption of the Taylor model it can be inferred that the deformation of crystal pairs must be equal to the deformation of the surrounding to avoid incompatibility to occur with the surrounding. Thus, for ideal plane strain deformation the compatibility constraints require that the resulting shear of the crystal aggregate has to vanish, but each grain itself can relax all shears. This can be obtained by two mechanisms. The first one corresponds to the model of opposite shears and the second one incorporates the concept of Geometrically Needed Dislocations (GND) [81-83]. In the here used model, both mechanisms are used [82, 84]. The incompatibilities with other crystals of the aggregate or with the surrounding are removed by GNDs to fulfill the FC prescription of the whole aggregate. The relaxation of strain components in the single grains is only allowed, if the total energy of deformation and GND creation falls below the energy for an FC deformation of all the grains with no relaxation. The creation of GNDs makes a relaxation unfavorable because it causes extra energy consumption. These energy terms depend on the Elastic modulus, strain hardening and grain morphology. The strain rate and temperature effects are considered. The effect of additional slip activity at different strain and temperature creates significant changes in texture.
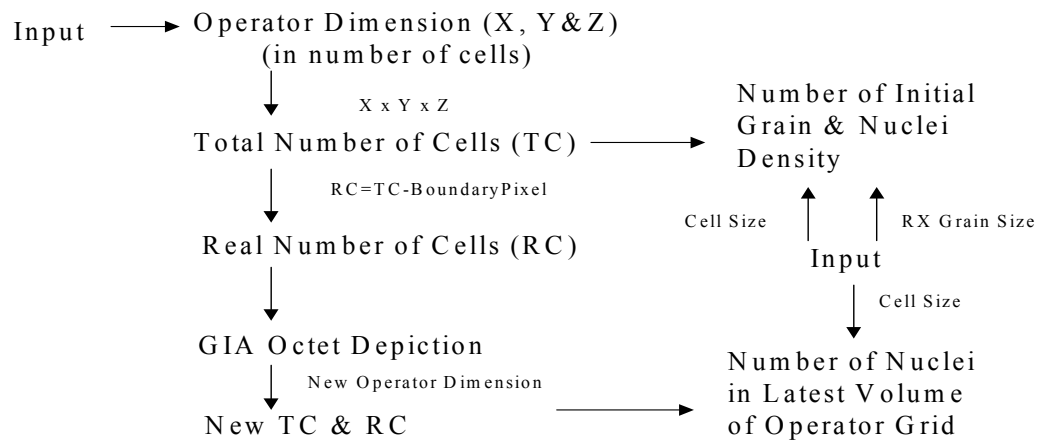
Fig. 16 Calculation of number of initial grains and nuclei density

New Operator Size for Octet Depiction: The initial size of the cellular operator is changed after 8 grain cluster depiction. The new operator dimension after 8 grain cluster depiction is obtained in following way.

Firstly the number of grains along three different directions (x,y,z) are calculated from the initial Operator dimension and the grain size.

$$N_{GXD} = \frac{X_{DX}}{X_{GSX}}, N_{GYD} = \frac{X_{DY}}{X_{GSY}}, N_{GZD} = \frac{X_{DZ}}{X_{GSZ}} \qquad (4.1a - 4.1c)$$

N_{GXD} – Number of grains along X direction of Operator. X_{DX} – Operator dimension along X direction. X_{GSX} – Calculated deformation grain size with prescribed deformation mode along X direction.

N_{GYD} – Number of grains along Y direction of Operator. X_{DY} – Operator dimension along Y direction. X_{GSY} – Calculated deformation grain size with prescribed deformation mode along Y direction.

N_{GZD} – Number of grains along Z direction of Operator. X_{DZ} – Operator dimension along Z direction. X_{GSZ} – Calculated deformation grain size with prescribed deformation mode along Z direction.

Secondly the number of octet grains along all three directions (x,y,z) are calculated from the number of grains in the respective direction.

$$N_{OjD} = 0.5 N_{GjD} \qquad (4.1d)$$

jD – X, Y, Z directions. N_{OjD} – Octet number along specific directions.

After calculation of number of octets the size of the octet grains are calculated from the initial grain size along all three directions.

$$X_{OjD} = 2X_{GjD} \qquad\qquad (4.1e)$$

X_{OjD} – Octet size, X_{GjD} – Grain size.

The new operator dimension obtained from the octet size and the octet number along each direction.

$$X_{NjD} = N_{OjD} X_{OjD} \qquad\qquad (4.1f)$$

X_{NjD} – New operator dimensions.

The real number of cell in the new octet depicted cellular operator grid is calculated the multiplying the operator dimension along X, operator dimension along Y and operator dimension along Z.

$$N_{RC} = X_{NXD} X_{NYD} X_{NZD} \qquad\qquad (4.1g)$$

N_{RC} - Real number of cells.

$$N_{TC} = N_{RC} + N_{BC} \qquad\qquad (4.1h)$$

Total number of cells = Real Number of Cells + Boundary Cells.

Dislocation density from 3IVM model: A microstructural flow stress model based on the consideration of three dislocation densities as internal state variable is used here to generate the deformation energy input for recrystallization model. This model consists of a kinetic equation of state and evolution laws for dislocation densities [85]. It simulates the flow stress at a given temperature and strain rate for a specific material, characterised by solute level, average particle size and volume fraction, grain size and texture. It is also applied for interpass rolling recovery simulation. The cellular microstructure is represented in the model discriminating dislocation densities between cell walls and dislocation in cell interiors. The third internal variable is the density of mobile dislocations, which bears the imposed strain rate. Due to the use of dislocation densities as internal variables, it results in output of the same, which is directly taken as input for subsequent modelling of static recovery and recrystallization during annealing. The use of the 3IVM in FE code results in the spatially resolved dislocation density in the deformed material.

The initial microstructure and nuclei texture and the deformation energy data obtained so far from the GIA and 3IVM model consists of different members [Fig. 18] like the index to each orientation, three Euler angles, volume fraction, width of scattering, the deformation energy and status of each orientation. While the index of each orientation

provides ease in computations the status of the orientation helps in finding the nuclei location for different sources.
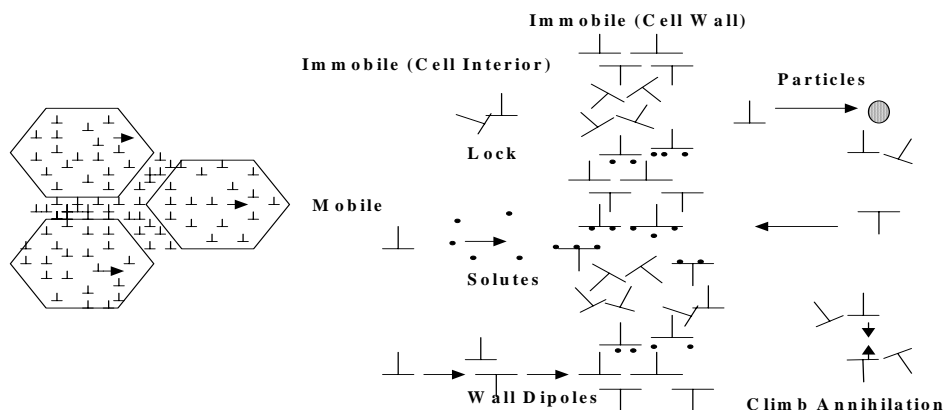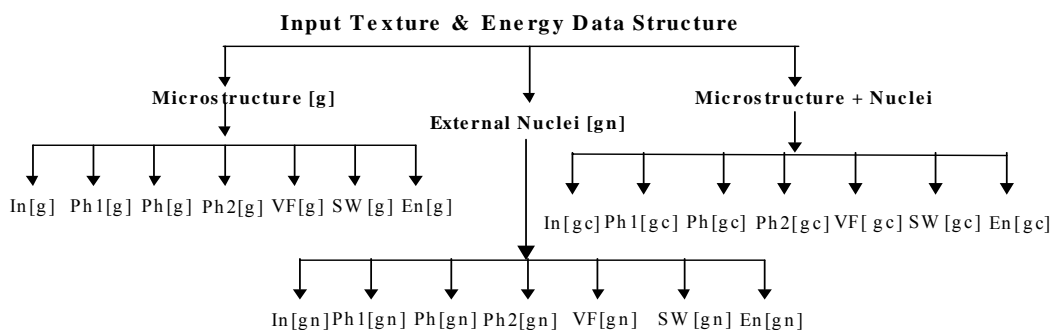

Fig. 17 Schematic representation of the 3IVM model. (Courtesy G. Goerdeler et. al: Aluminium June 2004; 80:666)

In - Number of microstructure items.

Ph1, Ph and Ph2 - Three Euler Angles.

VF - Volume Fraction.

SW – Scattering Width.

En – Deformation Energy.

Status of Orientation is another member, which is not shown here. It helps in finding the nuclei location for different sources.

Fig. 18 Data structure of input microstructure and nuclei.

Precipitates and solutes from classical nucleation and growth model (ClaNG): The output of this statistical model, which is capable of simulating the simultaneous nucleation and growth coarsening of spherical precipitates during homogenization, was taken as input for recrystallization model. A detailed description of this model can be found elsewhere [86]. A combination of thermodynamic and kinetic database including properties of materials is applied to calculate the driving force for precipitation,

interface energy and mobilities of different elements respectively. The nucleation rate is defined by the thermodynamic nucleation condition fulifilled by the slowest moving element and the subsequent growth law is obtained in form of a continuity equation involving the respective mobility. The total number of precipitates, precipitate size classes and matrix solute concentration obtained from this model, were used to calculate the number of particle stimulated nuclei, back driving force for recrystallization and solute drag force.

Properties of each cell:
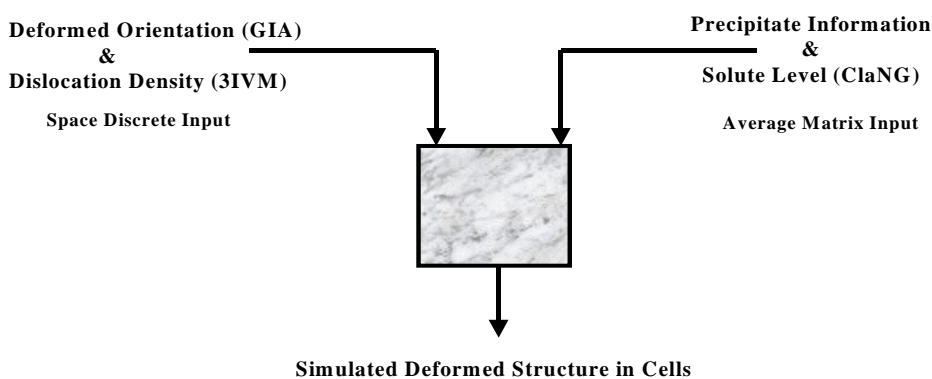
Fig. 19 Description of initial characteristics of starting microstructure.

4.3 Preferential nucleation based on space discrete variables: The
formation of new strain free grains may not resemble the initial stage of phase transformation [87]. The critical nuclei size and the number calculated from those thermodynamic factors do not match the reality. It is now understood that nucleation takes place gradually through some physical processes involving small pre-existing volume entity in terms of either cell or subgrains. New grains evolve during recrystallization from the deformed microstructure. Sources of recrystallization are deeply rooted in the deformation characteristic of material. Many research works have been dedicated to understand the deformation characteristics of aluminium [25-29, 88-91]. For aluminium alloys it is known that the recrystallization nuclei do not appear homogeneously but they nucleate at certain locations like near particles, along grain boundaries and deformation bands in a deformed grain [79, 92-95].

Grain boundary nucleation: Nucleation during recrystallization near the prior grain boundaries has been frequently observed. The most probable reason is that both strain and disorientation accumulate near grain boundaries during deformation, which make

Kinetic Instability - Presence of Mobile High Angle Boundary.

Segment of Boundary of Length Lc Which has no subgrain boundary entering it from one side and has n boundaries entering it from other side.

Subgrain Boundary
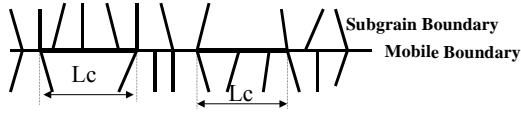
Mobile Boundary

Fig. 20 Cell wall/subgrain boundary impingements on mobile boundary.

Fig. 21 Localized process of dislocation rearrangements and nucleation.

the grain boundary a preferred site for nucleation. From that consideration each and every site along the grain boundary could be a site for nucleation, which in turn gives an over prediction of the number of grain boundary nuclei. In this present modelling approach grain boundary nucleation is treated as a localized phenomenon, which can be experimentally observed. Nucleation is considered to occur in those segments of a boundary, which have subgrains or cells on both sides of boundaries with the difference in intercept distances. In a simplified way the number of nuclei per unit volume from grain boundaries can be expressed as $N_{GB} = [\{N_A . A(\varepsilon)\}/V_0]$ where, N_A is the number of nuclei per unit area, $A(\varepsilon)$ is the instantaneous grain boundary area, i.e. $A(\varepsilon) = 2[a_0 b_0 + b_0 c_0 \exp(-\varepsilon) + a_0 c_0 \exp(\varepsilon)]$ and V_0 is the initial volume of the grain $(a_0 b_0 c_0)$. If the presence of irregularly shaped subgrains makes the grain boundary area (A) segmented and the segment size complies with a $P(A) = 1/A_{avg} \exp(-A/A_{avg})$ distribution, and if the probability of finding n subgrains on the other side of any of these segments follows the distribution, $P(n) = 1/n!(A/A_{avg})^n \exp(-A/A_{avg})$, then the number of area segments per unit area of grain boundaries which have n subgrains in one side and only one on the other side is given by

$$N(A) = \int_0^\infty P(n)P(A)\frac{dA}{A_{avg}} \quad \text{or} \quad N(A) = \frac{1}{n! A_{avg}} \int_0^\infty \left(\frac{A}{A_{avg}}\right)^n \exp\left(\frac{-2A}{A_{avg}}\right) \frac{dA}{A_{avg}} \tag{4.2}$$

The number of nuclei (N_A) per unit area is the sum of the grain boundary segments of critical size, which has n_c or more number of subgrains in one side and only one on the other side, can be obtained summing up grain boundary segments from critical value of n_c to infinity.

$$N_A = \left(\frac{2}{2^{n_c} A_{avg}} \right)$$

(4.3)

Where, $n_c = (A_{crit}/A_{avg}) = (d_{crit}/d_{avg})^2$, $A_{crit.}$ and $A_{avg.}$ represent the critical and average size of the grain boundary segments.
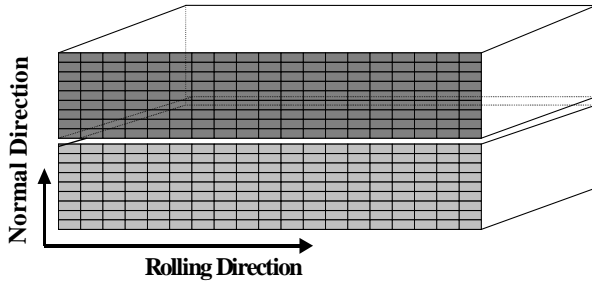

Fig. 22 a) Position for grain boundary nucleation along a grain boundary

Fig. 22 b) possible grain boundary nucleation along a grain boundary

The average subgrain size can be calculated from the dislocation spacing $d_{avg} = \dfrac{15}{\rho_{mean}^{0.5}}$

where ρ_{mean} is the mean dislocation density. The ratio of the critical to the average subgrain diameter is chosen in such a way that the thermodynamic criterion for nucleation by high angle boundary bulging is satisfied. $d_{crit} > \dfrac{4\gamma_{gb}}{0.5Gb^2 \rho_{mean}}$ where d_{crit} is

the critical subgrain diameter, γ_{gb} is the grain boundary energy, G is shear modulus and b is Burgers vector. Since during hot rolling of a material the cube orientation may be stable [19,96,97] the grain boundary nucleation is divided into two classes with respect to the orientation of the nuclei involved.

(a) Grain boundary nuclei from stable cube components mainly RD rotated cube and the respective number of nuclei can be written as

$$N_{GB\_Stable-Cube} = [\{N_{A\_Stable-Cube} \cdot F_{V-Cube} \cdot A(\varepsilon)\}/V_0],$$

(4.4)

where, $N_{A\_Stable-Cube}$ represents the nucleation probability, F_{V-Cube} gives the initial volume fraction of cube grains.
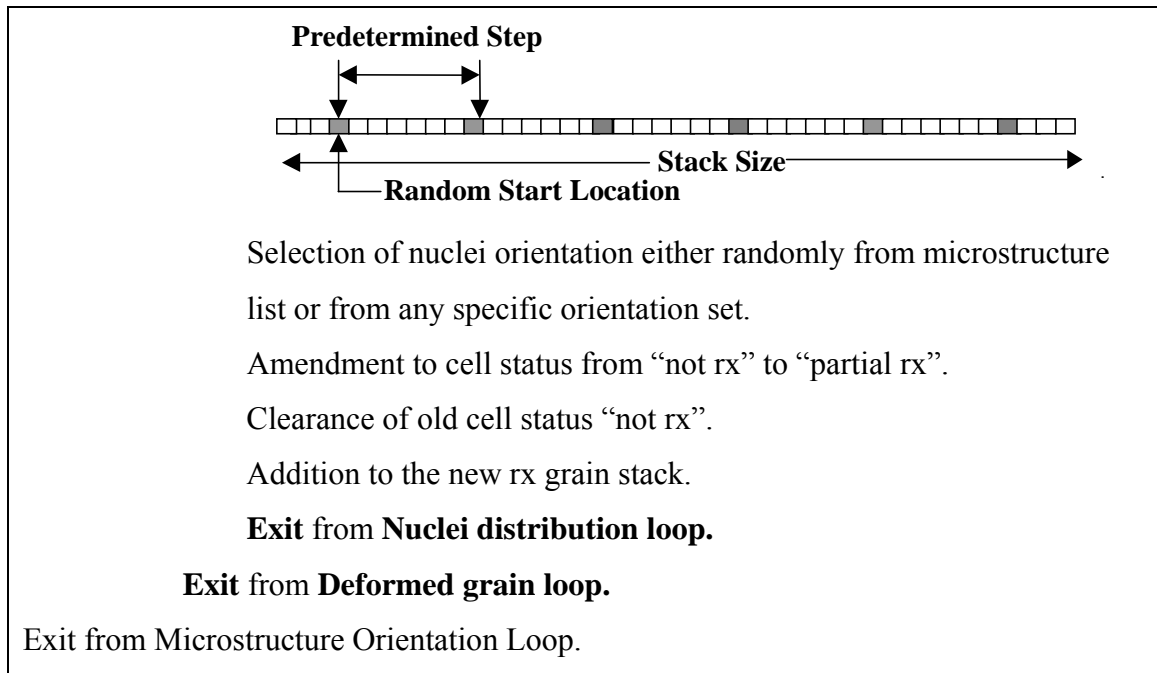
(b) Grain boundary nuclei from highly frequent rolling texture components

$$N_{GB\_ROLG} = [\{N_{A\_ROLG} \cdot (1- F_{V-Cube}) \cdot A(\varepsilon)\}/V_0]$$

(4.5)

where, N_{A_ROLG} is the nucleation probability from the rolling texture orientations.

In this space resolved modelling approach the grain boundary nucleation is kept restricted within cells from all six surfaces of virtual grains.

Initialise: Number of grain boundary nuclei from calculation = 0.
Calculation of number of grain boundary nuclei of each time step for different time dependent nucleation: 1. Increasing nucleation. 2. Decreasing nucleation. 3. Constant nucleation. Necessary correction for the number of nuclei of last nucleation time step so that the total number of nuclei calculated from the thermodynamic criterion remains unaltered.

Microstructure orientation loop:
 	
Distribution of available nuclei for each time step among all microstructure orientations according to criteria:
 	
    Nucleation based on high dislocation density.
 	
    Nucleation based on low dislocation density.
 	
    Nucleation based on mean dislocation density.
 	
    Number of grain boundary nuclei from calculation: Summed up nuclei available for different microstructure orientations after distribution.
 	
        Deformed grain loop:
 	
        Positioning of nuclei on all deformed grains of different orientations:
 	
        Determination of individual grain origin in X, Y, Z co-ordinate.
 	
        Determination of grain size in X, Y, Z directions in terms of cells.
 	
        Scanning of all surface cells of individual grains on the basis of their cell co-ordinates and grain size.
 	
        Addition of all empty cell locations available from all surface scans for further use of nucleation.
 	
        Nuclei distribution loop:
 	
        Nuclei cell location in not rx surface cells:

Selection of nuclei orientation either randomly from microstructure list or from any specific orientation set.

Amendment to cell status from "not rx" to "partial rx".

Clearance of old cell status "not rx".

Addition to the new rx grain stack.

Exit from **Nuclei distribution loop.**

Exit from **Deformed grain loop.**

Exit from Microstructure Orientation Loop.

Nucleation from deformation bands inside grains: In a number of materials subject to large plastic strain, it is observed that deformation becomes localized to bands, which penetrate the entire cross section of the polycrystalline material. Some investigations interprets that the formation of microband are more frequent in a matrix of diffused tangled dislocations which do not contain well defined cell or any evidence of lamellar structure and delivers a regular array of dislocation and high disorientations [25,30,98]. It is also shown that the broadening of microband may cover the entire cross section of deformed grains resulting in a local shear or random texture. An irregular array of immobile dislocation makes the cell formation difficult while a regular arrangement of comparatively free dislocations forms cells very easily. The variation in the density ratio of immobile to mobile in aluminium alloys with different compositions may introduce a
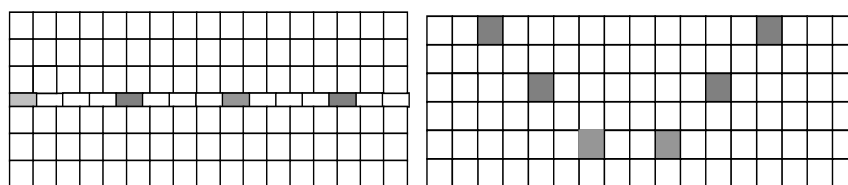
Fig. 23 Nucleation from initial microstructure heterogeneities

different tendency of cell formation for different alloys. There are efforts to simulate the deformation characteristic of polycrystalline material by Taylor type deformation texture model [GIA]. The major interpretation is that the difference in the number of

active slip system brings the disorientation [99]. The experimentally observed dense dislocation wall under gradual deformation creates microbands, which may spread gradually because of local slip process [98]. Another substructural feature, which seems to be an important factor for modelling Taylor type deformation texture models is a Geometrically Necessary Dislocation Boundary.
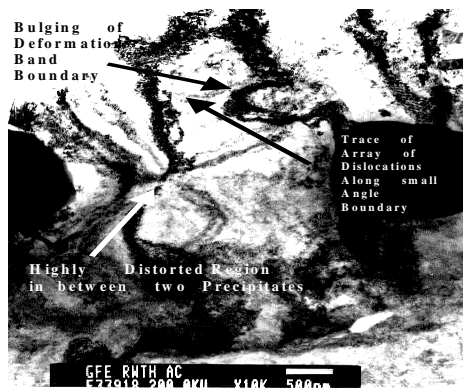

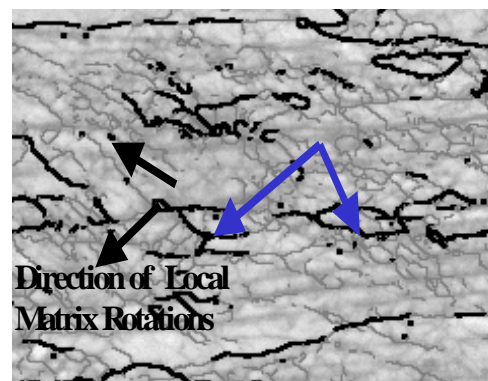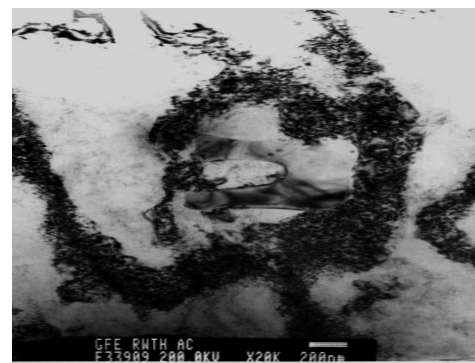Fig. 24 a) Nucleation from the deformation heterogeneities from a region in between two particles.

Fig. 24 b) Nucleation from the middle of the elongated grain.

Fig. 25 a) The nucleation of grain near precipitate.

25 b) Dislocation free entities near precipitate surrounded by dense dislocation in deformation zone.

These GNDs hold the disorientation between comparatively dislocation free cellular entities inside Taylor lattice. The initial nuclei texture of the material, which is a prerequisite for recrystallization modelling, is obtained from the GIA model. A microscopic view of this type of band as obtained from Fig. 24b) was tried to simulate in the Cellular Operator. Fig. 23 shows the simulated nuclei locations. The deformation transition bands can be created inside deformed grains, which are found to split under imposed deformation mode by GIA model [99]. As discussed before, a similar type of probability term is applied to calculate the effective number of sites for nucleation.

Particle stimulated nucleation: The difference in degree of plastic deformation makes a particle-containing alloy to be strain hardened much faster than a single phase material and also results in a deformation gradient which stores additional arrays of dislocation to bring the compatibility between differently deformed parts of material. This local non-uniform deformation mode adds new sets of dislocations, which are required for geometrical reason. Hence, the sources of dislocations for the deformation of these materials are of two types namely uniform deformation and non-uniform deformation. The uniform deformation generates statistical and non-uniform deformation produces geometrically necessary dislocations. A simplified model based on this assumption may give a very high dislocation density at a very low strain level. At a higher strain level the situation may change because of nucleation of dislocations in those places around the hard precipitates, where local stress is high enough to make dislocation sources active to generate more dislocations. The configuration of dislocations around particles naturally depends on particle size, spacing and on the deformation level and gradually becomes more complicated when a higher strain level is approached. A very high dislocation density and a prominent lattice rotation are expected consequences. Though a considerable lattice rotation is observed in practice around large particles at high strain level, the dislocation density is found to be less than expected high range because of local recovery process. As shown in Figs. 21 and in Fig. 25b), the local recovery process creates localised zone of lower energy and gradually constricts the dense dislocation wall, resulting in a sharp disorientation contrast between different adjacent parts inside the deformation zone either just beside particles or away from the particles depending on the nature and number of slip systems activated at different locations of deformation zone. The deformation zones around certain precipitates fulfill both thermodynamic and kinetic nucleation conditions and serve as possible nucleation sites (Fig. 25 a)). The critical condition for PSN is reached when the radius of curvature of a recrystallization nucleus equals the particle radius (r) [100]. In order to quantify the number of recrystallized grains per unit volume of the material, contributed by different precipitate size classes, the deformation zone volume is taken into account for each class of precipitate along with the number frequency of each class. In a simplified approach the total number of PSN nuclei can be written with the help of a probability of nucleation per unit volume of deformation zone ($C_{n/v}$) as

$$N_{PSN} = C_{n/v}\,(N1V1 + N_2V_2 + N_3V_3 + \ldots\ldots\ldots + N_nV_{n)} = C_{n/v} \sum_{ri}^{r\,max} N_iV_i \qquad (4.6a)$$

where V_i is the volume of deformation zone of ith class of precipitates having a super critical size ($ri = r_{crit.} \geq 2\gamma / (0.5Gb^2\rho)$) where G is shear modulus, b is Burgers vector, ρ is the dislocation density and N_i is the number of ith class precipitates per unit volume of the material. The volume of the deformation zone around the precipitates can be written as $V_i = 4/3\pi Z_i^3$, while the size of the deformation zone Z_i is a function of particle radius, $Z_i = f_{zone} . r_i$.

There is another approach for particle stimulated nuclei number calculation, which considers the nucleation from the surface of the deformation zone due to the growth of certain subgrains or cells situated in between precipitates and the boundary of deformation zone.

$$N_{PSN} = C_s \sum_{ri}^{r\,max} \frac{NiAi}{NiVi} \qquad (4.6b)$$

where Ai is the area of the deformation zone of ith class of precipitates having a super critical size ($ri = r_{crit.} \geq 2\gamma / (0.5Gb^2\rho)$). The nucleation probability (C_s) for this approach is calculated in a similar manner as nucleation probability for grain boundary nucleation.

Calculation of number of random nuclei of each time step for different time dependent nucleation:
Necessary correction for the number of random nuclei of last nucleation time step so that the total number of nuclei calculated from the thermodynamic criterion and precipitate data remains unaltered.
Random Nuclei Loop:
Nuclei positioning in the operator grid, Orientation Setting and cell status updating:
Random position selection from the not recrystallized cells.
Selection of orientation of nuclei from the available nuclei orienation list.
Reseting the cell status from "not rx" to "partial rx".
Clearance of old cell status "not rx".
Addition to the new rx grain stack.
Exit from **Nuclei Distribution Loop.**

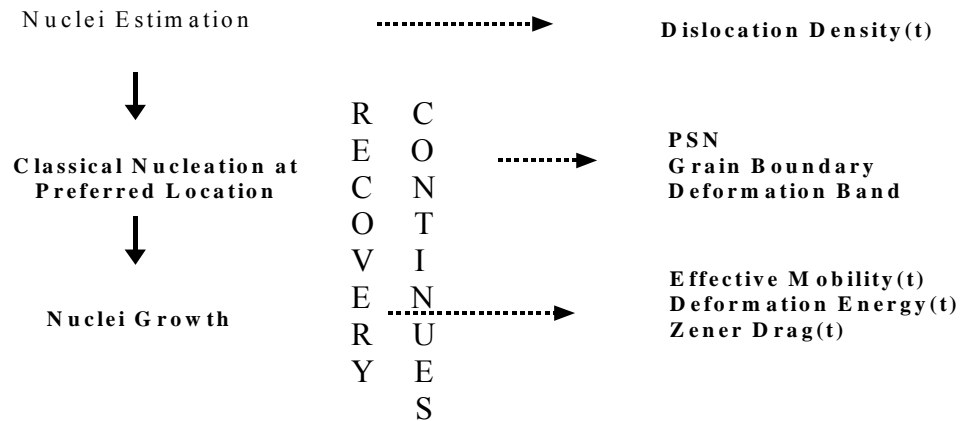**Static Recrystallization Process in Cellular Operator**

Nuclei Estimation · · · · · · · · · ▶ Dislocation Density(t)

↓

R C
E O
Classical Nucleation at   C   N · · · · · · ▶   PSN
Preferred Location   O   T   Grain Boundary
                            V   I   Deformation Band

↓

E   N
Nuclei Growth   R   U · · · · · · · · ▶   Effective Mobility(t)
                 Y   E   Deformation Energy(t)
                      S   Zener Drag(t)

Fig. 26 Sequence of functioning of different subroutines.

4.4   Time dependent nucleation: Five different modules of time dependent nucleation are given below. The optimization factors f_{ED} , f_{EI} , f_{LD}, f_{LI} and f_C and total number of nuclei, N_T form the relation between the number of nuclei and the simulation time step, $t_{SIM.}$

1. Decreasing Nucleation:

$$N_t = f_{ED} \exp(-t_{SIM})N_T \qquad (4.7a)$$

2. Increasing Nucleation:

$$N_t = f_{EI} \exp(t_{SIM})N_T \qquad (4.7b)$$

3. Decreasing Nucleation:

$$N_t = (f_{LD}t_{SIM})^{-1}N_T \qquad (4.7c)$$

4. Increasing Nucleation:

$$N_t = f_{LI}t_{SIM}N_T \qquad (4.7d)$$

5. Constant Nucleation:

$$N_t = f_C N_T \qquad (4.7e)$$

4.5 Nuclei number distribution:

Depending on the dislocation density of microstructure orientations different possible nuclei distributions per microstructure orientations are considered in the model. The orientation discrete dislocation densities obtained from the 3IVM model nucleate

different number of new grains depending on the deformation energy of the microstructure orientation. The following equations deal with different possible nuclei distributions.

$$N_{AHD} = \frac{N_T N_{OI} \theta \rho_n [Oi]}{N_{TDG} N_{OI}}$$ (4.8a)

N_{AHD} is the number of nuclei per microstructure orientation, when nuclei are distributed according to the normalised dislocation density value, $\rho_n[Oi]$ of individual orientation. θ is the optimisation factor. N_T denotes total number of grain boundary nuclei. N_{TDG} represents total number of deformed grains and N_{OI} stands for total number of microstructure orientations.

$$N_{ALD} = \frac{N_T N_{OI} \theta (1 - \rho_n [Oi])}{N_{TDG} N_{OI}}$$ (4.8b)

N_{ALD} is the number of nuclei obtained per microstructure orientation, when nuclei are distributed in reverse order of the normalised dislocation density value, $\rho_n[Oi]$ of individual orientation. θ is the optimisation factor.

In above mentioned nuclei distributions the individual dislocation density is normalized to maximum dislocation density available from the microstructure orientations. Another type of nuclei distribution is considered in the model where the maximum dislocation density of N_{AHD} is substituted by the mean dislocation density of the microstructure orientations.

Optimisation factor (f_{opt} or θ): It brings the total number of nuclei obtained from the deformation energy based distribution [$\sum_{O_1}^{O_N} N_{AHD}$ or $\sum_{O_1}^{O_N} N_{ALD}$] closer to the number of grain boundary nuclei (N_R) obtained from earlier mentioned calculation.

f$_{opt}$ =Middle Level (ML)

$$ML = \frac{UB - LB}{2} + LB$$

Upper Bound(UB)

Either

2nd Condn. UB=ML

Predefined

Or

3rd Condn. LB = ML

Lower Bound(LB)

1st Condn.

UB Condition $\sum_{O_1}^{O_N} N_{NHD} > N_R$
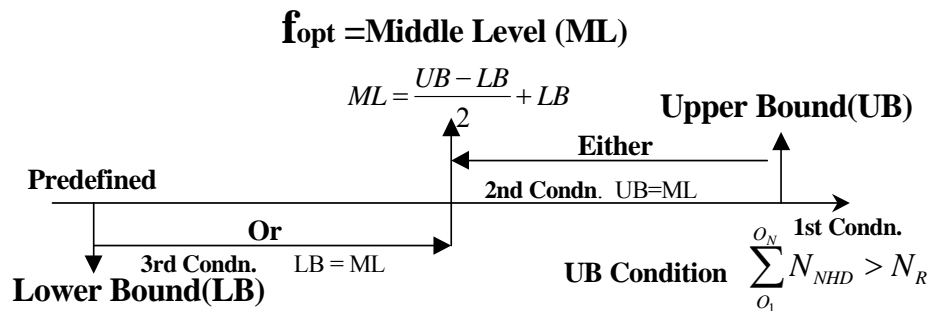
Fig. 27 Calculation of prefactor for grain boundary nucleation.

4.6 Recovery models: The high energy associated with dislocation density of deformed matrix makes the system thermodynamically unstable. The lowering of high energy takes place by recovery and recrystallization process. The movements of dislocations through climb and glide reduce the dislocation density and rearrange them in special configuration of low angle boundary. This process may take place during deformation, before or during recrystallization annealing. Though changes in microstructure remain limited to a very small scale, a significant effect of recovery on the nature and extent of recrystallization can be found under favourable process and material conditions. Under certain condition recovery might be competent enough to restrict completely the recrystallization process.

The type and the extent of the associated dislocation motion are determined by the stacking fault energy, chemistry of materials and strain, temperature of the material processing. From the point of energy consideration the climb of edge dislocation by that of jogs is favoured. The details of the process suggest that it may take place either by vacancy emission at the jogs along the dislocation line or by the supply of material by diffusion from the dislocation line to sink. The rate of the first process is determined by the activation energy associated with low concentration of jogs while the rate of the second process is indifferent to the high jog concentration and is determined by the activation energy of self-diffusion [101,102]. Depending on stacking fault energy and degree of vacancy saturation the configuration of climbing dislocation may change. Possibilities of climb of partial dislocations by constriction of jogs and by the pressure imbalance through the vacancy disc nucleation adjacent to a partial are also reported [103].

The reduction of dislocation density by cross slip is not very frequent in the fcc structure. It occurs when the gliding dislocation changes its own slip plane finding another slip plane with high atomic density and with parallel direction vector for gliding. Generally it is considered that the screw component of a dislocation loop can undergo this process. In fcc structures the interaction of similar type of stacking faults at the point of intersection of different orientations creates sessile dislocations, called stair rod dislocations. Neither of these two intersecting orientations contains the direction vector for gliding of this new dislocation. Since partial dislocation cannot cross slip without leaving a dislocation of this type, very high activation energy is required for this process.

The presence of solutes affects significantly the stacking fault energy and induces a wide split in partials, which are expected to have jogs of very high energy, where only a small fraction remains in thermal equilibrium. The climb would be much easier for the stacking fault absorbing or emitting point defects.

This model includes three different modules of recovery process. The climb of jogs of perfect and extended dissociated edge dislocations and the recombination process of splitted partials through gliding after first combination which is necessary for cross slip [104].

The climb velocity v_{climb} of the dislocation in a 3 dimensional network where the individual dislocation has a radius of curvature (R) under the influence of a force P is written as

$$v_{c\lim b} = \frac{dR}{dt} = \frac{D_T c_j P b}{kT}$$

(4.9)

where D_T is the diffusivity at temperature T, c_j is the concentration of jogs, b is the Burgers vector and k is the Boltzmann factor. Since force (P) on an individual dislocation line segment with radius of curvature (R) is given by

$$P = \frac{Gb^2}{R}$$

(4.10)

where G is the shear modulus.

The earlier equation is rewritten as

$$\frac{dR}{dt} = \frac{D_T c_j Gb^3}{kTR}$$

(4.11)

The integration of the Eqn. (4.11) and the dependency of dislocation density on dislocation spacing ($\rho \sim R^{-2}$) result in time (t) dependency of dislocation density (ρ) during recovery as

$$\frac{1}{\rho} = \left[\frac{1}{\rho_0} + \frac{2D_T Gb^3 c_j}{kT} t \right]$$

(4.12)

where ρ_0 is the initial dislocation density. The effect of stacking fault energy (SFE) on recovery through dislocation climb is included considering the climb of extended dissociated edge dislocations

$$\frac{1}{\rho} = \left[\frac{1}{\rho_0} + \left(\frac{2D_T Gb^3 c_j}{kT} \right) \left(\frac{SFE}{Gb} \right)^2 \left(\frac{33.9\pi(1-\nu)}{(2+\nu)} \right)^2 t \right]$$

(4.13)

where ν is the Poisson ratio.

The recombination model suggests that the cross slip of dislocation in fcc metals is possible if the splitted dislocations after first combination glide and make a curvature of certain length before a stable recombination which is necessary for cross slip. The activation energy for this is written as

$$Q_{CS} = \frac{Gb^2\lambda}{15}\left(\ln\frac{\lambda}{b}\right)^{0.5} \tag{4.14}$$

where λ is the width of separation of partial dislocations.

This activation energy term is included in the following equation which deals with time (t) dependent dislocation density (ρ) because of the thermal assisted glide of dislocation.

$$\rho = \rho_0 - \frac{8c}{G^2b^2}\exp\left(\frac{-Q_{CS}}{kT}\right)t \tag{4.15}$$

4.7 Growth of nuclei by grain boundary movement:
In Contrast to atomistic details of recrystallization, the energetic reasons for recrystallization are well understood. Basically there is always a driving force on a grain boundary if Gibbs free energy, G_F, of a crystal is reduced during motion of the boundary. If an area element dA of a grain boundary is displaced by an infinitesimal distance, dx, the free energy will be changed by

$$dG_F = -pdAdx = -pdV \tag{4.16}$$

Where dV is the volume swept by the moving grain boundary. The term $p = -dG_F/dV$ is referred to as driving force; it has the dimension of gained free energy per unit volume (J/m^3), but it can also be considered as a force acting per unit area on the grain boundary (N/m^2), i.e., as pressure on the grain boundary. If a recrystallized grain grows into the deformed microstructure, the dislocations in the swept volume are consumed by the boundary, and a volume with a substantially lower dislocation density is left behind (about $\rho_N = 10^{10}[m^{-2}]$ compared to $\rho_D = 10^{16}[m^{-2}]$ in heavy deformed metals). The energy of a dislocation per unit length is given by $E_d = 0.5Gb^2$ where G is shear modulus and b is Burgers vector. The driving force for primary recrystallization may be formulated as

$$p = (\rho_D - \rho_N)E_d = 0.5(\rho_D - \rho_N)Gb^2 \tag{4.17}$$

In cellular operator lattice each deformed grain represents a deformed orientation with its high dislocation density. The dislocation density of nuclei is set to a fixed value $\rho_N = 10^{10}[m^{-2}]$.

If a grain boundary moves under the action of a driving force p each atom gain the free energy pb^3, where b^3 is the atomistic volume, if it detaches from the shrinking grain and subsequently attaches to the growing grain. The velocity of a grain boundary is the displacement per unit time from the difference of thermally activated diffusional jumps from the shrinking to the growing grain, and vice versa.

$$V = b\upsilon_0 c_{vg}\left\{\exp\left(-\frac{G_m}{kT}\right) - \exp\left(-\frac{G_m + pb^3}{kT}\right)\right\} \tag{4.18}$$

Here υ_0 is the atomic vibration frequency, G_m the free energy for a diffusional jump through the grain boundary, and C_{vg} the vacancy concentration in the grain boundary since, as in self-diffusion, only a jump to an empty site in the grain boundary is possible. Because of small driving forces of recrystallization, at typical recrystallization temperature ($T>0.4T_m$) $pb^3<<kT$. Hence the velocity can be written as

$$V \cong b\upsilon_0 c_{vg}\exp\left(-\frac{G_m}{kT}\right)\left\{\frac{pb^3}{kT}\right\}$$
$$= b^4\upsilon_0 c_{vg}\frac{1}{kT}\exp\left(-\frac{G_m}{kT}\right).p = m.p \tag{4.19}$$

The relation between mobility, m, and diffusion coefficient, D_m, for jumps through the grain boundary with the activation energy, Q_m, is given with the Nernst-Einstein relation as

$$m = \frac{b^2 D_m}{kT} = \frac{b^2 D_0}{kT}\exp\left(-\frac{Q_m}{kT}\right) = m_0\exp\left(-\frac{Q_m}{kT}\right) \tag{4.20}$$

The mobility of a grain boundary also depends on the orientation relationship between the adjacent grains. Low angle grain boundaries have low mobilities, whereas grain boundaries with an orientation relationship 40°<111> show high mobility in aluminium. The experimentally observed grain boundary mobility values were used for all calculations [105].

A prefactor in the mobility term, calculated on the basis of disorientation relationships between nuclei and deformed grain orientations, was incorporated in the kinetic equation. Three different types of mobility were considered. Grain boundaries with special orientation relationship like 40°<111> were considered to have highest mobility. The low angle boundaries were assumed to be the slowest moving. The ratio of special to the average mobility factor was altered to identify its effect in recrystallization front movement.

Growth model from cellular operator evolution law:

Recrystallized Grain Structure

Grains of Time Step t [N]   **Grains of Time Step t +1[N]**

AcI[N]   PI[N]   FIPN[N]   FI[N]   SCI[N]   In[N- gc]   SR[N]

N: Number of new grains originated.
AcI: Actual index of new grains.
PI: Index of partially recrystallized grains.
FIPN: Index of fully recrystallized grains with partially recrystallized neighbors.
FI: Index of fully recrystallized grains.
SCI: Index of surface cells.
In: Orientation index.
SR: Sum of cells recrystallized.

Fig. 28 Data structure for recrystallized grains for two subsequent time steps.

Cell Status Not RX

Starting of RX

Cell Status Partial RX

100% RX

Cell Status Full RX
in Next Step

Neighbour Not RX

All Neighbours RX

Cell Status Full RX

Full RX with Not RX Neighbours
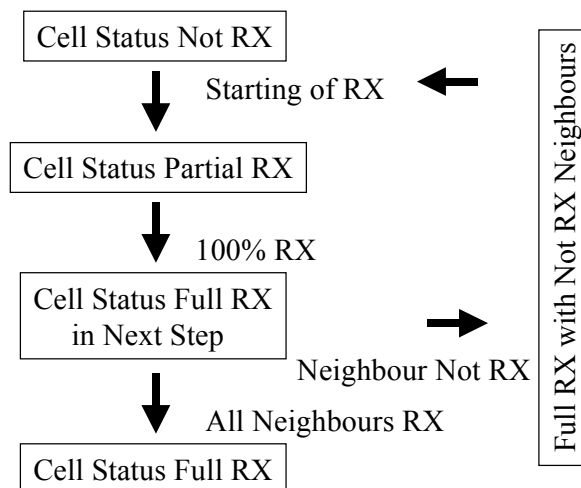
Fig. 29 The recrystallzed front transition in cells from the starting to the finishing of recrystallization (RX).

Conversion of time step (t_{step}) to real time (second):

The basic consideration behind the time step to real time conversion is that the recrystallization front crosses one cell in one time step when the velocity, defined by

the mobility and driving force parameters, is the maximum.

$$1\,t_{step} = \frac{cellsize(\mu)}{v_{max\,imum}\left(\dfrac{\mu}{sec\,ond}\right)}$$ (4.21)

The final form of the growth equation: Any velocity of recrystallization front is scaled in terms of the maximum velocity of recrystallization. The normalised velocity can be expressed as

$$v_{n\_timestep} = \frac{v_{timestep}}{v_{max\,imum}} = \left(\frac{R_f E_{cell\_timestep}}{E_{max\,imum}} - \frac{Z_{timestep}}{E_{max\,imum}}\right)\left(\frac{O_f m_{timestep}}{m_{max\,imum}}\right)$$ (4.22)

where $v_{timestep}$ is the velocity at a particular time step and $v_{maximum}$ is the maximum possible velocity. The recovery factor is expressed as a ratio of dislocation density at a particular time step to the initial mean dislocation density.

$$R_f = \left(\frac{\rho_{timestep\_mean}}{\rho_{initial\_mean}}\right)$$ (4.23)

The time dependent deformation energy encountered by the growing nuclei is written as

$$E_{cell\_timestep} = 0.5Gb^2\rho_{cell\_timestep}$$ (4.24)

while the maximum deformation energy available is given by

$$E_{max\,imum} = 0.5Gb^2\rho_{max\,imum}$$ (4.25)

The time dependent loss in the recrystallization driving pressure because of the Zener drag ($Z_{timestep}$) depends on the particle/precipitate radius ($R_{p\_timestep}$), number ($N_{p\_timestep}$) and grainboundary energy (γ_{gb}).

$$Z_{timestep} = 6.28N_{p\_timestep}R_{p\_timestep}^{2}\gamma_{gb}$$ (4.26)

The grain boundary mobility at a particular time step

$$m_{timestep} = m_0 \exp\left(-\frac{Q_m}{kT_{timestep}}\right)$$ (4.27)

is normalized to the maximum mobility of the grain boundary

$$m_{max\,imum} = m_0 \exp\left(-\frac{Q_m}{kT_{max\,imum}}\right)$$ (4.28)

Where m_0 is the pre-exponential factor, Q_m is the activation energy for grain boundary mobility, k is the Boltzmann constant and T is the temperature. The mobility becomes orientation dependent because of the orientation dependent factor O_f.

The modification of the mobility term because of solutes drag: The interaction of solute with the recrystallization front is included in the model through different physical parameters like diffusivity of the solute (D_{solute}), interaction energy ($E_{exchange}$) parameter, concentration of solute (C_{solute}) near grain boundary etc. [106]. The lowering of energy because of solute entrapment along the grain boundary is given by

$$E_{exchange} = \frac{4}{3}\pi\left(\frac{1+v}{1-v}\right)Gr_{material}{}^3\left|\frac{r_{material} - r_{solute}}{r_{material}}\right| \tag{4.29}$$

where G is the shear modulus, v is the Poisson ratio, $r_{material}$ is the radius of the matrix and r_{solute} is the radius of the solute.

The activation energy (E) for grain boundary mobility in presence of solutes includes the previously mentioned interaction energy ($E_{exchange}$) and the activation energy for solute diffusion (Q_D). The time dependent mobility of grain boundary under this conditions is written as

$$m_{timestep\_solute} = \left(\frac{N_a D_{solute}}{kT_{timestep} C_{solute\_timestep}}\right)\exp\left(-\frac{E_{exchange} + Q_D}{kT_{timestep}}\right) \tag{4.30}$$

where the pre-exponential term takes the number of atoms available ($N_a = \frac{4\sqrt{2}}{a_{material}^2}$),

the time dependent solute concentration ($C_{solute\_timestep}$) and diffusivity of solute (D_{solute}) in account.

Conversion to cell fraction: $E_{counter}$ denotes all volume elements or subcells of a complete cell, which is crossed by the recrystallization front in one time step with its maximum velocity. The recrystallization front velocity at any time step ($v_{n\_timestep}$) except the maximum velocity, crosses only a fraction of a cell, which is represented by the number of subcells ($V_{cell\_timestep}$)

$$V_{cell\_timestep} = E_{counter} d_{v\_cell} v_{n\_timestep} \tag{4.31}$$

The direction vector (d_{v_cell}) determines the counter size depending upon the direction of recrystallized front transition, shown in Fig 15 b).

Calculation of fraction recrystallized ($X_{cell\_timestep}$) from cell fraction: The summed up value of $V_{cell\_timestep}$ for all growing nuclei (N) in all directions (n) divided by all possible volume elements in the operator lattice describes the recrystallized fraction. The N_{RC} stands for real number of cells.

$$X_{cell\_timestep} = \frac{\sum\limits_{1}^{N} \sum\limits_{1}^{n} V_{cell\_timestep}}{N_{RC}\, E_{counter}} \tag{4.32}$$

4.8 Recrystallization texture and grain distribution:
The total number of subcells or cells recrystallized is calculated for every time step for each growing grain. The total recrystallized amount for a particular microstructure or nuclei orientation is obtained from a combination of members, which transforms the grain number to grain orientation and that to total amount of recrystallized subcells. The resulting recrystallized amount per nuclei (microstructure and external) orientation (SR) is converted to volume fraction (VF) (Fig. 30a).

$$VF = \frac{SR}{N_{RC}E_{counter}} \tag{4.33}$$

However, the recrystallization texture can also be derived from cell wise grain orientation checking along all three directions. This model consists of both these types of recrystallization texture determination.

A similar approach of grain orientation checking is applied for grain distribution. The orientation monitoring along all three directions are performed with a predetermined steps. Steps are expressed in number of cells. The initial orientation of the grain is noted. After transition to a new orientation the old orientation is substituted by the new orientation and the distance covered in between these two orientations is calculated. This procedure is continued till the end of the dimension of the lattice along each direction.
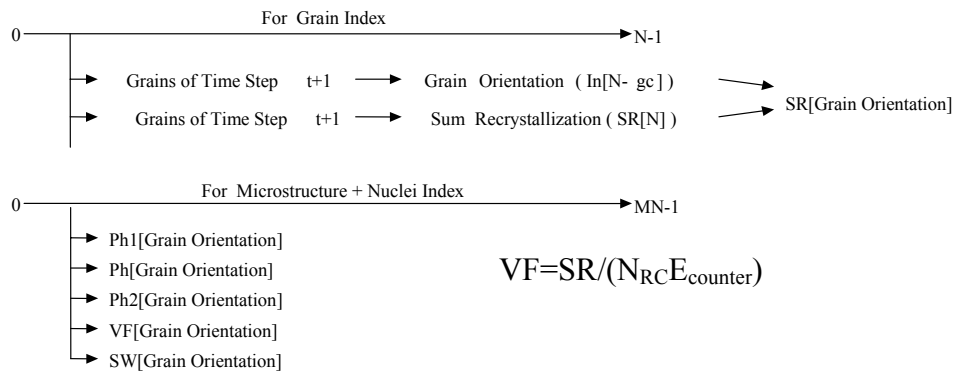
Fig. 30 a) Calculation of volume fraction of each recrystallized orientation from the total number of subcells recrystallized of that orientation (SR) and the total number of subcells of the three dimensional lattice.
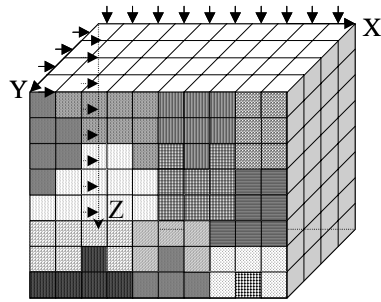
Fig. 30 b) Recrystallized grain distribution from cell wise grain orientation variation along all three directions of the fully-recrystallized lattice. The orientation variation on XZ face of the lattice is shown here.

5. Results.

5.1 Recrystallization exponent in site saturation nucleation and isotropic growth condition:
In order to check the model behaviour the recrystallization kinetics simulated with an isotropic growth and nucleation site saturation condition. All grain boundaries were given similar mobility and all cells were given an identical driving force. Since a similar condition was created as JMAK model, the recrystallization exponent obtained from this simulation should reflect the Avrami exponent. The calculated recrystallization exponent value obtained from this model is nearly equal to the Avrami exponent value for site saturation nucleation condition (Fig. 31).
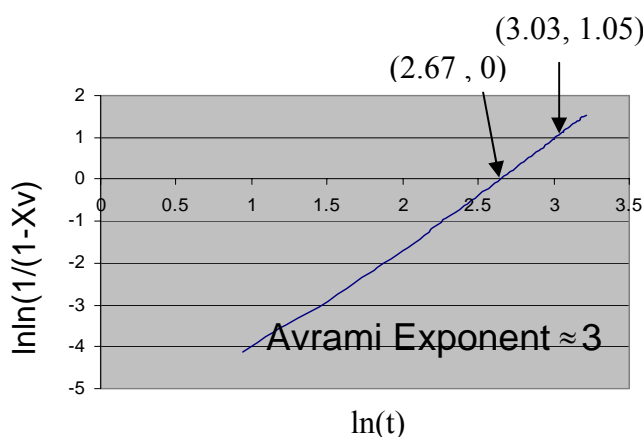
Fig. 31 The recrystallization exponent in site saturation nucleation and isotropic growth condition.

5.2 The effect of grain boundary nuclei distribution:
The distribution of nuclei in deformed structure can have a strong effect on the recrystallization texture, microstructure grain distribution. The deformed grain orientations (from GIA model) and their dislocation densities (from 3IVM model) create a heterogeneous initial microstructure in cellular grid and make different types of nuclei distributions possible. The number of nuclei per grain in distribution 1 is defined by the ratio of deformation energy of a grain to the mean deformation energy. The distribution 2 represents the ratio of deformation energy of a grain to the maximum deformation energy and the distribution 3 deals with the nuclei distribution reverse of that of type two. A clear difference is found in textures and in microstructure obtained from all three nuclei distributions (Fig. 32) with constant nucleation kinetics. The nuclei distribution 2

generates maximum intensity in texture, which is basically a weak rolling texture. The lowest intensity of texture is associated with the nuclei distribution 3 texture but it shows the strengthening of near cube texture. The nuclei distribution also changes the grain distribution. The grain distributions from nuclei distribution 1 and 3 are similar to normal distribution while the grain distribution 2 exhibits a log normal distribution.
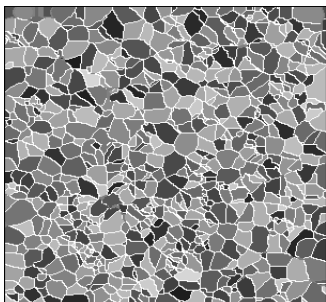
Simulated Recrystallization microstructure from nuclei distribution 1.
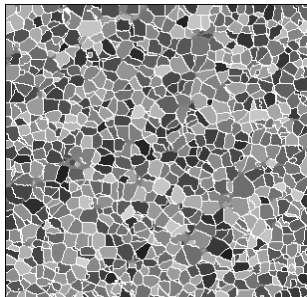
Simulated Recrystallization microstructure from nuclei distribution 2.
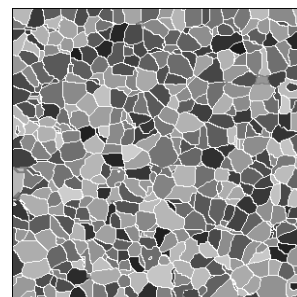
Simulated Recrystallization microstructure from nuclei distribution 3.
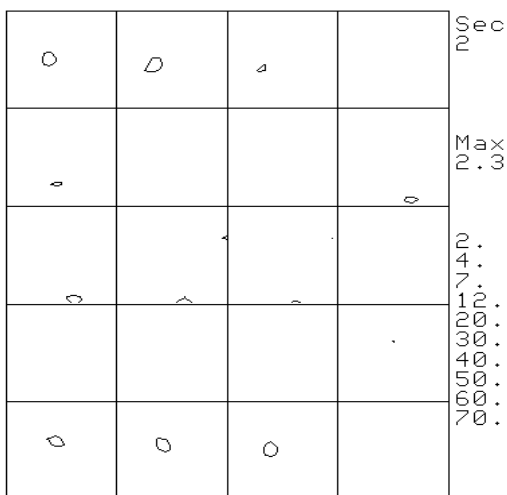
Simulated Recrystallization texture from nuclei distribution 1.
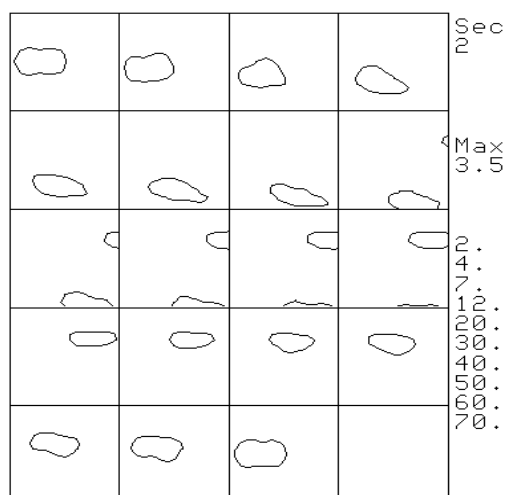
Simulated Recrystallization texture from nuclei distribution 2.
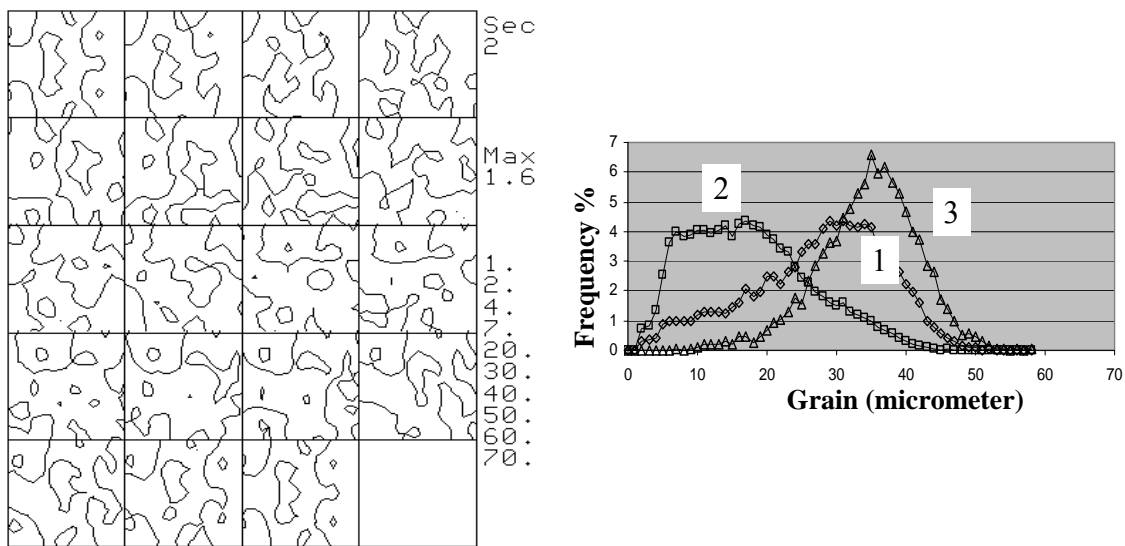
Simulated Recrystallization texture from nuclei
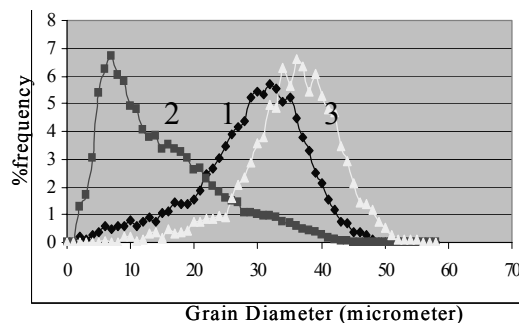distribution 3.

Fig. 32 Effect of different nuclei distributions on recrystallization microstructure, texture and grain distribution for constant nucleation kinetics.

The earlier results present the effect of nuclei distribution under constant nucleation rate. A change in nucleation kinetics from a constant to a decreasing one improves the recrystallization texture intensity and makes the cube, {100}<100> component stronger (Fig. 33). The nature of grain distributions does not change but the peak sharpening takes place. The texture intensities are found to decrease with the increasing type nucleation kinetics (Fig. 34). A detailed analysis of the induced grain morphology because of the decreasing nucleation kinetics requires a comparison study of recrystallized microstructures obtained from different nucleation kinetics.

5.3   Influence of time dependent nucleation: In time dependent nucleation module different types of nucleation time dependencies were applied (Fig. 35). Two types of increasing nucleation kinetics, two types of decreasing nucleation kinetics and a constant nucleation kinetics provide diverse results, which are consistent in their nature. A higher fraction of smaller grains below size (11 Cells -12 Cells) is associated with decreasing nucleation rate (Fig. 36). Increase in nucleation kinetics gives more fraction/frequency of larger grains. The fraction of larger grains increases and the fluctuation in the grain distribution curve also reduces with the increase in nucleation kinetics. The microstructure grain distribution obtained from the very slow nucleation

kinetics of increasing type two closely reflects that one obtained in many annealing operations. The size difference is created by the slowness of nucleation kinetics, which may not be identical with the real nucleation kinetics, which is not so slow in some cases, according to observations.
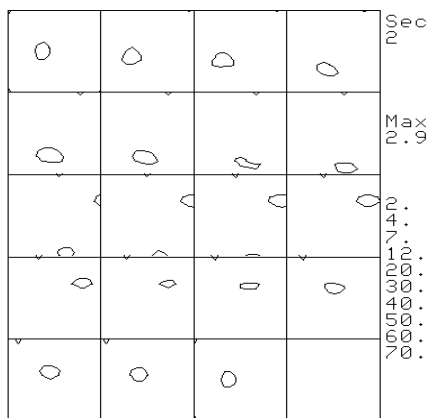
Simulated Recrystallization texture from nuclei distribution 1.
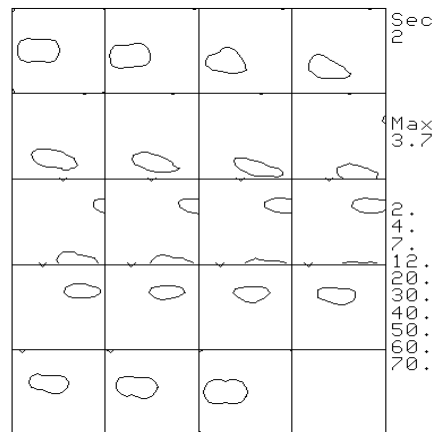
Simulated Recrystallization texture from nuclei distribution 2.
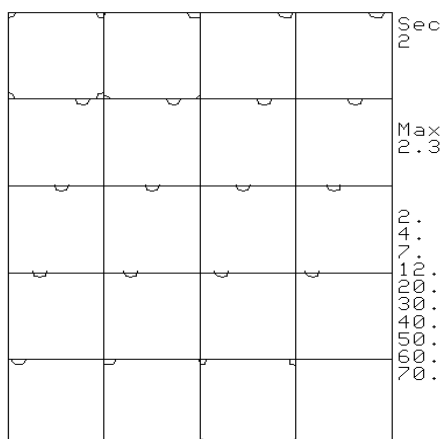
Simulated Recrystallization texture from nuclei distribution 3.

Fig. 33 Effect of different nuclei distributions on recrystallization texture and grain distribution for decreasing nucleation kinetics.

Simulated recrystallization texture from nuclei distribution 1.

Simulated recrystallization texture from nuclei distribution 2.

Simulated recrystallization texture from nuclei distribution 3.
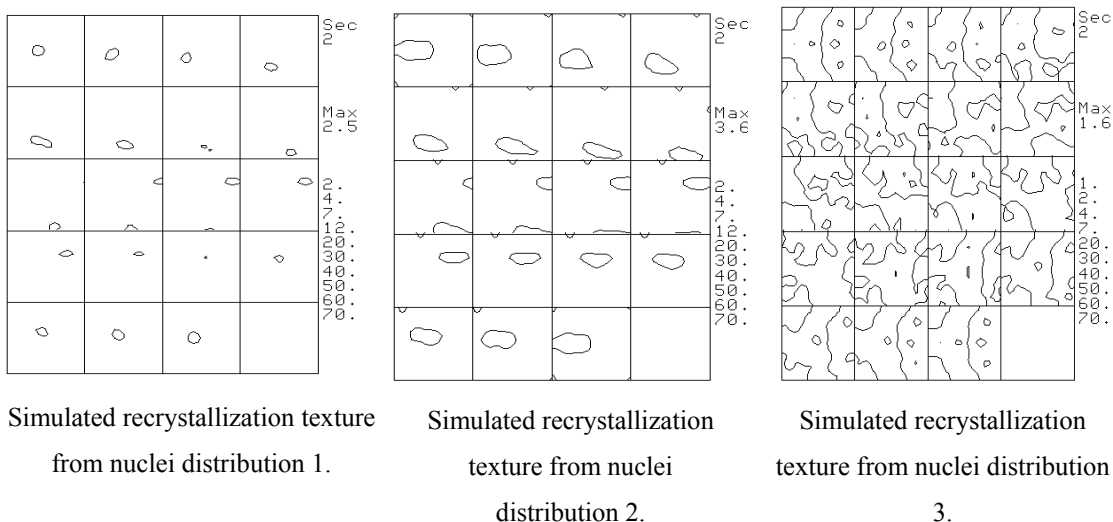
Fig. 34 The influence of nuclei distribution on recrystallization texture for increasing nucleation kinetics.
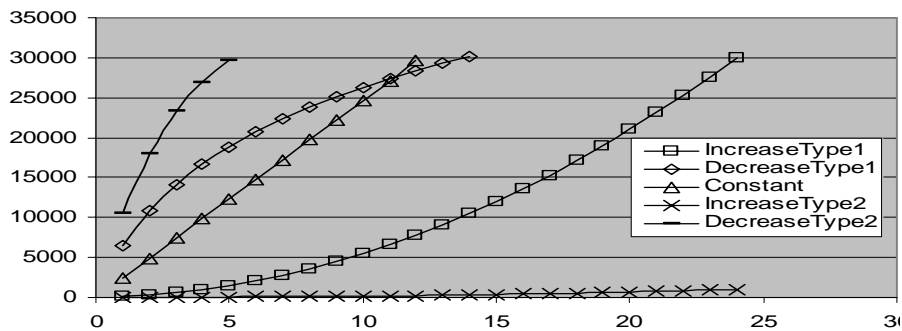
Fig. 35 Nucleation kinetics for time dependent nucleation.
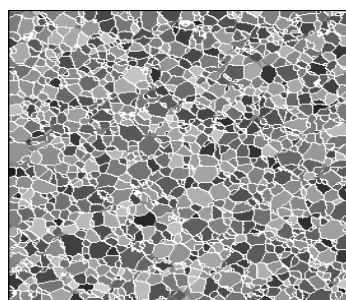
Simulated recrystallization microstructure for nucleation kinetics, Increase Type 1.
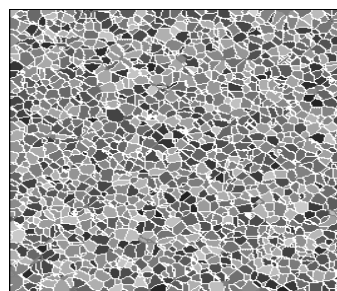
Simulated recrystallization microstructure for nucleation kinetics, DecreaseType 1.
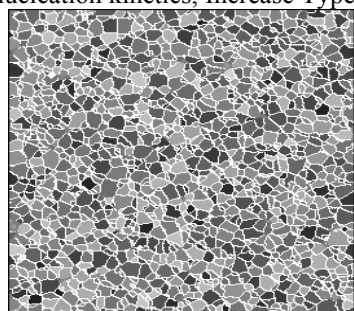
Simulated recrystallization microstructure for
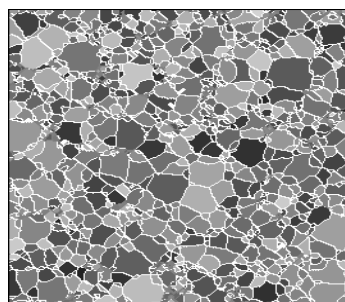
Simulated recrystallization microstructure for nucleation kinetics, IncreaseType 2.

nucleation kinetics, Constant.
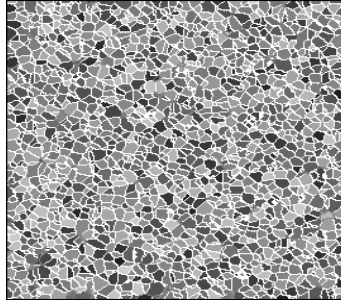
Simulated recrystallization microstructure for
nucleation kinetics, DecreaseType 2.
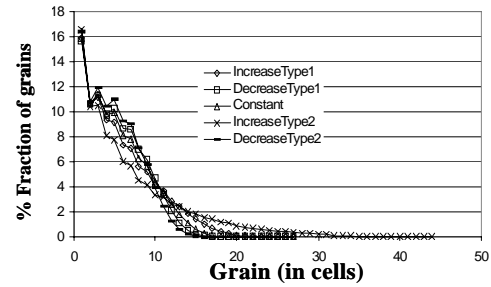
Grain distribution (Grains are in number of cells)

Fig. 36 Recrystallized microstructure and grain distribution from time dependent nucleation.

5.4   The effect of nuclei density:
The effect of nuclei density was studied with different nuclei densities with a same initial input data. The orientations of nuclei were randomly selected from the deformation texture orientations and the nuclei were randomly distributed inside grid. The initial deformation texture orientations and dislocation densities were kept unaltered for all studies.

The initial 2000 deformation texture orientations were distributed among 6000 grains in a 290x310x298 grid with cell size 2 micrometer. Simulations were conducted with different nuclei densities.
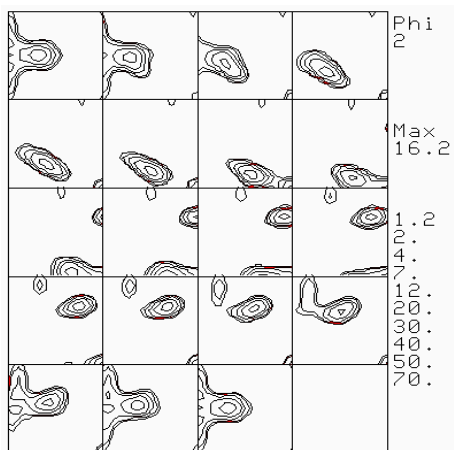
Starting Texture.
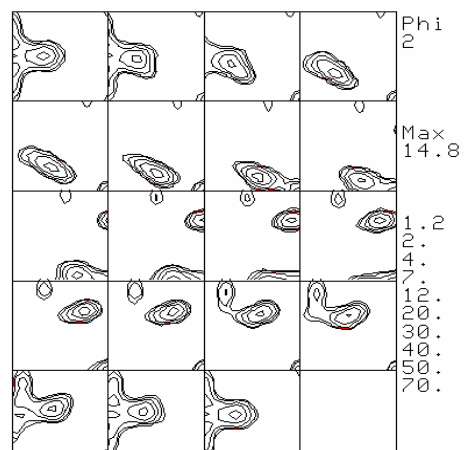
Simulated recrystallization texture with 10,000

Nuclei.

Simulated recrystallization texture with 42,000 Nuclei.

Simulated recrystallization texture with 68,000 Nuclei.
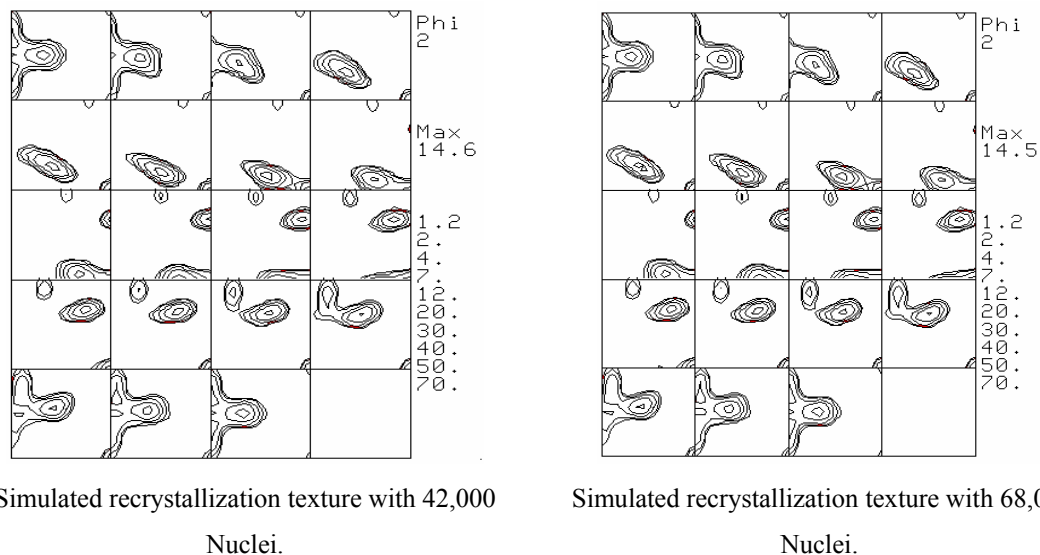
Fig. 37 Simulated recrystallization textures obtained from different nuclei densities.
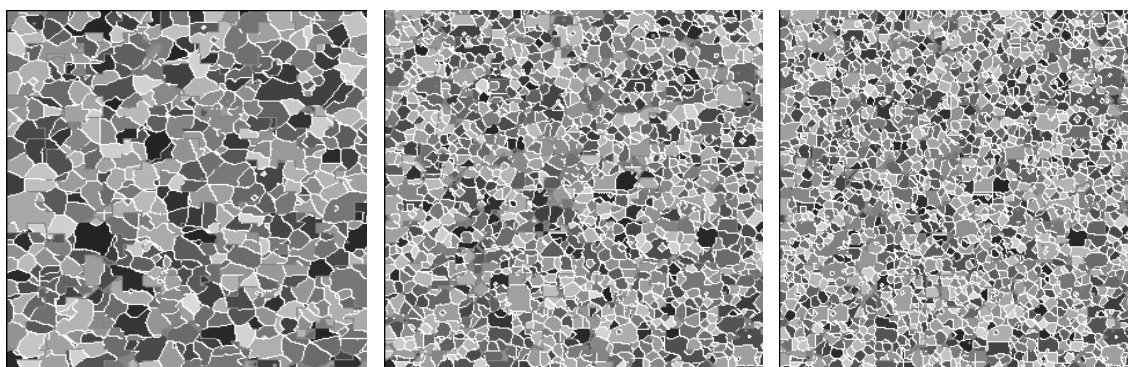
Fig. 38 The simulated microstructure obtained from different nuclei densities (left to right 10000, 42000 and 68000).

The recrystallization textures obtained from all calculations are a randomized deformation texture (Fig. 37). The intensity of rolling textures decreases slightly after recrystallization. An increase in the nuclei density decreases the recrystallization texture intensity. A very fast recrystallization kinetics at 760°K enables recrystallization to be finished within a very short period of time The nuclei density has strong effect on kinetics and the recrystallization exponent is found to vary from 2.16 to 1.92 for two extreme nuclei densities (Fig. 39). The grain distributions obtained from different nuclei densities are lognormal in nature with a long tail of larger grains with low frequency (Fig. 40). The increase in number of nuclei makes the distribution bimodal with a number of small peaks near the maximum of frequency. The profile becomes flat with the decrease in number of nuclei. The frequency preference of a particular size range, which increases with the number of nuclei, is observed.
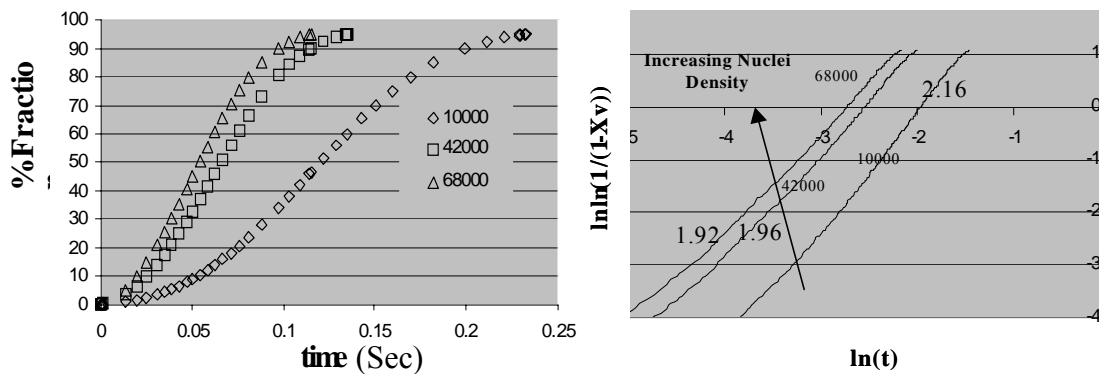
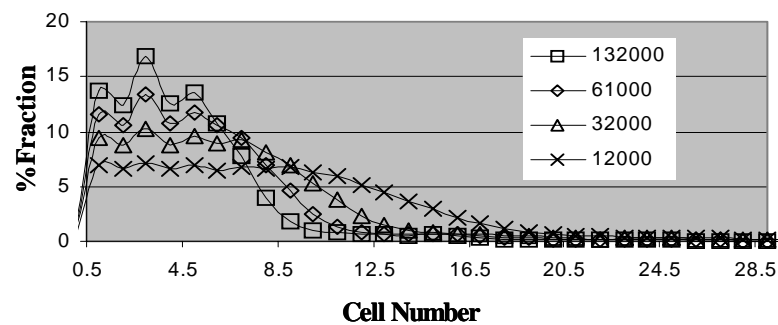Fig. 39 The calculated recrystallization kinetics obtained from different nuclei densities.

Fig. 40 The calculated grain distributions with number of nuclei. Grains are expressed in number of cells.

5.5 The effect of orientation discrete and average driving force: The dislocation density per orientation of the initial microstructure as an input for recrystallization simulation helps in finding the influence of orientation discrete and average dislocation density on the recrystallization kinetics. The maximum, minimum and the average driving pressures for recrystallization were calculated from the maximum, minimum and average dislocation dislocation density of the microstructure orientations. The different energy represents the driving pressure obtained from the orientation discrete dislocation density. Though the kinetics is affected by the variation in dislocation densities the grain distribution remains unchanged (Fig. 41). The average dislocation density calculated from initial orientation list is found to have the same effect as oriented discrete dislocation densities in recrystallization kinetics (Fig. 41c).
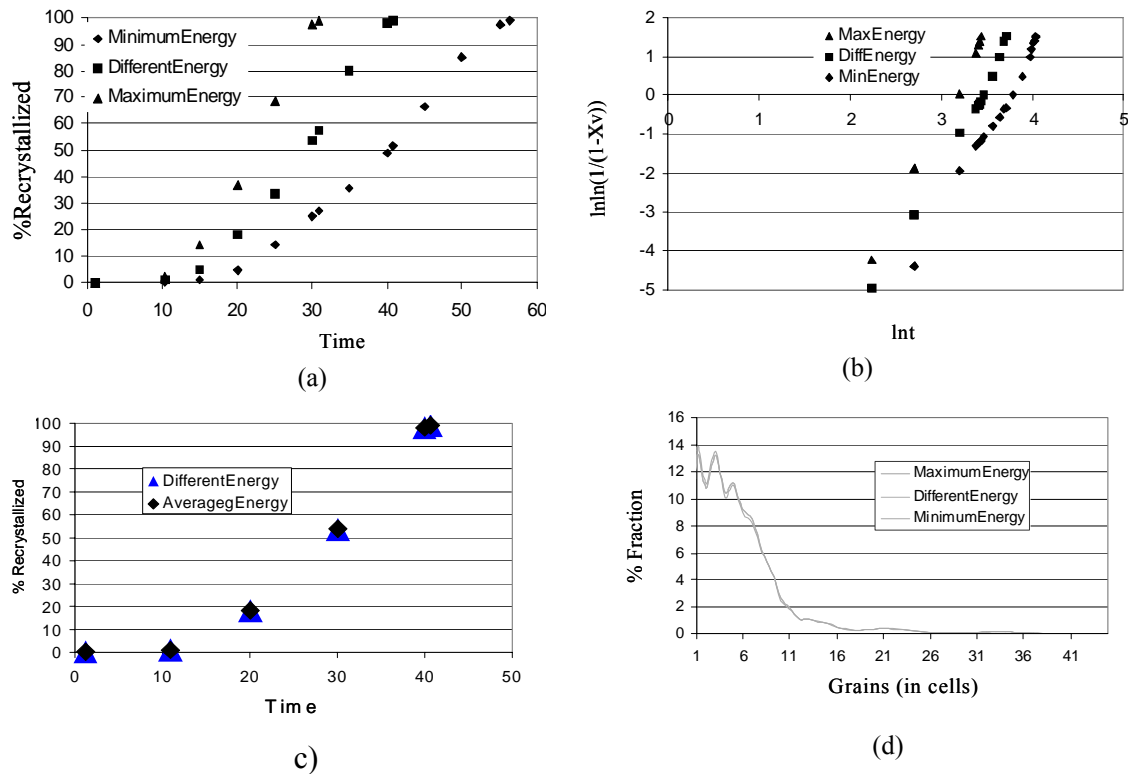
Fig. 41 (a) The calculated recrystallization kinetics with maximum, minimum and different energies. (b) Recrystallization exponent for maximum, minimum and different energies from simulation. (c) The calculated recrystallization kinetics with different and average energy. (d) Grain distribution for maximum, minimum and different energies from simulation.

5.6 Initial grain dimension on texture, microstructure and kinetics:

There are a number of aspects involving the deformed orientations may contribute different recrystallization behaviours in a material. These aspects are independent of material chemistry but evolve because of deformation orientation-disorientation and strain energy distribution in deformed orientations. Each initial grain has a particular orientation and an average dislocation density in this model. Experimental evidences of grain dependent deformation energy and accumulated long and short range disorientation were obtained from the substructure study of aluminium with similarly oriented grains with different diameter (200 micrometer and 400 micrometer) (Fig. 42). The substructure and disorientation development in smaller grain (200 micrometer) material is more pronounced than those of larger grain (400 micrometer) material. The effect of initial grain dimension dependent deformation energy and disorientation distribution goes in the recrystallization simulations through the combination of GIA and 3IVM model.

(a)
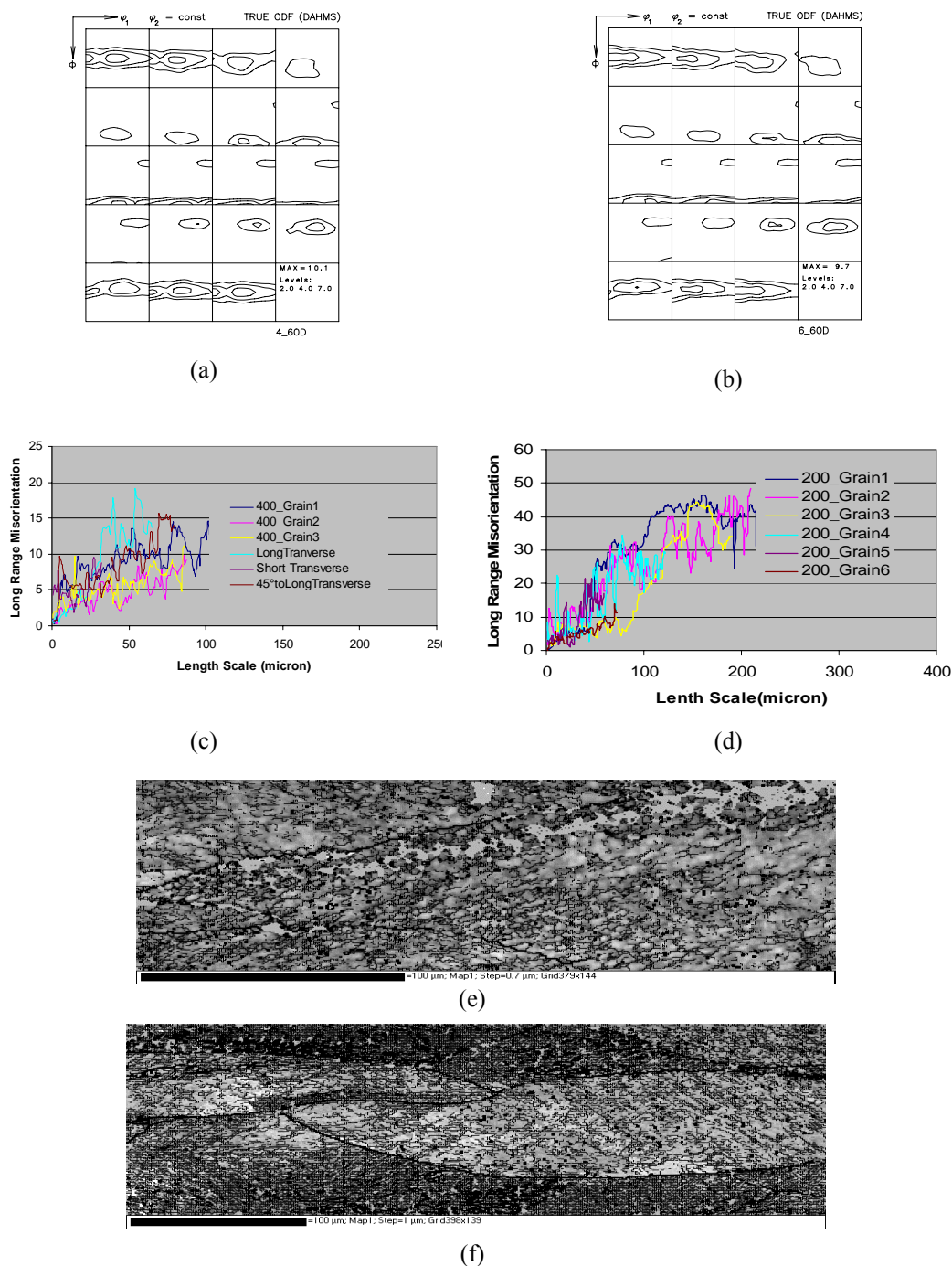

(b)

(c)

(d)

(e)

(f)

Fig. 42(a) Texture of aluminium with around 400-micrometer grain diameter, type 1. (b) Texture of aluminium with around 200-micrometer grain diameter, type2. (c) Long range disorientation for type 1 material. (d) Long range disorientation for type 2 material. (e) 60% cold rolled (true strain 0.8) type 1 material, (f) 60% cold rolled (true strain 0.8) type 2 material. (Courtesy: Prof. I Samajdar, S. Badirujjaman).

The deformed orientations with respective dislocation densities were randomly distributed in form of grain aggregates according to the GIA 8 grain cluster concept and necessary precautions were taken to restore the deformation texture. Recrystallization simulations were performed varying the initial grain dimension and keeping the nuclei

density constant for a particular distribution of deformed orientations to know the effect of initial grain dimension, the location of nucleation and the orientation of nucleation. The simulation parameters involving the nuclei locations and orientations are given below.

(i) Nuclei locations were random and orientations were randomly selected.

(ii) Nuclei locations were along grain boundary and orientations were randomly selected.

(iii) Nuclei locations were along grain boundary and orientations of original grains were selected.

Since texture orientations are randomly selected in simulation (i) and in simulation (ii), the difference in results should be created by the location of nuclei in terms of their surroundings.

The results from simulation (ii) and from simulation (iii) should clarify the effect of nuclei orientations where locations of nuclei in both simulations are along grainboundary.

In aluminium alloys there are possibility of nuclei orientation change depending on pre-recrystallization deformation. A very high degree pre-recrystallization deformation may randomise nuclei orientations otherwise the grain orientation should remain preserved in nucleation. Moreover, in a 2 phase aluminium alloy where majority of nuclei produced from precipitates the number of nuclei or new grains should not vary to a large extent with the pre-recrystallization deformation.

The following experimental work on aluminium alloys was performed to confirm the earlier mentioned possibilities. The alloy was recrystallized in salt bath furnace after pre-recrystallization 60%, 80% and 90% cold rolling. Necessary precautions were taken to avoid grain growth after recrystallization. The annealing operation were carried out in three different temperature levels i.e. 300°C, 350°C and 400°C. The microstructrure of annealed samples revealed that samples were fully recrystallized after 3.5 minutes of annealing at 400°C and microstrucrtures gain stability after that because of pinning of grain boundaries by precipitates. The results of 400°C annealed material show insignificant variation in total number of grains, maximum, minimum and in average grain dimension for all samples with different levels of pre-recrystallization deformations (Fig. 43). However, differences in recrystallization grain distributions and in recrystallization textures are very much clear for all three samples with different pre-recrystallization deformations. These findings are in favour of the fact that the degree of

pre-recrystallization cold rolling can change nuclei and recrystallization textures but it has less effect on the total number of recrystallization grains for an alloy which contains a large number of precipitates capable of stimulating recrystallization nucleation (Fig. 43 - Fig. 45).

A similar condition was tried to simulate in simulation (ii) and in simulation (iii) where the nuclei orientations were varied keeping nuclei locations and number constant.
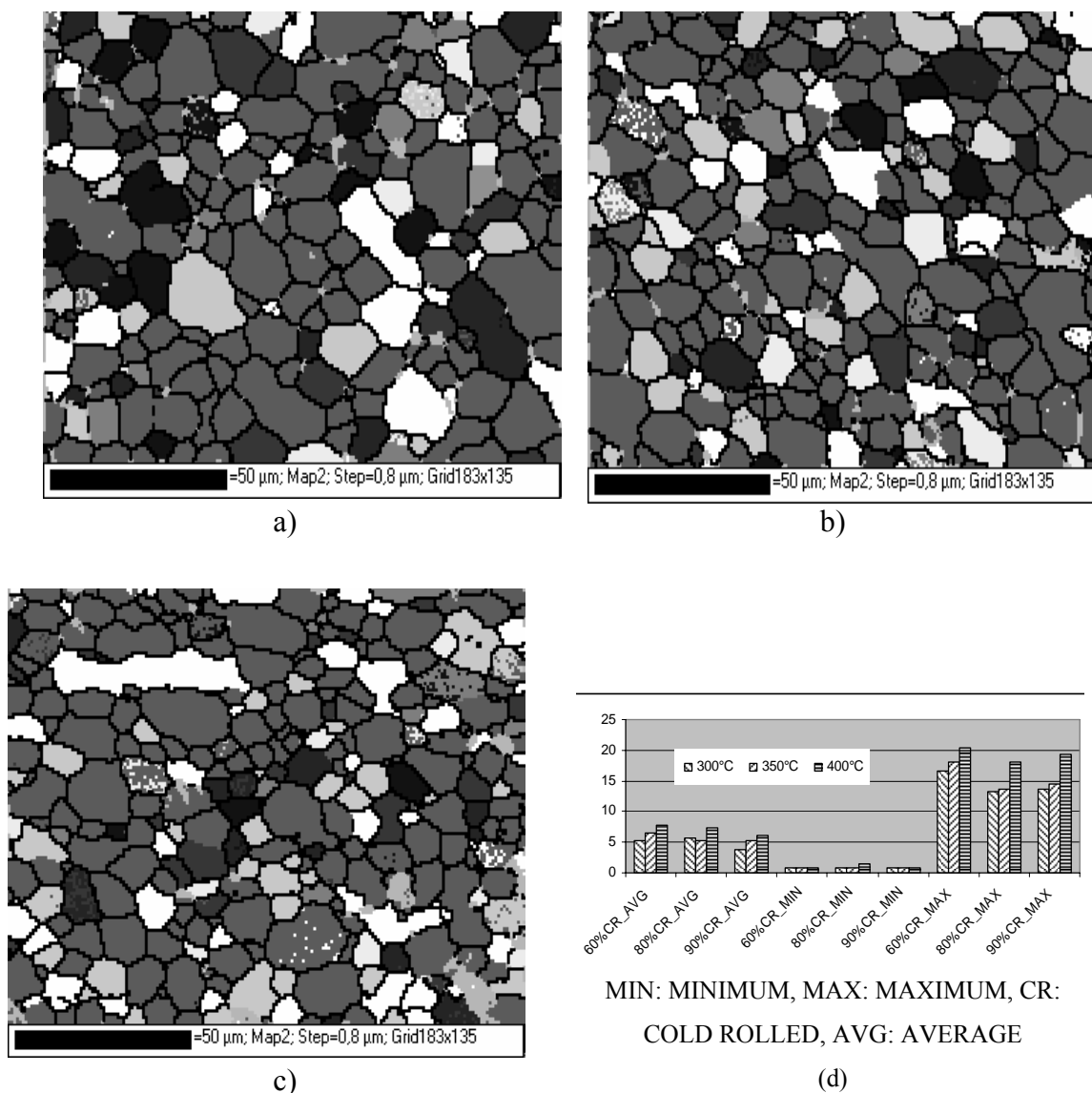

a)

b)

c)

MIN: MINIMUM, MAX: MAXIMUM, CR: COLD ROLLED, AVG: AVERAGE

(d)

Fig. 43 a) 60% cold rolled (true strain 0.8) and annealed (Salt bath 400°C), b) 80% cold rolled (true strain 1.6) and annealed (Salt bath 400°C), c) 90% Cold Rolled (true strain 2.4) cold rolled and annealed (Saltbath 400°C), d) Recrystallization grain size with different prior recrystallization cold rolling at different saltbath temperatures.
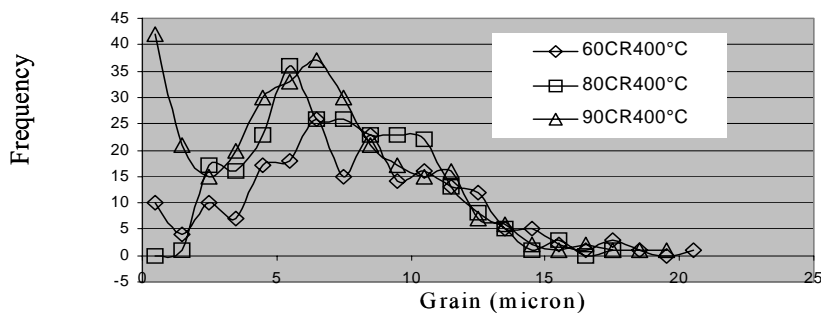
Fig. 44 Grain distribution in recrystallization microstructures obtained from salt bath annealing at 400°C for three differently cold rolled (60%, 80% and 90%) sample prior to the annealing.
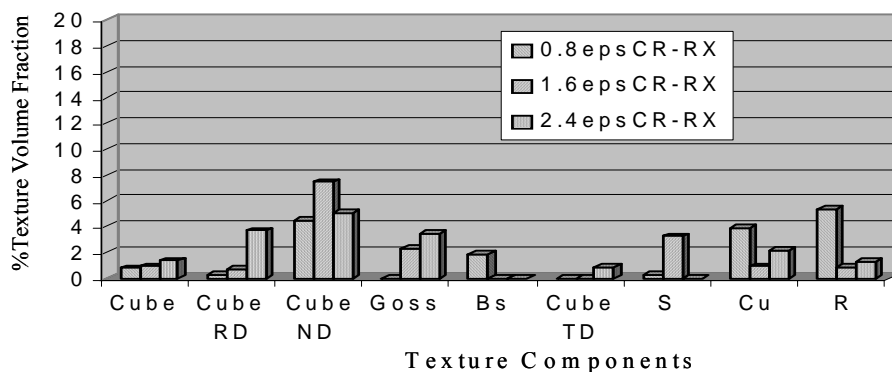

Fig. 45 Variation in volume fraction of different recrystallization texture components with prior recrystallization cold rolling (true strain 0.8, 1.6 and 2.4).

The results listed below obtained from varying the initial grain dimension where both nuclei locations and the nuclei orientations are random. The intensity of rolling texture components are found to reduce after recrystallization with the increase in the initial grain dimension. The increase in frequency of larger recrystallized grains with the increase in initial grain volume creates the textural change. The slight increase in near {100}<100> orientation and a faster recrystallization kinetics are associated with the increase in initial grain volume (Fig. 46). The comparison of recrystallization texture results from simulations (i) and (ii) (Fig. 46 and Fig. 47) shows no major variation which indicates a negligible effect of nuclei locations when the nuclei orientations are randomly selected.
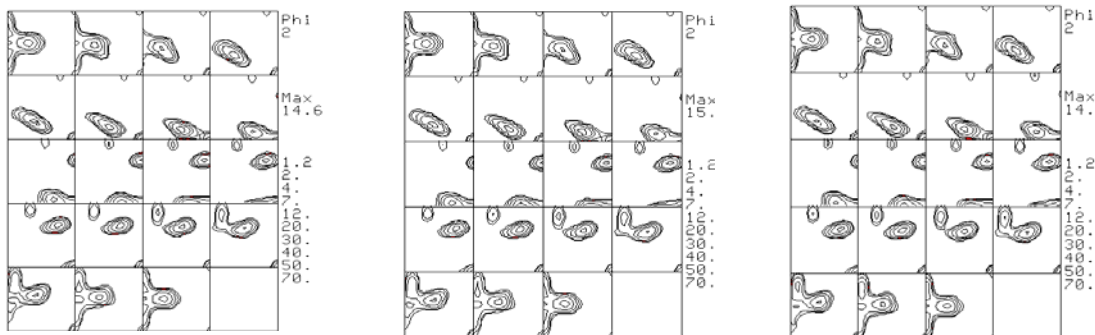
Fig. 46 a) The effect of initial grain dimension (Left to Right: (25-40-60) micron) on simulated textures.
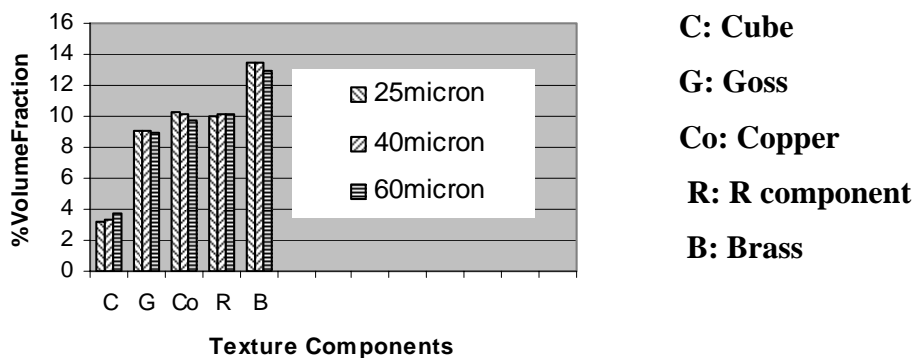

C: Cube

G: Goss

Co: Copper

R: R component

B: Brass

Fig. 46 b) The effect of initial grain dimension on volume fraction of simulated texture components.

Initial grain dimension
25micron

Initial grain dimension
40micron

Initial grain dimension
60micron
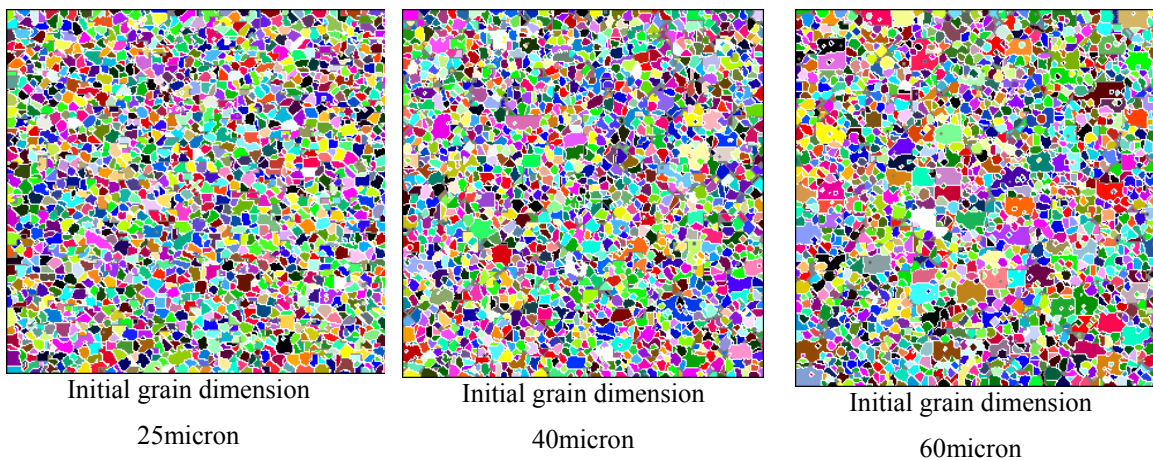
Fig. 46 c) The simulated recrystallized microstructure from initial grains of different dimensions.
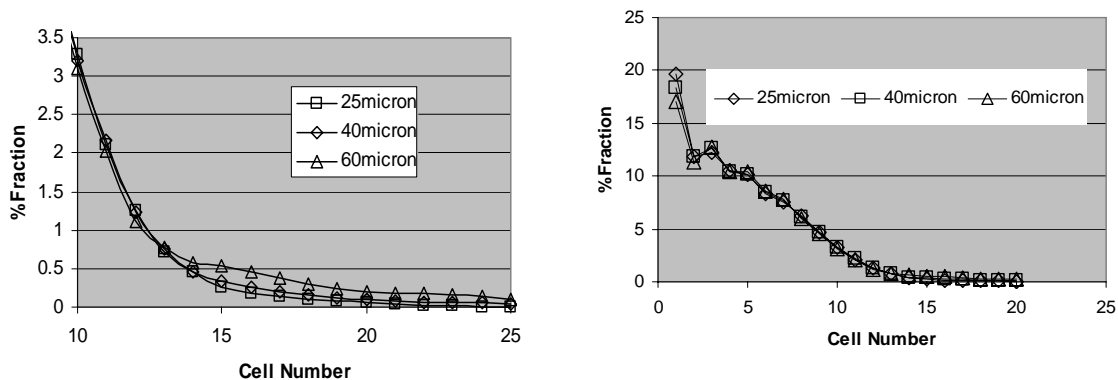
Fig. 46 d) The calculated recrystallized grain distribution with different initial grain dimensions. Grains are in cell numbers.
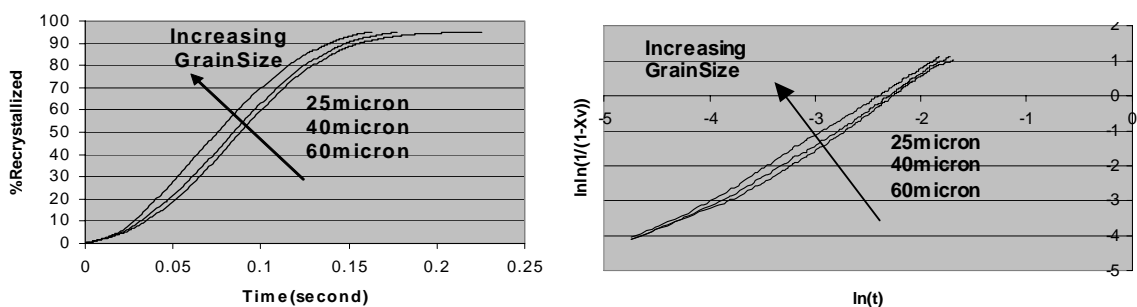

Fig. 46 e) The calculated Recrystallization kinetics and recrystallization exponents with different initial grain dimensions.

The variation in results obtained from two types of grain boundary nucleations in simulation (ii) and in (iii) is note worthy. The random selection of nuclei orientations generates weak texture. The intensity of texture increases sharply when the original grain orientation is selected (Fig. 47 b,d)). The major consequence of grain oriented nuclei selection is the significant reduction in intensity of Cu texture orientation after recrystallization. The previously found effect of initial grain dimension in recrystallization texture and grain distribution from simulation (i) is preserved in those of simulation (ii) and in simulation (iii). The random selection of nuclei orientations improves the recrystallization kinetics, which is faster than the recrystallization kinetics obtained from grain oriented nuclei (Fig. 51).

(a)   (b)

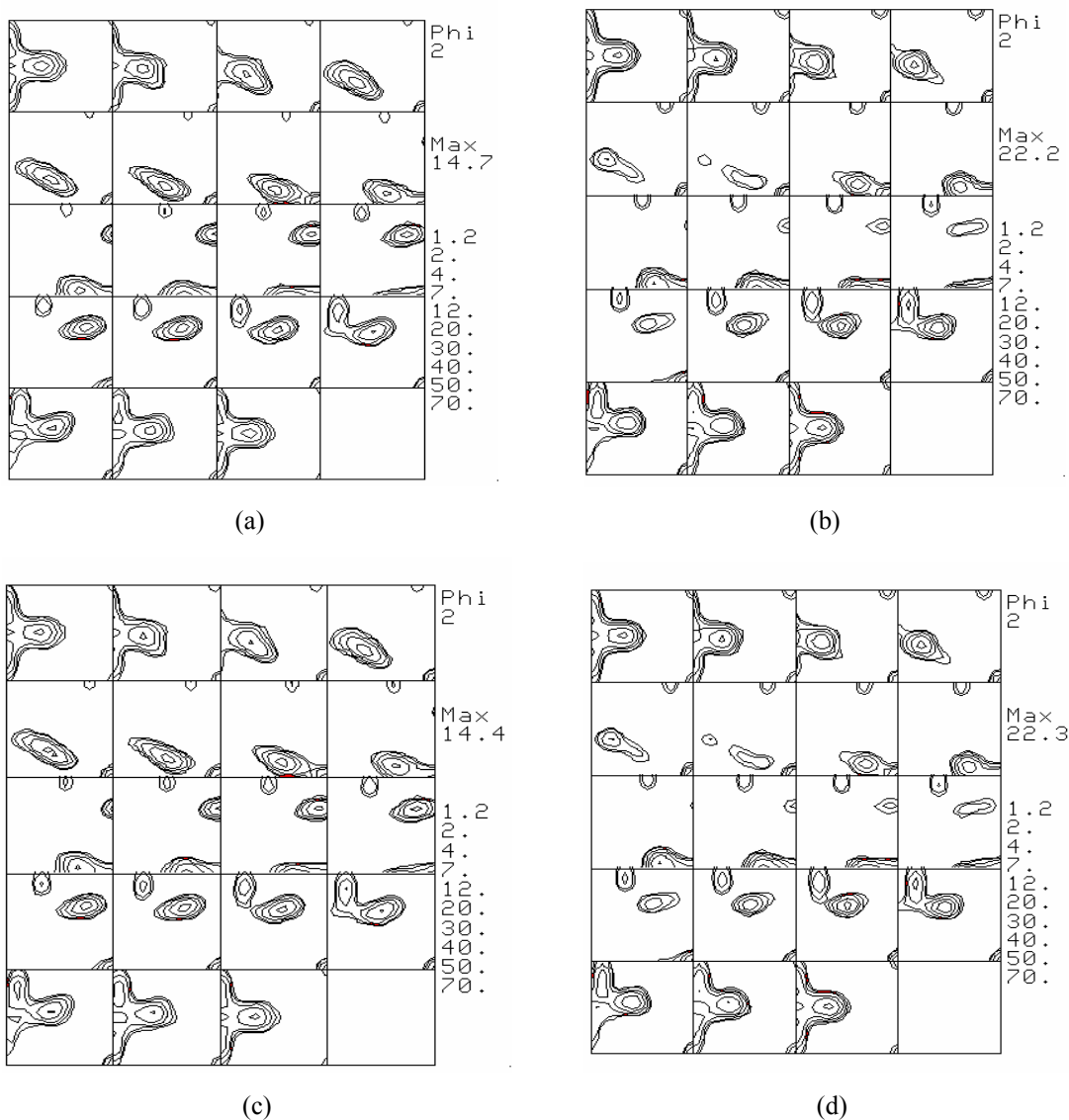(c)   (d)

Fig. 47 The effect of nuclei orientation and grain dimension on the simulated recrystallization texture.
a) 25-micrometer initial grain diameter. Nuclei orientation randomly selected, b) 25-micrometer initial
grain diameter. The grain orientation is selected as nuclei orientation. c) 60-micrometer initial grain
diameter. Nuclei orientation randomly selected. d) 60-micrometer initial grain diameter. The grain
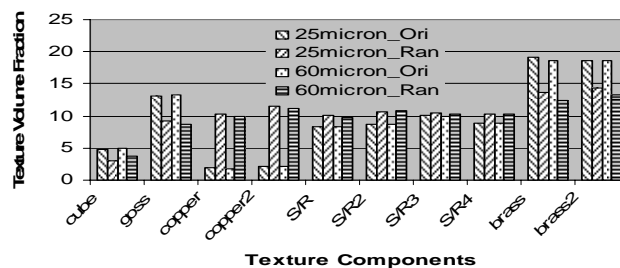orientation is nuclei orientation.

Fig. 48 The simulated volume fractions of texture components from different nuclei orientations (Ori:
initial grain orientation and Ran: random orientation) and different initial grain dimensions (25 micron
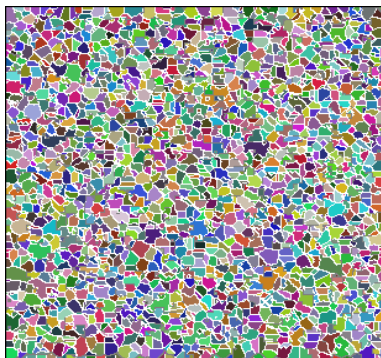and 60 micron).

Fig. 49 a) The effect of nuclei orientation and initial grain size on simulated recrystallization microstructure. 25-micrometer initial grain size. Nuclei orientation randomly selected.
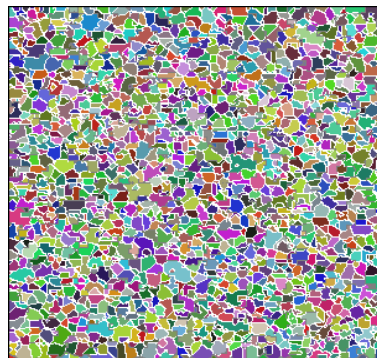

Fig. 49 b) The effect of nuclei orientation and initial grain size on simulated recrystallization microstructure. 25-micrometer initial grain size. Nuclei orientation is grain orientation.

Fig. 50 a) The effect of nuclei orientation and initial grain size on simulated recrystallization microstructure. 60-micrometer initial grain size. Nuclei orientation randomly selected.
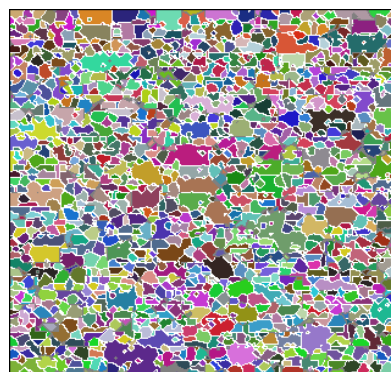

Fig. 50 b) The effect of nuclei orientation and initial grain size on simulated recrystallization microstructure. 60-micrometer initial grain size. Nuclei orientation is grain orientation.
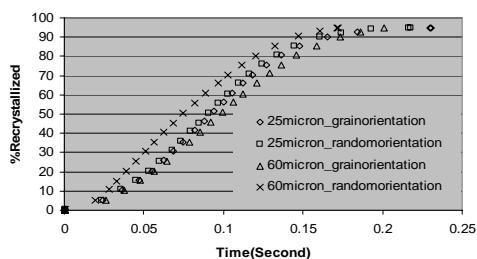

Fig. 51 a) The simulated recrystallization kinetics with variable initial grain diameter and nuclei orientation (random and grain orientation).
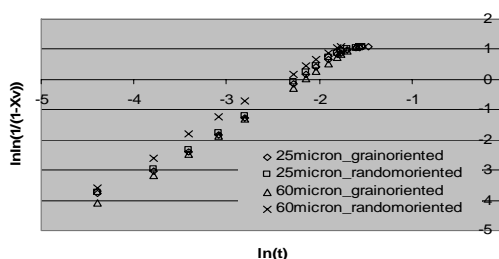

Fig. 51 b) The simulated recrystallization exponents with variable initial grain diameter and nuclei orientation (random and grain orientation).

The effect of change in intensity of oriented growth was studied with the 60 micron size initial grains, constant number of grain oriented nuclei. Though the texture intensity reduces compared to that of Fig. 47 d), The volume fraction near {100}<100> grains

increases with the increase in degree of oriented growth. The frequency of larger grains also increases (Fig. 52).
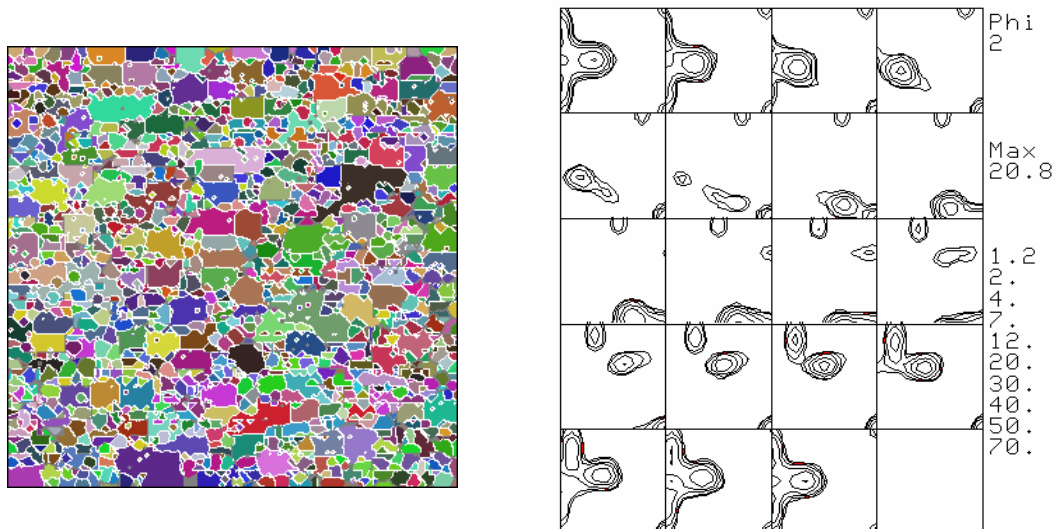

Fig. 52 Simulated recrystallization microstructure and texture with improved oriented growth.

5.7 Variation in subgrain size and particle radius:

In reference to equations shown earlier the contribution of different nuclei sources are displayed with variable subgrain and particle radius. A nominal value of subgrain and particle size of the order of 10^{-6} meter was increased by 1.5, 2.0 and 2.5 times. A strong impact of these variations shows the sensitivity of the model, which can follow minute changes in average dislocation density and precipitation in nucleation stage. Particle and ParticleRadii represent contributions of subgrain and precipitate/particle radius variations in particle-stimulated nucleation (Fig. 53).
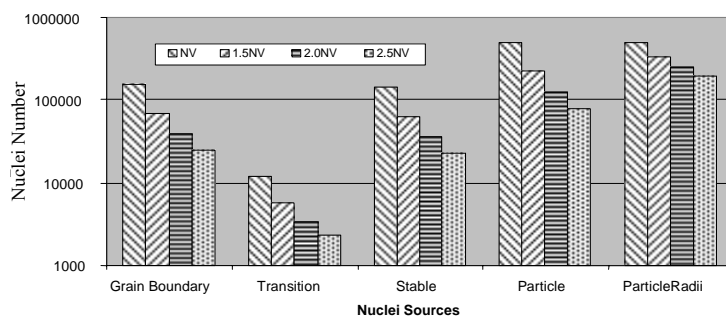

Reference volume around (318x289x289) cubic micrometer. Nuclei density = (Nuclei number / Reference volume).

Fig. 53 Effect of subgrain and particle radius on different categories of nuclei.

5.8 Back driving force on recrystallization kinetics:

The presence of precipitates stimulates the nucleation but hinders the subsequent growth restricting the grain boundary movement. The loss in recrystallization driving pressure depends on the precipitate radius and precipitate number. This drag force per unit area which acts against the recrystallization driving pressure is called Zener drag or back driving pressure. This model includes this effect in the velocity term of the recrystallization front. The employment of scalable subgrid technique can take care of the minute variation in grain boundary motion because of grain boundary impingements by particles or precipitates. A precipitation kinetic model (ClaNG), mentioned earlier was used to obtain the nominal value of precipitation number per cubic meter of an AlMgMn alloy and that was 10, 20, 30, and 100 times increased to obtain different levels of back driving pressures. All simulations were performed with constant nuclei density and a constant precipitate size. The effect of increased precipitate number on nucleation was not considered. About 15% increase in complete recrystallization time is found changing the precipitate number 100 times per cubic meter (from 10^{11} to 10^{13}) (Fig. 54 a), b)).

A clear effect of precipitate radius change is found in kinetics when the precipitate number is kept constant but the radius value is increased by 2.5, 5, 10 and 15 times. A similar 15% increase in complete recrystallization time is found in recrystallization kinetics when the precipitate radius is increased 10 times from 0.1micron to 1 micron. The grain distributions in both cases remain unaffected (Fig. 54 e) f)).

a)   (b)
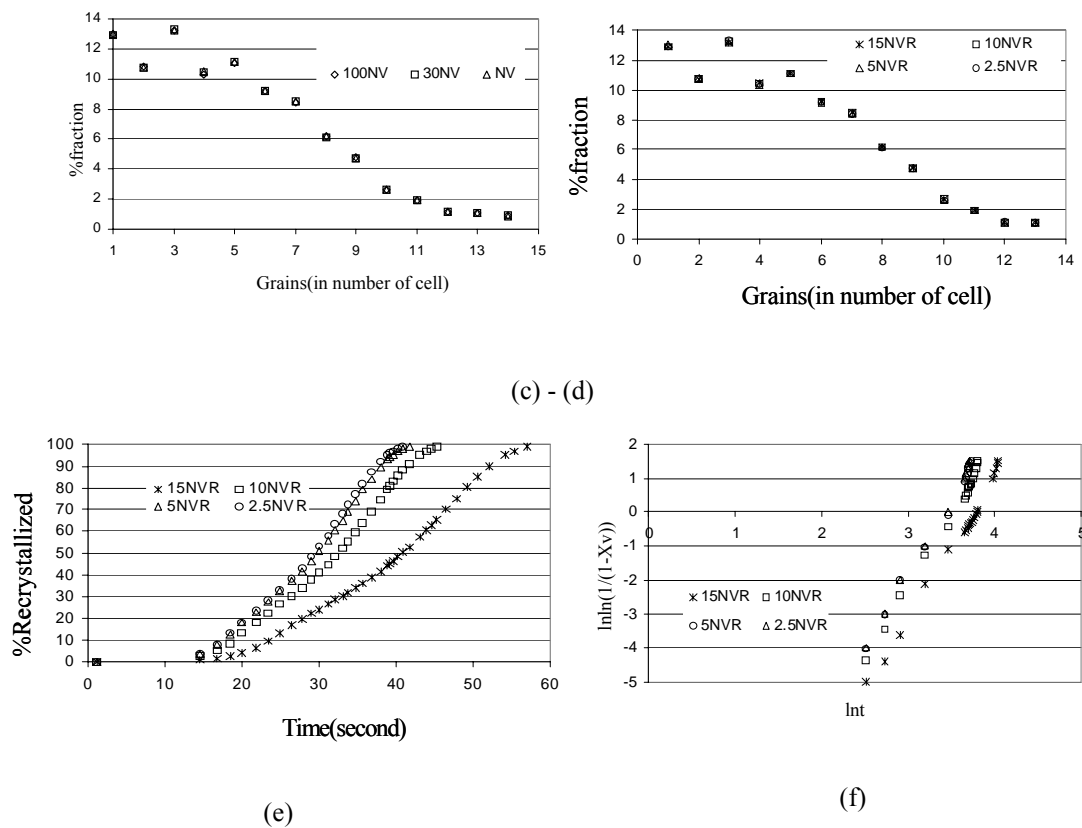
(c) - (d)

(e)

(f)
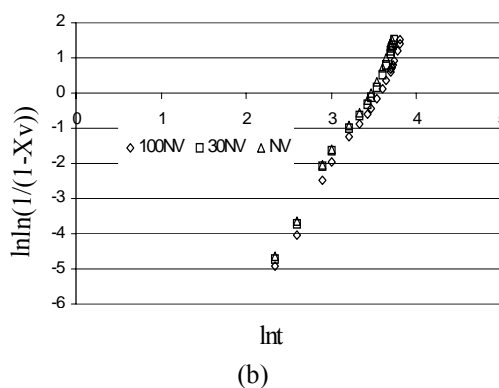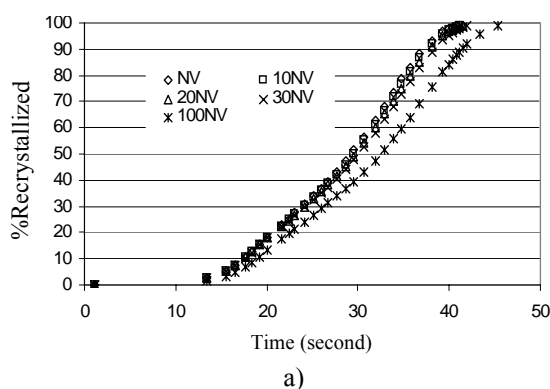
Fig. 54 a) Recrystallization kinetics with variable precipitate number. The available particle number is 10, 20, 30 and 100 times increased to see the effect of particle number in recrystallization kinetics b) Recrystallization exponent with variable precipitate number. c)-d) Grain distributions with variable precipitate number and radius. e) Recrystallization kinetics with variable precipitate radius. The available particle radius is 2.5, 5, 10 and 15 times increased to obtain the effect of particle radius in recrystallization kinetics. f) Recrystallization exponent with variable precipitate radius.

5.9 Solute drag on recrystallization kinetics:

The interaction of solutes with the recrystallization front is included in this model in the velocity of recrystallizing front boundary. The changes in any solute concentration during the recrystallization process may alter the mobility of recrystallization front involved because of elastic interaction between grain boundary and solute. The temporal concentration change of different solutes of aluminium alloys with temperature, obtained from the ClaNG model, was taken as reference to examine the solute drag effect on recrystallization kinetics. In order to get an impression of preciseness of this model a solute whose concentration varied not in monotonic fashion was chosen. As shown in Fig. 55 a) and 55 b) the recrystallization kinetics responds to the concentration variation of solute Fe. The initial increase in solute concentration

hinders the kinetics and finally the recrystallization stops before completion because of a sharp increase in solute concentration following a fluctuation near minima after the initial increase. The falling of solute concentration below the initial peak is well recognized by the model. A small steep step in between two sluggish parts of kinetic curve indicates that.
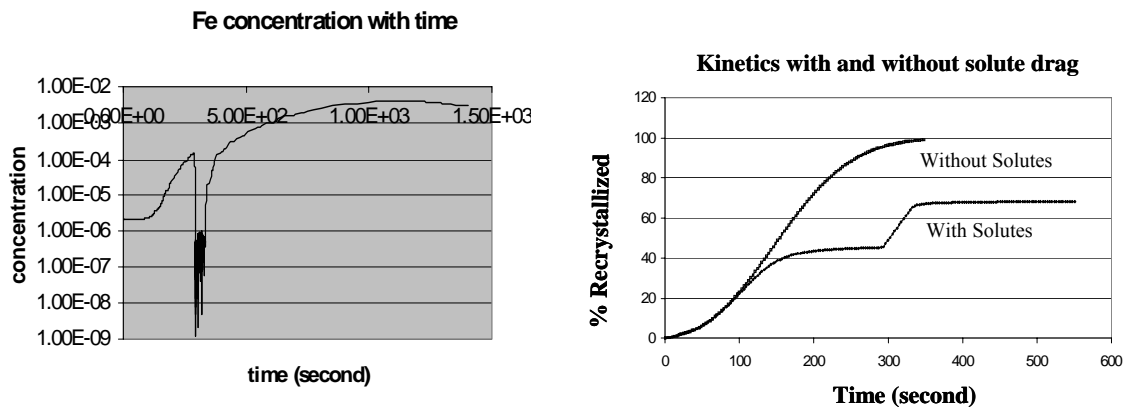

Fig. 55 a) Change in solute (Fe) concentrations with time.b) Recrystallization kinetics with and without solute (Fe) drag effect. The time dependent Fe concentration is shown in earlier figure.

5.10   Recovery on recrystallization kinetics:

This model is capable of simulating the simultaneous recovery phenomenon through different types of recovery kinetics, which involves the climb of jogs of perfect, extended dissociated edge dislocations, and the gliding of splitted partials before stable recombination. It assumes that the characteristic of dislocations and that of dislocation motion during recovery vary with the chemistry and with the intrinsic properties like the stacking fault energy of different alloys. Since kinetics of different dislocation motions are distinct in their nature, the system will choose only one of them for a particular condition set by internal and external parameters. The following results show effects of recovery kinetics on recrystallization. The recovery kinetic depends strongly on the activation energy of dislocation steps commonly known as jogs and the stacking fault energy. The earlier mentioned recovery factor decreases with the increase in stacking fault energy for a particular value of jog activation energy ($0.10Gb^3$) (Fig. 56a). This recovery factor is included in the velocity of recrystallization front. The result indicates that the maximum velocity calculated for each time step of recrystallization can also bear the impression of time dependent decrease in dislocation density because of

recovery (Fig. 56b). The cumulative effect of strong recovery for this lower value of dislocation step activation energy ($0.10Gb^3$) is best expressed in the recrystallization kinetics, which indicates an incomplete recrystallization for all stacking fault energy values even at a high (700°K) constant recrysatllization temperature (Fig. 56c). The batch annealing time and temperature data are quite different from that of constant temperature annealing (Fig. 56d). The recrystallization kinetics during different batch annealing temperatures with simulatneous recovery and without recovery were simulated (Fig. 57). The temperature of a batch annealing operation (data_1 or 1.0 NV) was increased 1.1 and 1.2 times to generate different input time vs. temperature data for recrystallization. A stacking fault energy value was selected which matches the stacking fault energy of aluminium. The simulations were performed with different dislocation step activation energies like $0.2Gb^3$, $0.25Gb^3$ and a higher value, which could stop recovery completely. The recrystallization and the recovery kinetics are found to be afftected by minor variation in batch annealing temperature for a particular value of dislocation step activation.
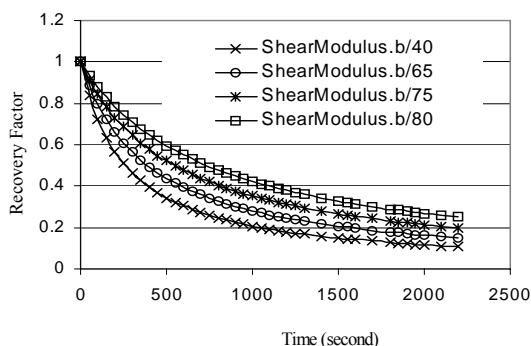

Fig. 56 a) Recovery factor with stacking fault energy. The stacking fault energy is considered to be a function of shear modulus (G) and Burgers vector (b).
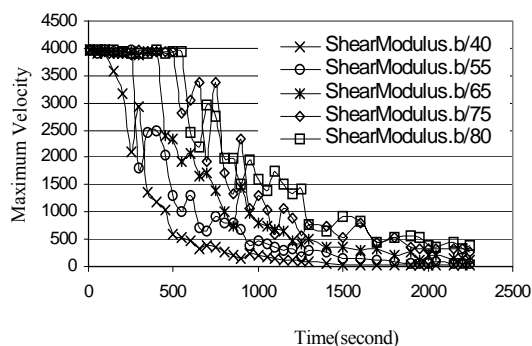

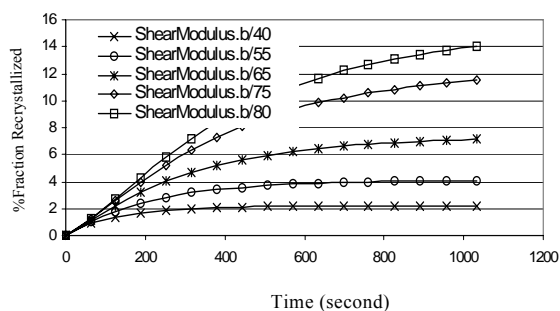Fig. 56 b) The decrease in maximum velocity with stacking fault energy.
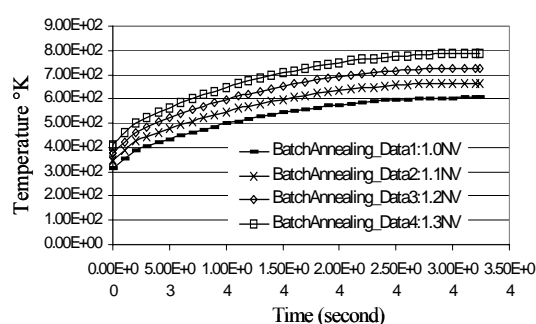

Fig. 56 c) Fraction recrystallized with stacking fault energy.

Fig. 56 d) Different batch annealing cycles.
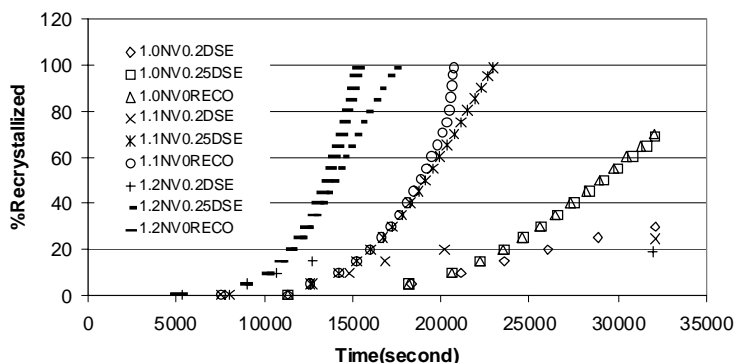
Fig. 57 Recrystallization kinetics for different batch annealing cycles with different jog activation energy. 1.0NV, 1.1NV and 1.2 NV denote different batch annealing data. 0.2DSE and 0.25DSE represent different dislocation jog activation energy. 0RECO stands for no recovery.

5.11 Location discrete nucleation approach: The deformation heterogeneity predicted by deformation texture model helps to identify different microstructure orientations responsible for different types of nuclei orientations like grain boundary, transition band and meta-stable/stable nuclei (Fig. 58a,c,d). These nuclei orientations were derived from the basis of splitting tendencies of differently oriented grains. The initial microstructure orientation list indicated the type of nuclei each microstructure orientation can provide. The locations of nuclei are different and are based on the experimentally observed nuclei locations. The grain boundary nuclei were distributed among surfaces of the deformed grains, the transition band nuclei were placed along the transition band which could be a couple of

a) Grain boundary nuclei.

b) Near precipitate nuclei.
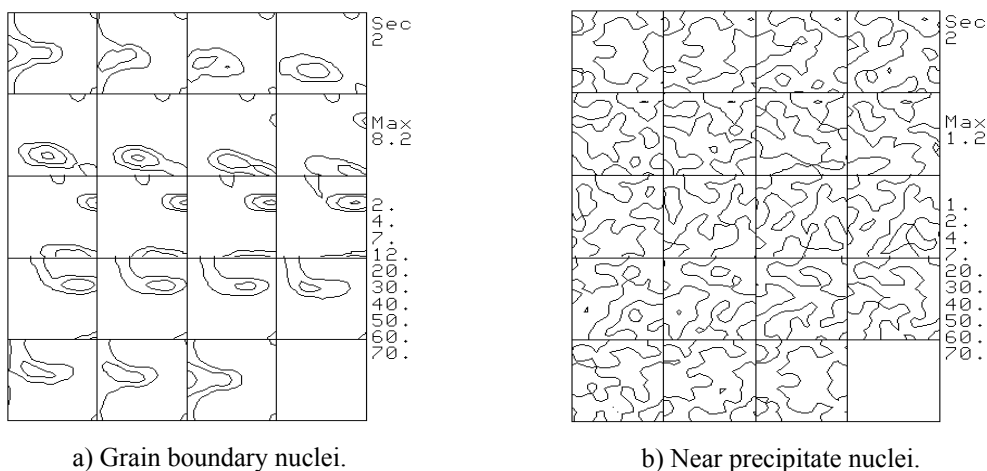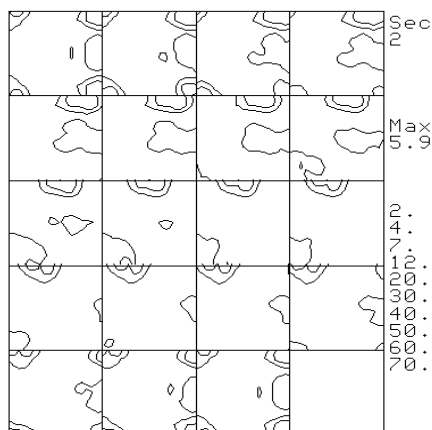
c) Transitionband nuclei.
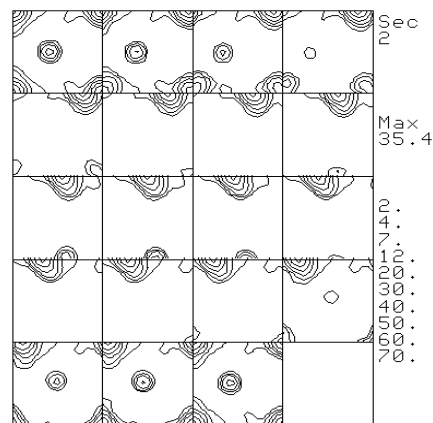
d) Metastable orientation nuclei.

Fig. 58 a), c) and d) Nuclei texture from obtained from GIA model. b) Nuclei texture obtained from local texture measurements.

Grainboundary

Meta-Stable/Stable

TransitionBand
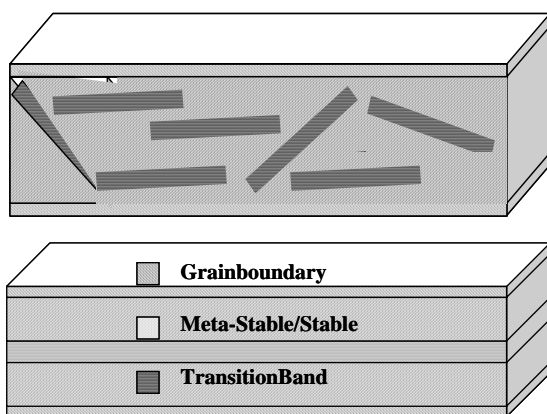
Nuclei Sources in deformed grain

top: severely deformed.

bottom: moderately deformed.

(a)
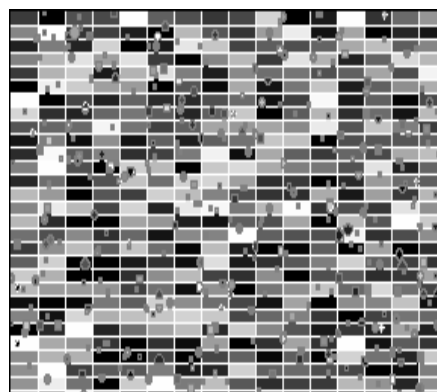
(b)
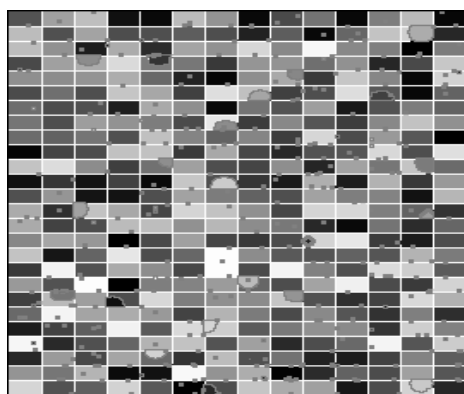
(c)
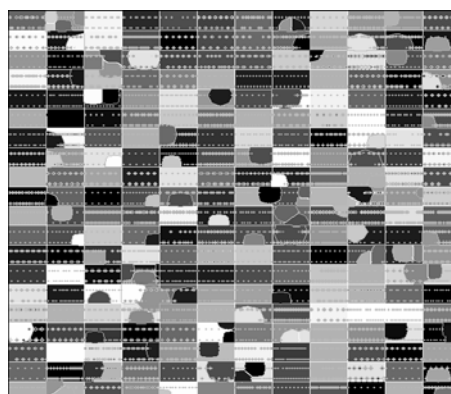
(d)

Fig. 59 a) Initial grain, b) Random nuclei, c) Grainboundary nuclei and d) Stable or metastable nuclei.

subgrain thick band parallel to the largest axis of transition band forming deformed grains and the metastable/stable nuclei were located in between grain boundary and

stable orientations. A random location distribution for transition band and the metastable/stable nuclei can also be considered, where the degree of deformation and the developed in grain strain heterogeneity too intense to have a certain pattern with well distinct transition band and region of stable orientations. This may give rise to a condition where different categories of nuclei orientations remain well defined but locations become non conservative. An example of different types of nuclei orientations and their locations are shown here (Fig. 59a). The schematic diagrams present geometrical locations of different sources in a deformed grain for small and large degree of deformations. The locations indicated in schematic drawing were tried to obtain in simulation for an aluminium alloy during nucleation of recrystallization after small deformation (Fig. 59c, d). The presence of precipitates brings another source of nucleation, which may not always random but possesses certain texture intensity of preference. An experimentally found nuclei orientations is shown here for this category (Fig. 58b). In through process modelling this was simulated with orientations obtained from list of equidistant orientations in Euler space, which under oriented growth mode could give similar texture as obtained from experiments. Since locations of precipitates were not well defined and were considered to be random, positions of these nuclei were randomly selected.

5.12 Through thickness microstructure heterogeneity:

The inherent anisotropic nature of engineering metals or alloys is enhanced many folds in conjugation with external reference system for engineering of those materials. Once a discrepancy initiates in meso-macroscale, it increases with the subsequent production steps of that material. The point of initiation is solidification, which gives textural and microstructural heterogeity because of difference in rate of solidification. The different microstructural features like chill zone, columnar region and equiaxed zone are associated with difference in textures. The subsequent through thickness heterogeneity during hot and cold rolling stages is accumulated because of difference in mechanical constraints exerted by the pass line, roll geometry, roll gap etc. on surface and in centre of the metals and alloys. The macroscopically imposed strain rotates orientations in different regions of the sheet differently not only because of local strain developed for each orientation but also because of frictional ease/difficulty for rotations caused by constraints. Whatever is the most effective reason, the resulting recrystallization texture

after subsequent processing stage becomes through thickness non-uniform. The through thickness non-uniform microstructure was simulated here on the basis of deformation texture simulated by Taylor type deformation texture model (GIA) and oriention dependent deformation energy from flow stress model (3IVM). The focus was mainly on the effect of local strain gradient on orientation change during deformation. Two different types of input deformation microstructures for surface and centre as obtained from deformation modeller were superimposed on cellular lattice. The difference in properties of initial microstructures creates diverse nucleation probabilities on the surface and in the centre of the lattice. Higher deformation energy of the surface microstructure than that of the centre one, induces more recrystallized grains along surface. The temporal developments of the recrystallization microstructure are shown in result (Fig. 60). This simulation considered uniform precipitate density for the surface and the centre. Since nucleation density depends on particle density, less particle density along surface compared to that in centre may change results.
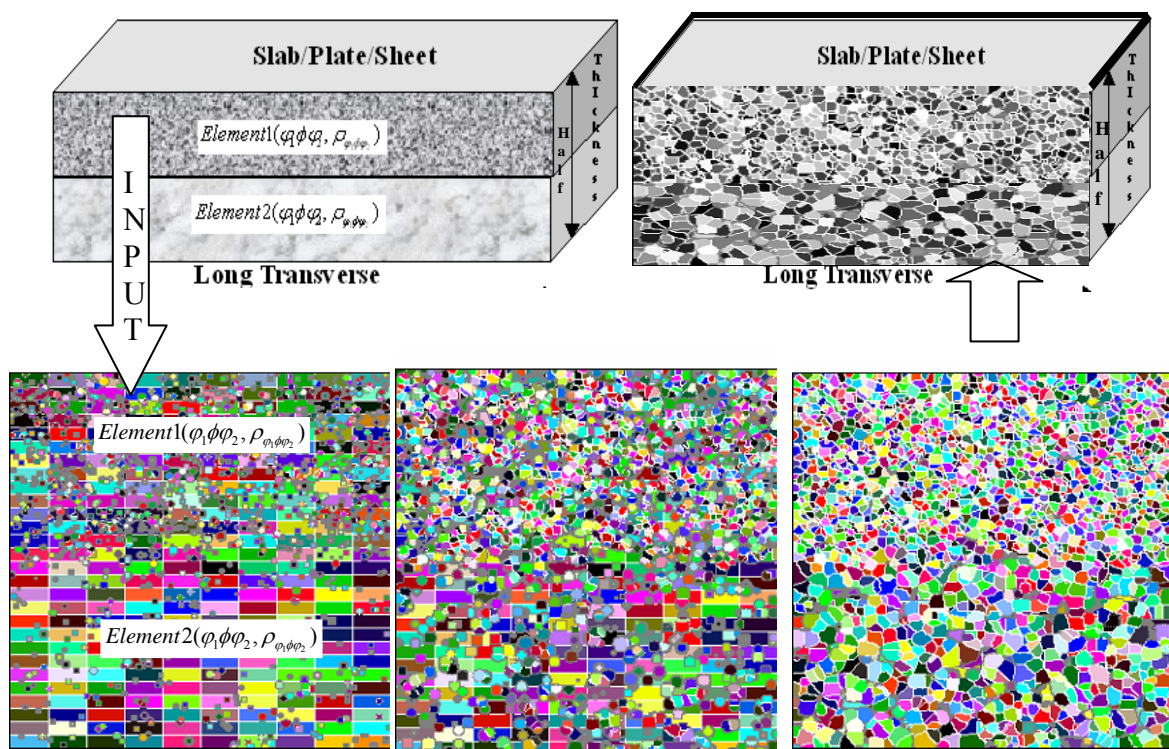
Fig. 60 Temporal development of through thickness recrystallization microstructure gradient from dual (surface and centre) input parameters.

5.13 Time dependence of different nucleation sources: The local energetic variation may sometime activate different nucleation with certain kinetic variations. This model consists of several independent nucleation subroutines. These subroutines of nucleations can be called before the start of the growth or they can be called during the growth stage. The first type of simulation denotes site saturation condition for nucleation while the second type represents time dependent nucleation. The nucleation kinetics is found to vary with degree of deformation, grain size and presence of precipitates etc. Even for a particular material this may vary with engineering history. Different modules of this model were applied for obtaining versatile effects of nucleation kinetics on recrystallization texture. All four categories of nuclei were considered. The initial microstructure and nuclei density of each category were kept constant. As found in the Fig. 61 a fast nucleation of grain boundary nuclei retains rolling textures after recrystallization. An early nucleation of particle-stimulated nucleation randomizes the texture. The intensity of {100}<100> orientation increases with the faster nucleation of meta-stable/stable orientation.

(a)   b)

(c)   (d)
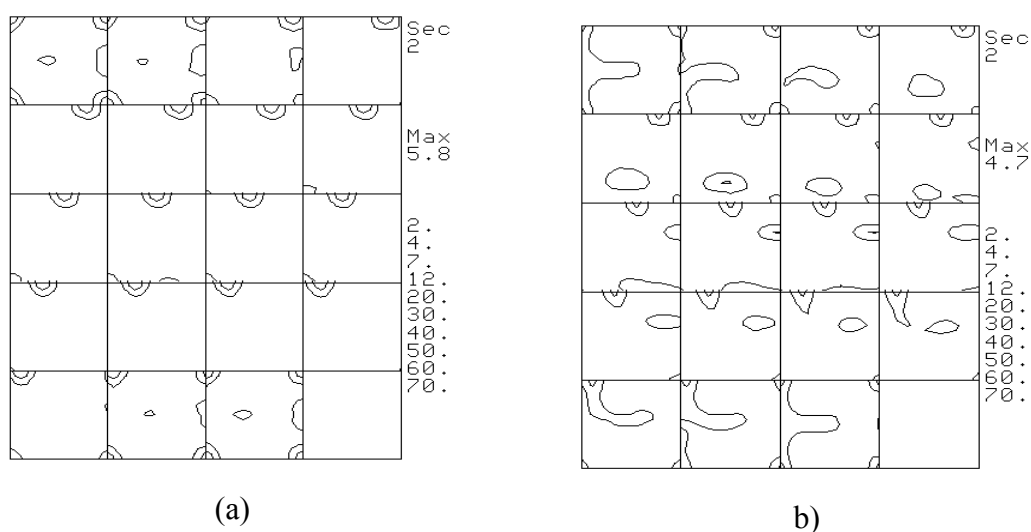
Fig. 61 (a) All Nucleations, Grain boundary, stable orientations, transition band and random nucleation are time dependent; (b) All nucleations except grainboundary nucleation are time dependent; (c) All nucleations except random nucleation are time dependent; (d) All nucleations except stable orientation nucleation are time dependent.

5.14 Oriented growth: The development of {100}<100> orientation after recrystallization is found in an AlMnMg alloy. The results of an experimental study of co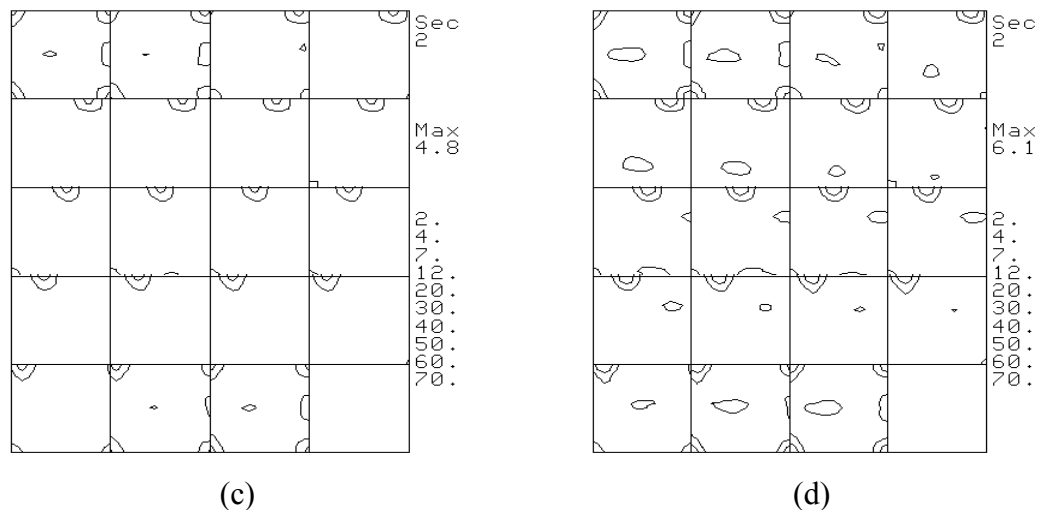ld rolling (cold rolling levels 40%, 60%, 80% and 90%) and subsequent annealing at a temperature about 700°K in saltbath are given below (Fig. 62). The initial fully recrystallized hot band had an accumulation of grains near Bs and S texture component with very less Cu texture component (a similar texture was developed in earlier simulation with grain boundary nucleation using grain oriented nuclei). The intensity shift in β−fibre from Bs and S components to Cu component with increasing cold rolling is noticable here apart from the reduction in {100}<100> orientation. The hot band texture randomizes with the increase in degree of deformation. The decrease in Bs, S and increase in Cu texture orientation with deformation make this alloy a little bit different from the usual one. The resulting experimental recrystallization textures conform the intensity variation of initial rolling texture up to the last stage of cold rolling. A sudden increase in the intensity of {100}<100> orientation in the recrystallization texture of 90% cold rolled alloy is also note worthy. Since the texture intensity variation accords the variation in rolling texture, the first trial of simulation was done considering rolling texture orientations (discretized with orthorhombic crystal symmetry) and distributing nuclei of rolling texture orientations according to their volume fractions in the deformed microstructure. No other nucleation sources were used The aim was to reproduce a strong intensity of {100}<100> or cube orientation from

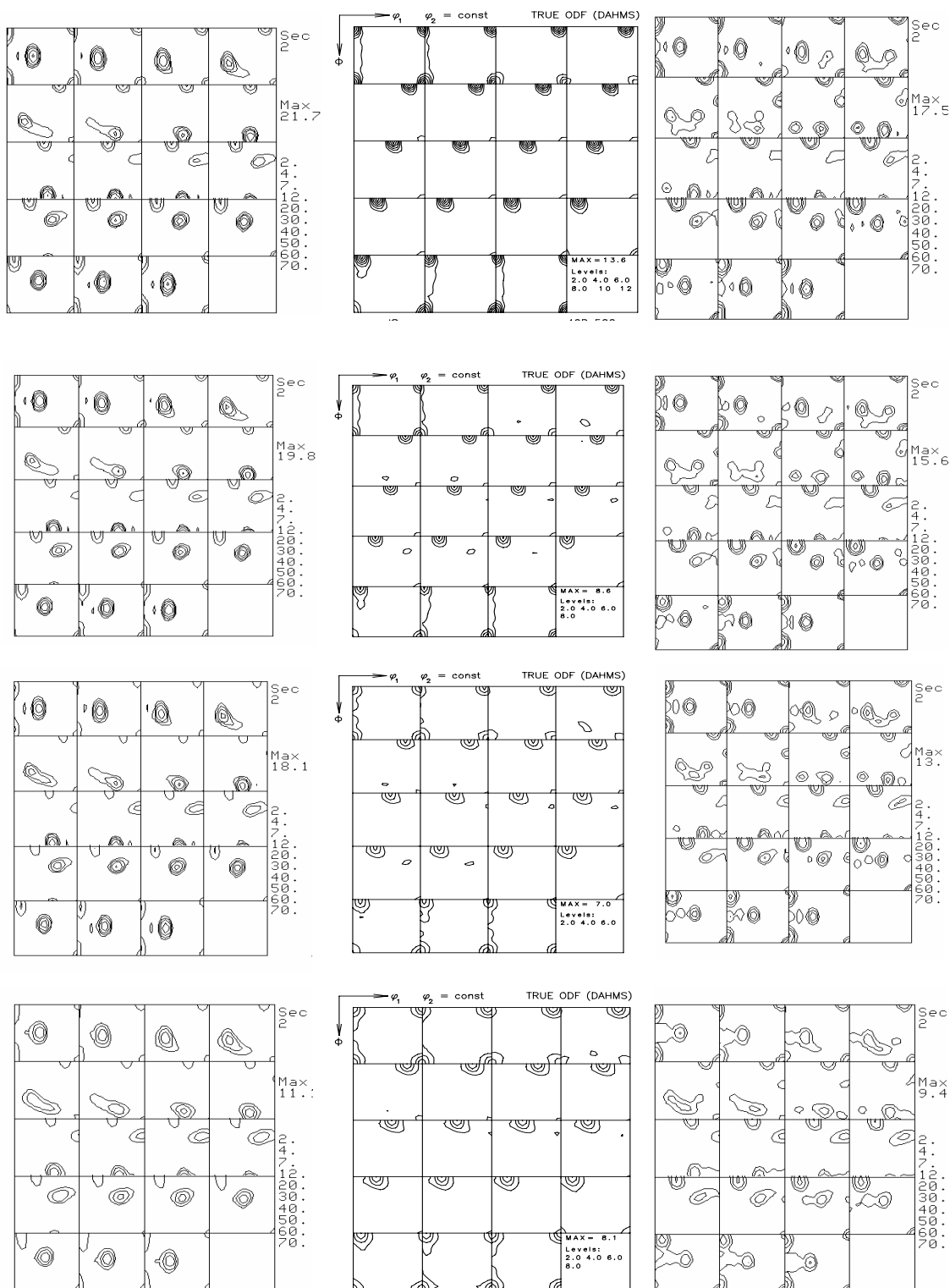Fig. 62 Row wise Texture: 1st row textures: 40% cold rolled, annealed, simulated annealed. 2nd row texture: 65%cold rolled, annealed, simulated annealed. 3rd row texture: 80% cold rolled, annealed, simulated annealed. 4th row texture: 90% cold rolled, annealed, simulated annealed.

initial microstructure orientation with the help of strong oriented growth. A strong oriented growth was applied. The simulated recrystallization textures show a stronger

intensity than that of experiments. Though the strength of cube component in simulated results are found to be stronger intensity than that of experimental results, the reduction in rolling texture intensities in simulation are not well reproduced. The intensity of rolling texture especially Bs and S decreases but not up to the level defined by experimental recrystallization textures. The gain and in loss in volume fraction of different texture components both in experiments and in simulations are explained in table 1 and in table 2. The important finding from the annealed microstructure of this material is that the recrystallized microstructure at a particular annealing temperature becomes stable beyond the 60% pre-recrystallization deformation but it varies with the annealing temperature (Fig. 64).

Table 1. Volume fraction of texture components in cold rolled and simulated recrystallized condition.

Components	40%CR	40%CR-RX	65%CR	65%CR-RX	80%CR	80%CR-RX	90%CR	90%CR-RX
cube	7.2	14.21	5.45	11.04	4.07	9.81	4.35	8.75
goss	2.1	4.1	2.53	4.73	2.1	4.42	2.63	4.62
copper	8.78	8.04	9.94	7.73	10.89	10.06	13.04	12.02
S/R	38.16	24.79	37.86	24.18	38.89	23.31	35.13	24.23
brass	33.11	17.79	30.89	17.03	29.19	16.52	23.34	15.19

Table 2. The change in volume fraction of different texture components during recrystallization, obtained from simulation and experiments.

Components	dRX40Sim	dRX40Exp	dRX65Sim	dRX65Exp	dRX80Sim	dRX80Exp	dRX90Sim	dRX90Exp
cube	7.01	5.5693	5.59	2.4479	5.74	4.0549	4.4	6.0825
goss	2	1.9272	2.2	1.8093	2.32	1.3138	1.99	0.4215
copper	-0.74	-3.1317	-2.21	-3.0494	-0.83	-4.6049	-1.02	-6.8868
S/R	-13.37	-29.1691	-13.68	-26.8786	-15.58	-25.7896	-10.9	-23.905
brass	-15.32	-27.0351	-13.86	-25.198	-12.67	-23.3681	-8.15	-17.8666
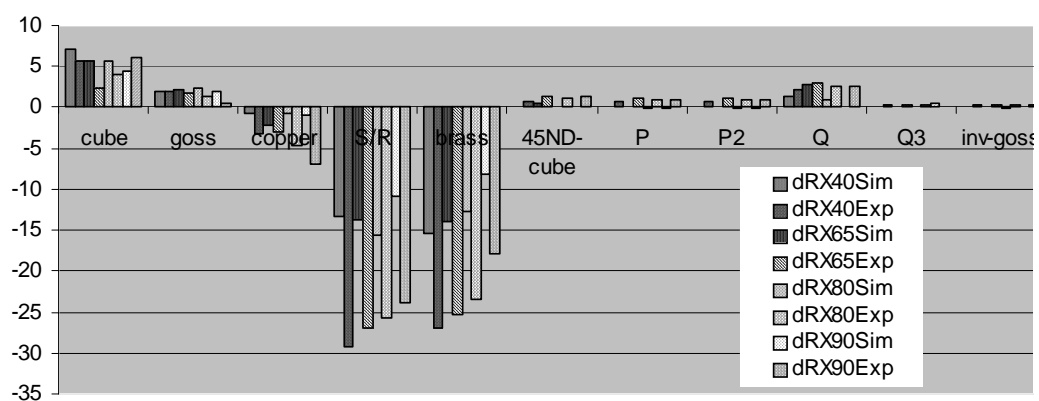
Fig. 63 Textural strengthening and weakening of different components.
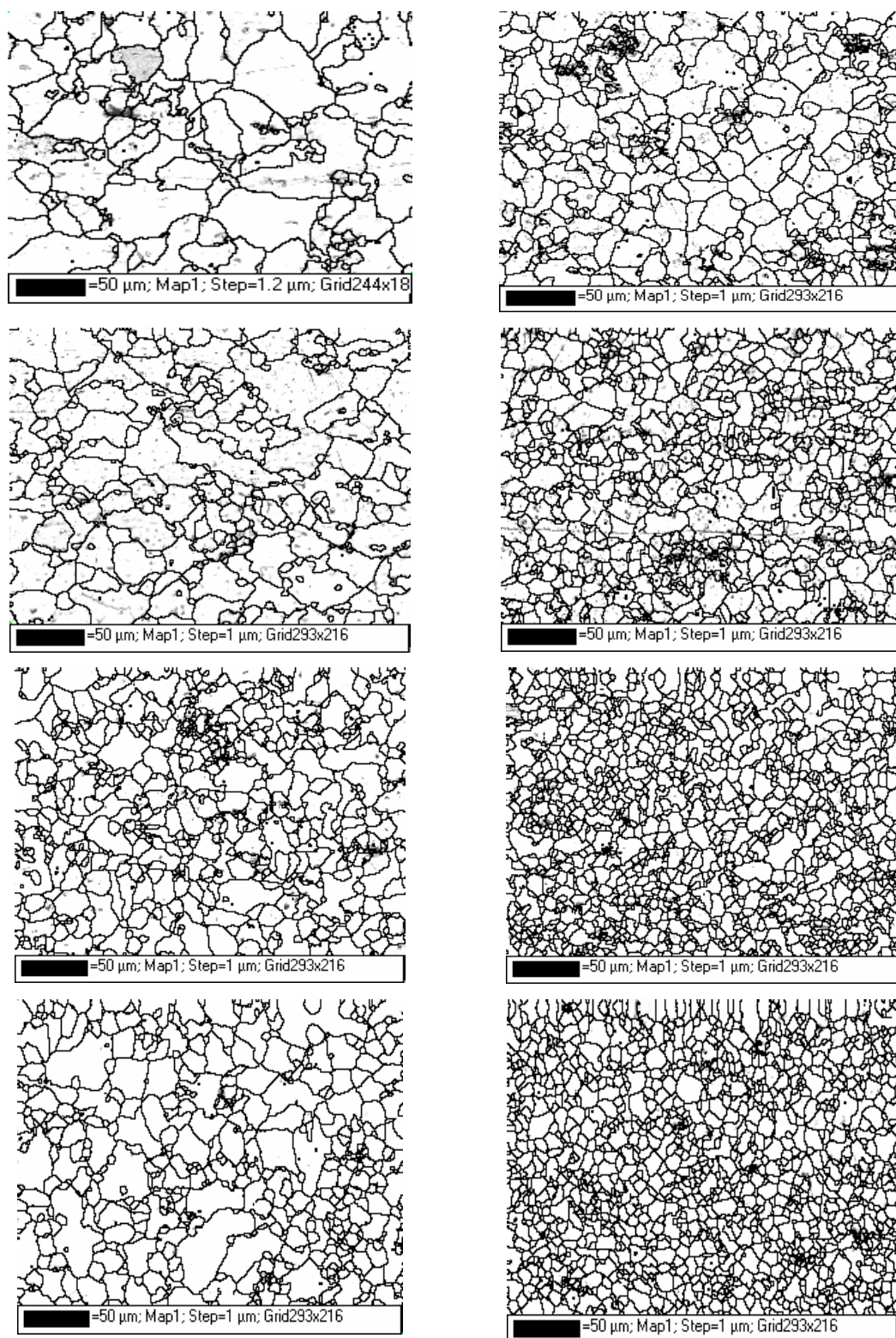
Fig. 64 Column wise: Al1%Mn1%Mg alloy Annealed Microstructure. 1st column: 300°C salt bath annealing of 40%, 65%, 80% and 90% pre-recrystallization deformed samples. 2nd column: 500°C salt bath annealing of 40%, 65%, 80% and 90% pre-recrystallization deformed samples.

5.15 The particle stimulated nuclei orientations in deformed microstructure:

It is well known that the presence of particles randomizes the

recrystallization. In the earlier study we have seen that simulated recrystallization textures had higher intensity than experimental one. Incorporation of random texture in initial microstructure nuclei can decrease the texture intensity. The following results show the variation in different recrystallization texture components with the increase in random nuclei texture components (Fig. 65, Fig. 66) in initial microstructure. The variation in random fraction from 10% to 20% is shown in different orientation distribution functions. The volume fraction analysis of 90% cold rolled and recrystallized sample shows insignificant variation in {100}<100> texture orientation with the variation in random fractions from 10% to 20%. The volume fraction of Cu and S/R components decrease but virtually no change in Bs orientation is noticed. It is clear from these results that the incorporation of random or nearly random nuclei texture from precipitates reduces the rolling texture intensity more than that of near cube orientation in presence of intense oriented growth. This is due to the fact that random nucleation can also create cube texture under intense oriented growth. This was extensively studied earlier [31]. In principle these nearly random orientations should remain in microstructure orientations. The probable reason for not identifying them in initial texture is that they belong to deformation zone of precipitates with very less volume and with wide scatter in orientation. A very high nucleation potentiality brings them into limelight after recrystallization. The possible reasons for the sudden increase in cube or {100}<100> orientation after recrystallization of final gauge (90% cold deformed) are

a) the effective use of full stability of stable {100}<100> orientation because of the presence of surroundings favourable for better compromise growth.

b) geometrical constrains on nucleation near particles because of band thinning.

c) massive reorientation near particle and formation of some preferred orientations.

With the present status of the model outlined so far, all above mentioned possibilities can be addressed.
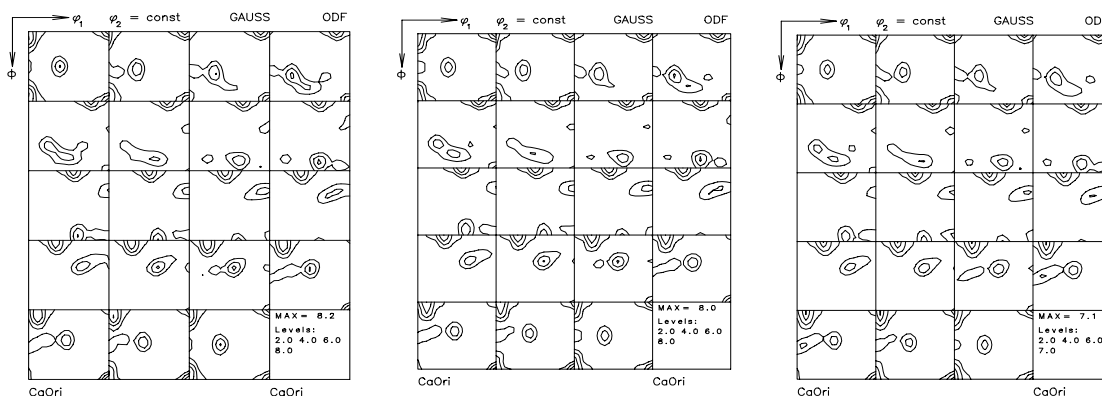
Fig. 65 90% cold rolled and annealed with increasing contribution of random texture (left to right 10%, 15% and 20%).
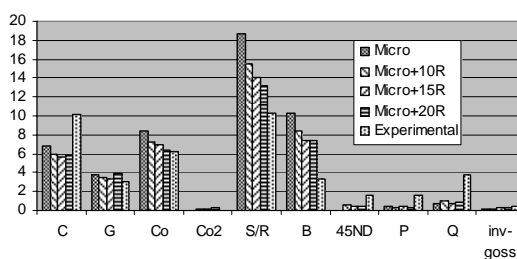
Fig. 66 Strength of simulated recrystallization texture components with 10%, 15% and 20% contributions of random texture in microstructure orientations (C for cube, G for Goss, Co for Copper, B for Brass etc.).

5.16   Texture engineering from laboratory scale to industrial scale:

The texture of sheet determines the quality of final product after subsequent forming operation. An intense textural strength of any or a few texture components may cause defects during forming operation of sheet. Hence the controlling of texture is an industrial interest. A laboratory scale experimental work was performed to find out a cold rolling and a batch-annealing schedule, which randomized the recrystallization texture of Al4.5Mg0.5Mn alloy after final deformation level. The hot rolled alloy was cold rolled to true strain level 2.4 by different routes with or without interannealing (Fig. 67). The rolling texture intensities along β fibre and intensity of rolling direction oriented {100}<100> orientation for different deformation stages are shown in Fig. 68. The deformation texture intensity transition from Cu-S-Bs of cold deformed samples follow a normal trend. The presence of inter-annealing after true strain levels 0.80 and 1.60 changes this Cu-S-Bs intensity variation. The rolling texture intensity along this ß fibre is changed significantly (Fig. 69). The recrystallization textures obtained from of all three different paths (Fig.70-Fig.72) involves the maximum texture intensity

variation 4.0-3.4-6.7 in final cold rolled sheet. The interannealing reduces the recrystallization texture intensity of the final gauge.
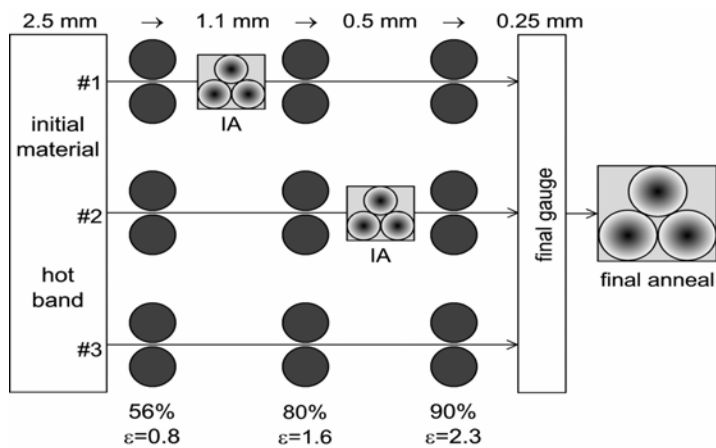
Fig. 67 Different process routes with or without inter-annealing.
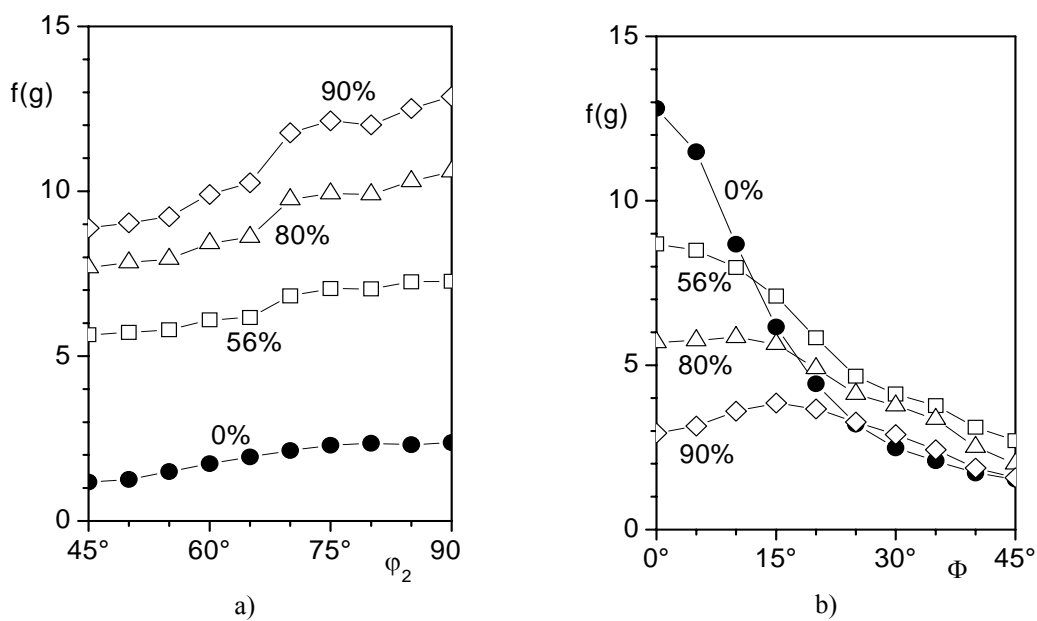
Fig. 68 a) ß Fibre rolling texture with deformation. b) Rolling Directional {100}<100> with cold rolling.
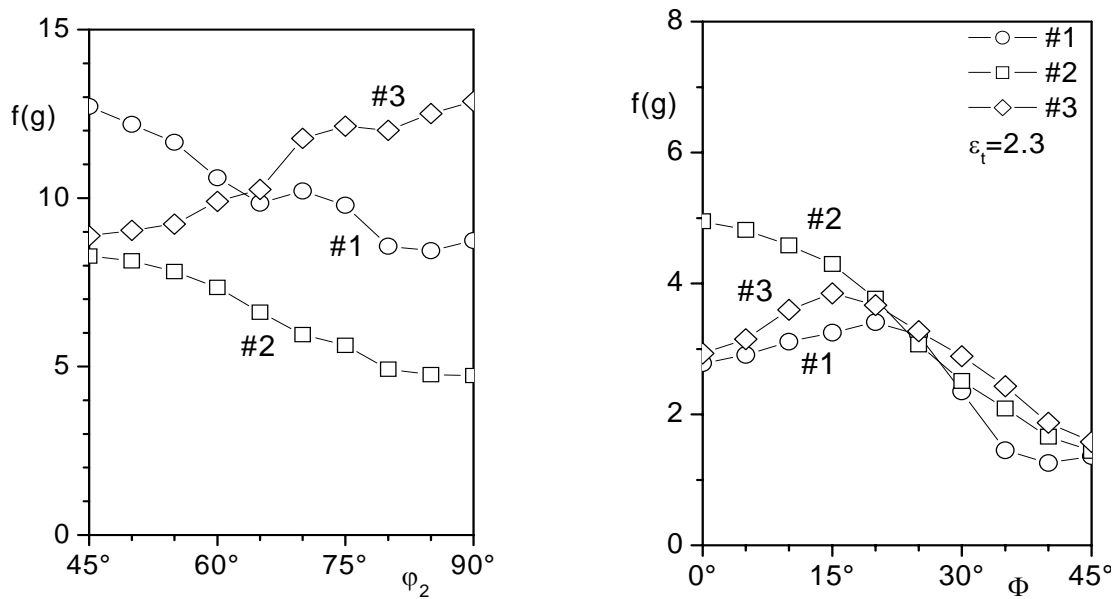
Fig. 69 a) Deformed final ß fibre textures from all routes. b) Final Rolling Directional{100}<100> from all routes.
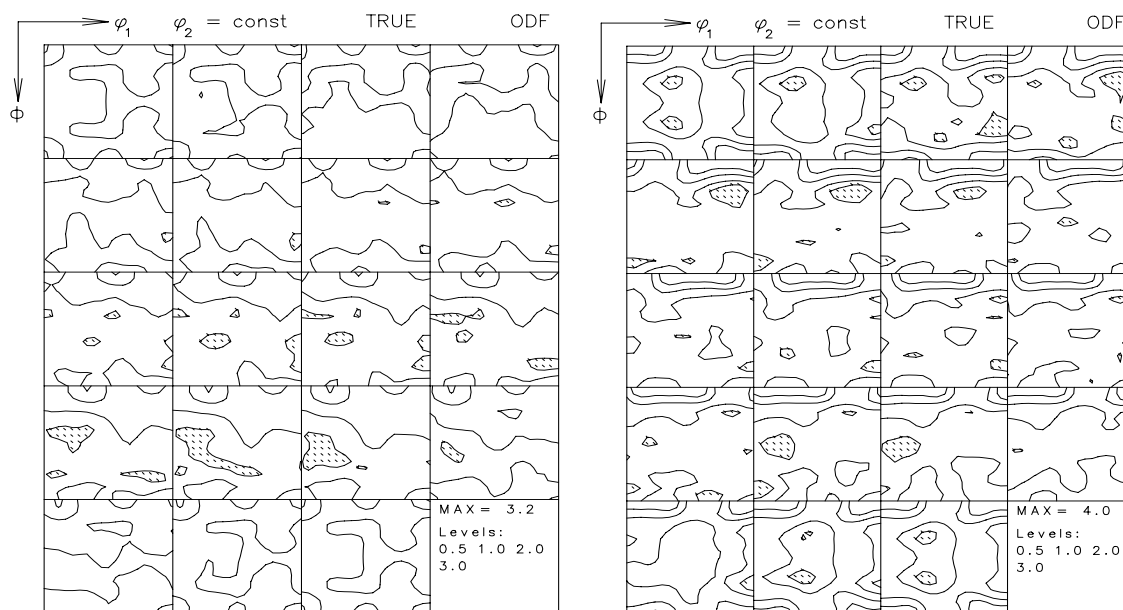
Fig. 70 a) Recrystallization texture after 0.8eps (true strain). b) Recrystallization texture after 2.4 eps (true strain) from route 1.
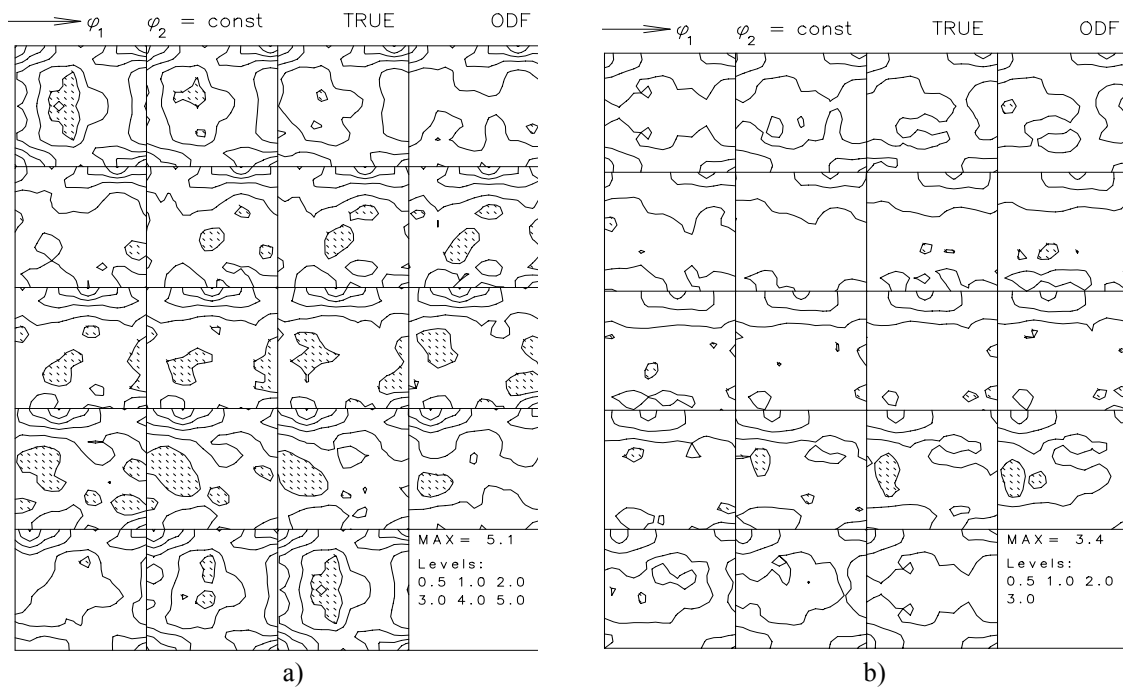
Fig. 71 a) Recrystallization texture after 1.6eps (true strain). b) Recrystallization texture after 2.4 eps (true strain) from route 2.
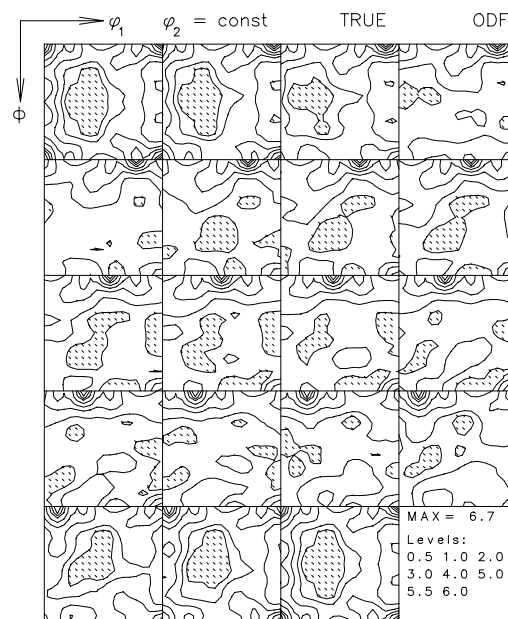
Fig. 72 Recrystallization texture after 2.4eps (true strain) from route 3.

5.17 Industrial AA5182 strip production: The following diagram shows different stages of the industrial engineering of this aluminium alloy, used for this study (Fig. 73a). It includes both the hot rolling and the cold rolling steps. The rolling stands from No. 3 to No. 5 were used for hot rolling where transfer slab from the break down mill were deformed at higher temperatures, 666°C, 621°C and 606°C respectively. The

hot rolled coil obtained from rolling stand No. 5 was subsequently cold rolled in following rolling stands from No. 6 to No. 9. A series of inter-annealing operation was incorporated to recrystallize material after small cold deformation in order to control and to achieve weak texture of the annealed finishing gauge. The time temperature cycle of the interannealing operation is shown in subsequent diagram (Fig. 73b). All interannealing operations were performed with same heat treatment parameters.

The simulation was started from the transfer slab material. There were three hot rolling stands. The final hot rolling texture and the grain diameter of material were calculated step by step taking output of one rolling stand as an input for the subsequent recrystallization. The deformation texture and deformation energy data of each rolling pass obtained from other models mentioned ealier. The starting texture of transfer slab was considered to be random. The average grain diameter for each recrystallization stages, expressed in terms of stand number, was calculated according to the earlier mentioned equations. The GIA model delivered the nucleation texture for each recrystallization process. One example of orientation spectrum of different nuclei categories used for recrystallization is shown in Fig. 79.
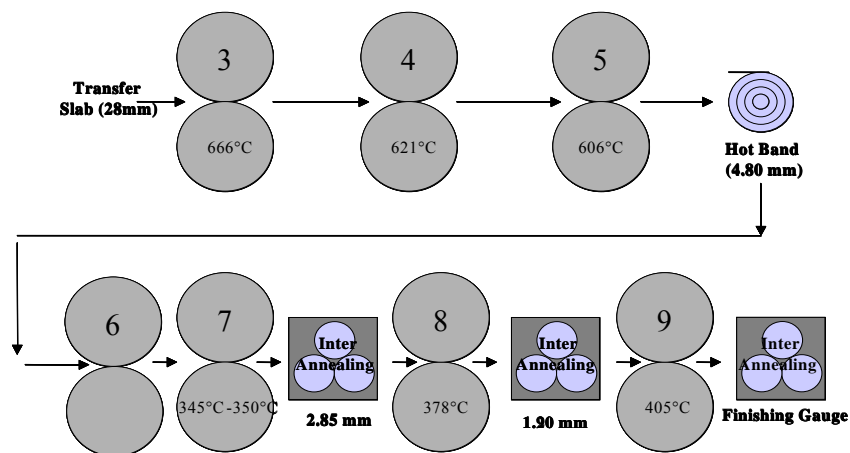
Fig. 73 a) AA5182 Strip processing stages from transfer slab to finishing gauge.
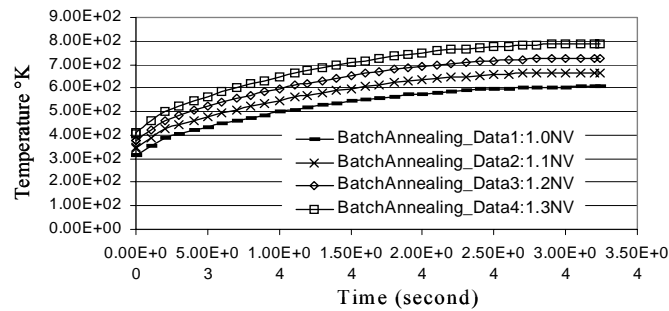
Fig. 73 b) Time-Temperature cycle (Batch annealing_Data1:1.0NV) of the interannealing operation.
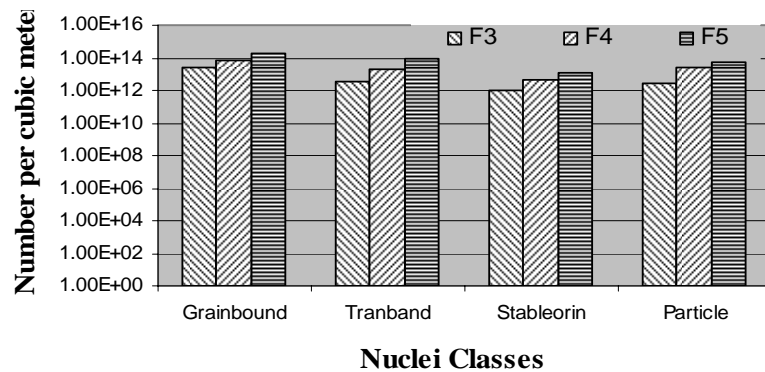
Fig. 74 Calculated nuclei density of recrystallization during the intermediate stages of hot rolling process. F3 to F5 represent the rolling stand no 3 to 5.

The nuclei contributions of different categories like grain boundary, transition band, stable and particle stimulated nuclei during recrystallization after hot rolling are shown in Fig. 74. The average grain diameter for each recrystallization in between the transfer slab and the final sheet was calculated from the total number of nuclei obtained from the method mentioned earlier. The average recrystallization grain diameter through out the production of sheet is shown in the Fig. 75. It also describes the effect of minute variation in the nucleation probability. An accurate measure for dislocation density and the selection of proper nucleation probability can alter the result. Two different calculations gave DATA1 and DATA2 results. DATA2 presents an improvement in result. DATA2 calculations were done according to the nuclei density shown in earlier diagram (Fig. 74). The nucleation probability was in the range of 10^{-4}. A recovery during the nucleation was assumed. A prior recovery process for dislocation density reduction was considered to keep dislocation density in the order of 1.0e+15 for subsequent calculation of nuclei density or grain diameter.
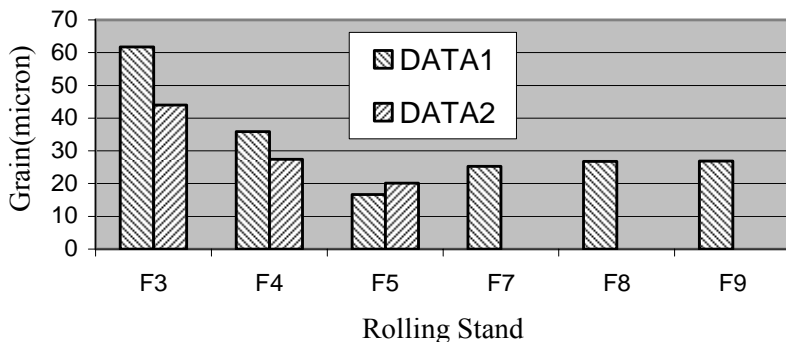
Fig. 75 The calculated recrystallized grain diameter through out the production chain. F3 to F9 denotes the rolling stand no 3 to 9.
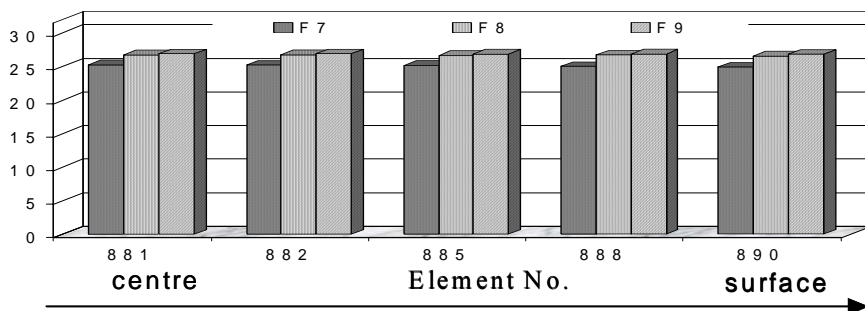
Fig. 76 The calculated through thickness variation of recrystallized grain diameter after batch annealing.
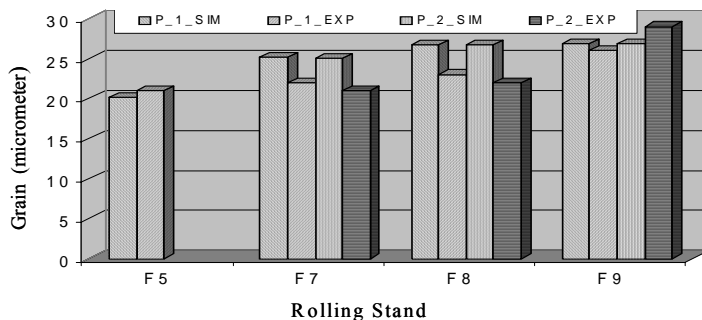
Fig. 77 Experimental and calculated recrystallized grain diameter. The position P_1 denotes position near centre level while the position P_2 represents position near surface level of the sheet.

The through thickness average grain diameter variation after three different batch annealing is shown in Fig. 76. The rolling stands from no.7 to no.9 are denoted as F7 to F9. An identical nucleation probability and extent of recovery in time scale before the onset of nucleation were applied for all nuclei density calculation during batch annealing. Fig. 77 represents the experimental and simulated recrystallization grain diameter for near surface and near centre regions of the sheet after hot rolling, after cold rolling and annealing stages.
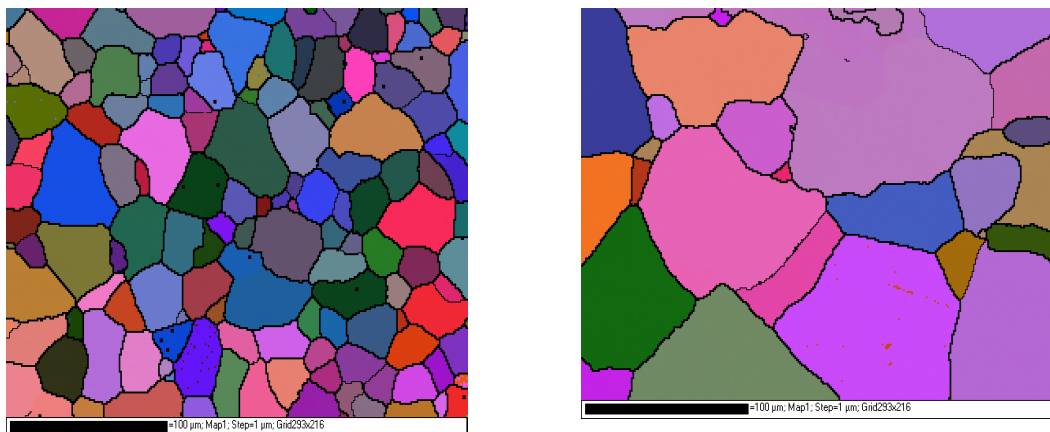
Fig. 78 Through thickness microstructural change in transfer slab (left to right near centre, near surface).

grainboundary nuclei

transition band nuclei

Stable orientation nuclei

random nuclei from particles
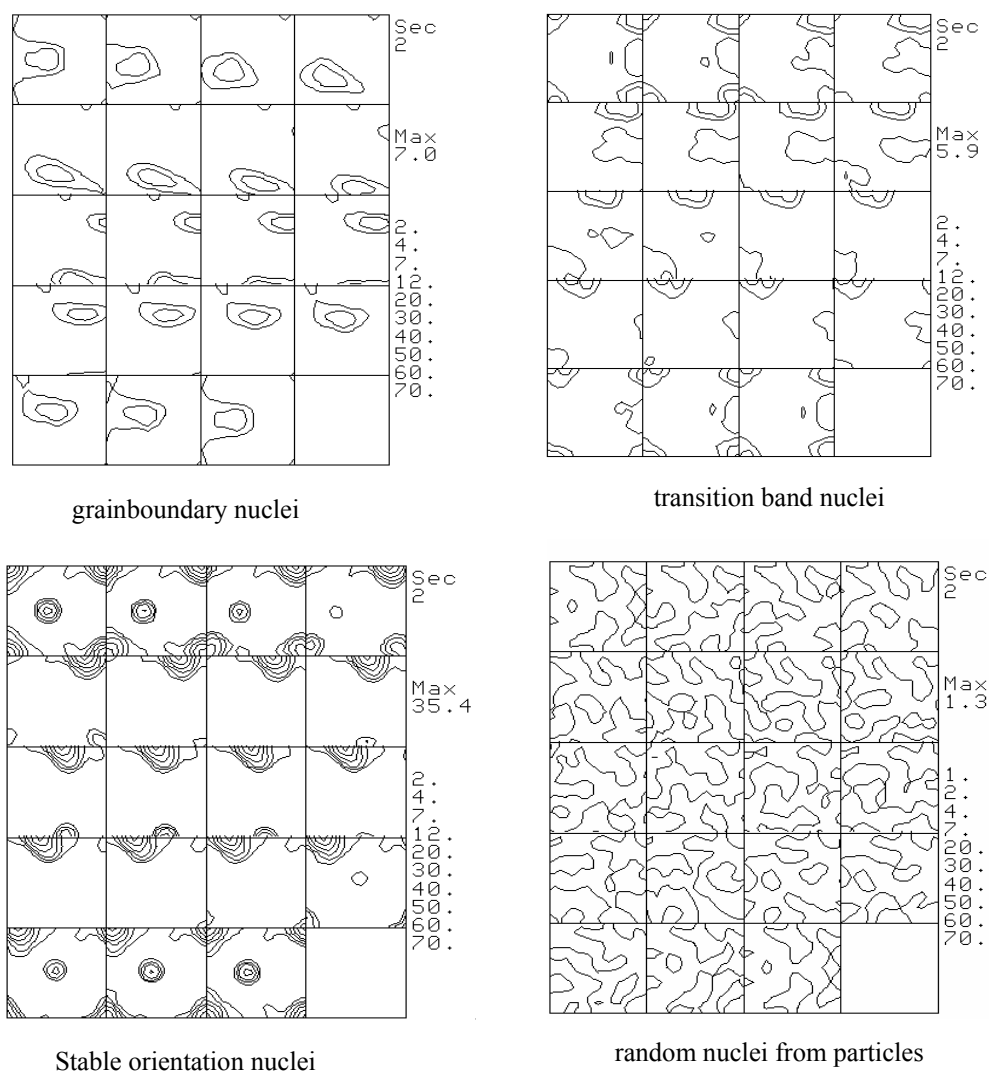
Fig. 79 Starting nuclei texture for F3-F4 intermediate recrystallization.

The following figures deal with the initial textures, recrystallization textures, microstructures and grain distribution. The hot and cold rolled textures are compared

with the experimentally obtained one (Fig. 82, Fig. 85). Simulated microstructure of hot rolled sheet and that from experiments are shown in Fig. 83 and in Fig. 84. The temporal development of the simulated texture of hot rolled material shows that the texture intensity first decreases because of the nucleation of different types of nuclei including random orientations. The near cube texture at the later stage of recrystallization becomes stronger and lifts the intensity of the texture (Fig. 82). The salt bath annealing of the final gauge produce very weak texture.The experimentally observed weak annealing texture of the final gauge material is reproduced in simulation (Fig. 85). The fully recrystallized texture of final gauge material obtained from simulation is compared with the recrystallization texture obtained from salt bath annealing in laboratory. The batch annealed final gauge material had a partially recovered microstructure and a higher intensity of rolling textures (Fig. 86, 87).
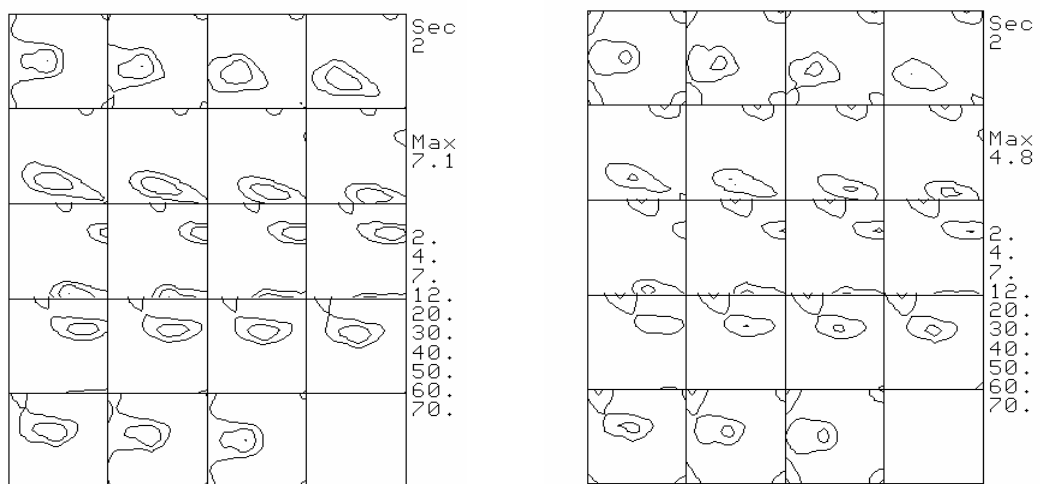
Fig. 80 Starting rolling (left) and simulated recrystallization (right) texture of F3-F4 intermediate recrystallization.
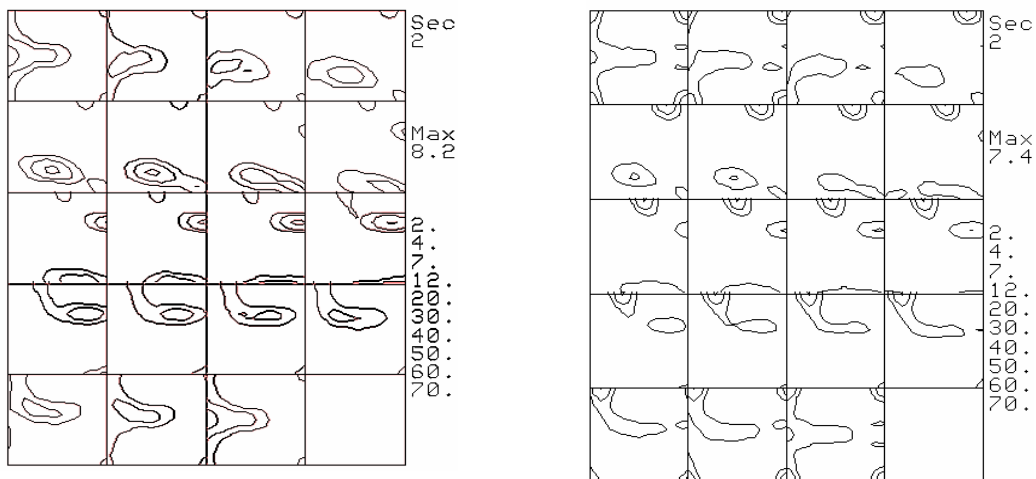
Fig. 81 Starting rolling (left) and simulated recrystallization texture (right) of F4-F5 intermediate recrystallization.

a)

b)

c)

d)

e)

f)
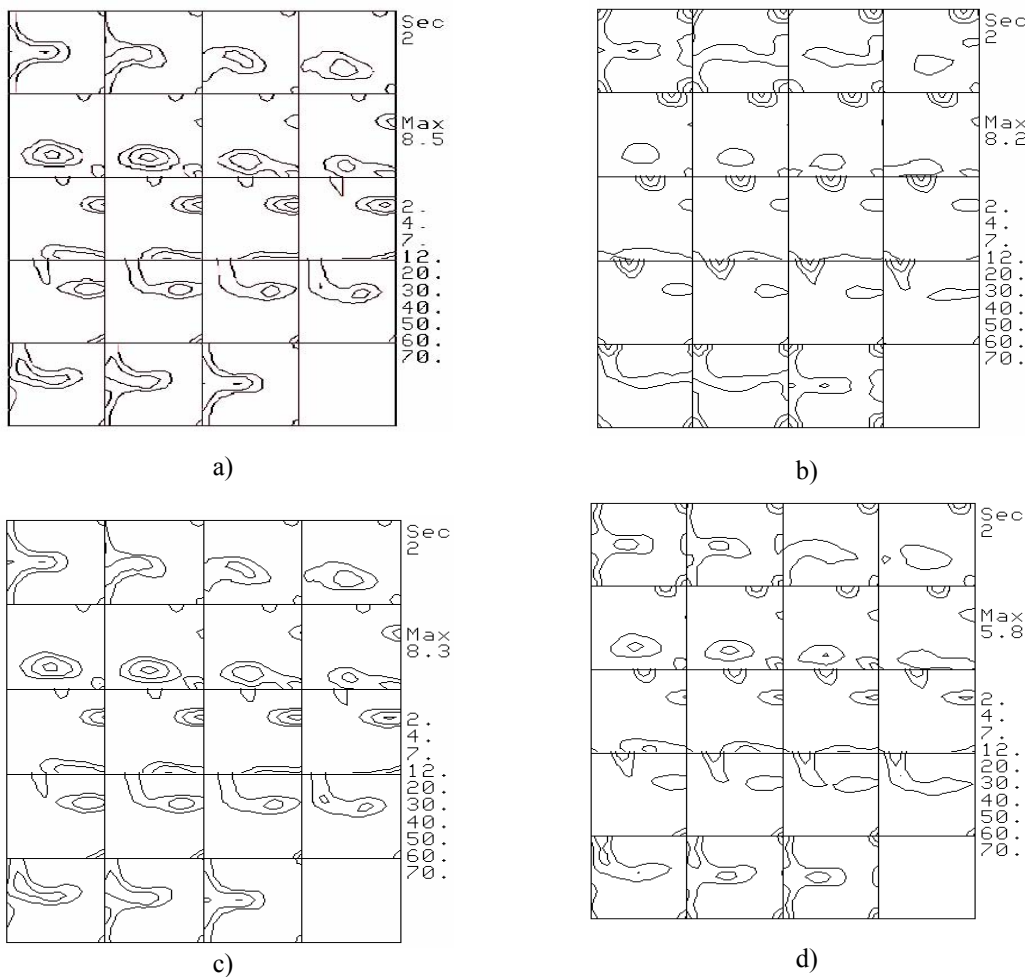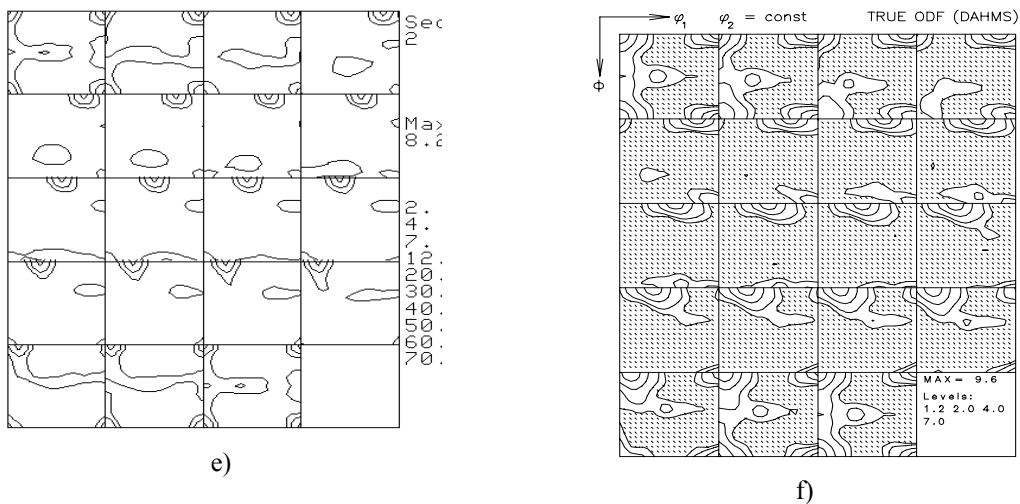
Fig. 82 a) F5 initial texture, b) Simulated recrystallized texture, c) to e) Temporal developments in simulation, f) Measured hot band texture.

a)

b)

c)

d)
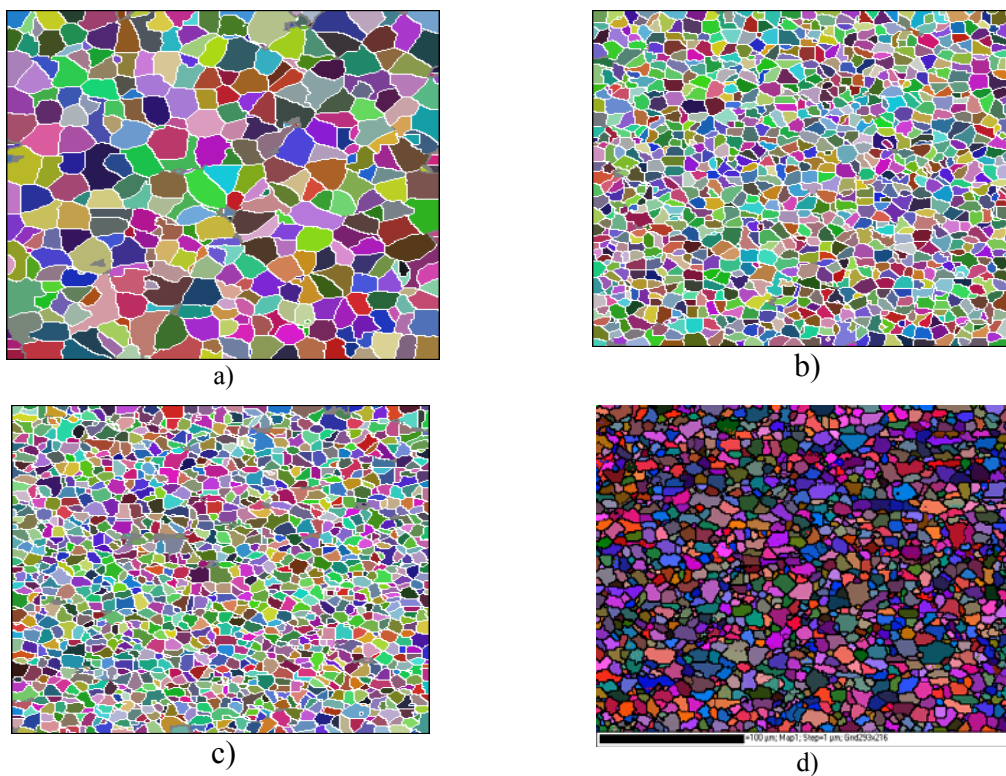
Fig. 83 a) Simulated F3-F4 intermediate microstructure, b) Simulated F4 -F5 intermediate microstructure, c) Simulated hot rolled microstructure and d) Measured hot rolled microstructure.
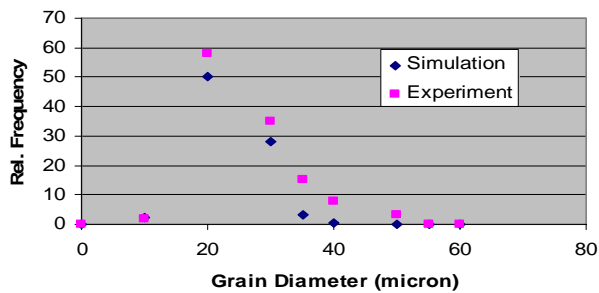
Fig. 84 Measured and simulated grain distribution of hot rolled sheet.
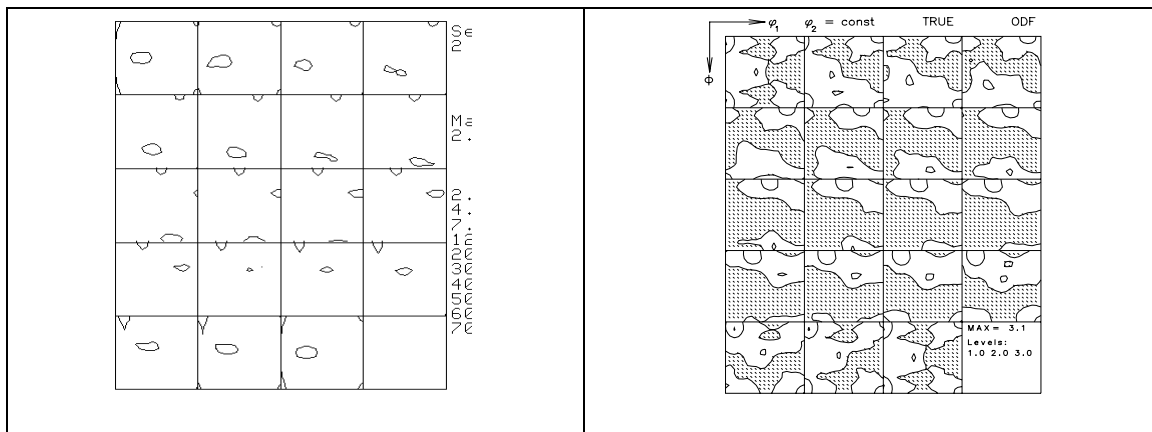
Fig. 85 Simulated fully recrystallized texture of the final gauge (left) and measured texture of fully recrystallized material with similar prior recrystallization deformation (right).

•
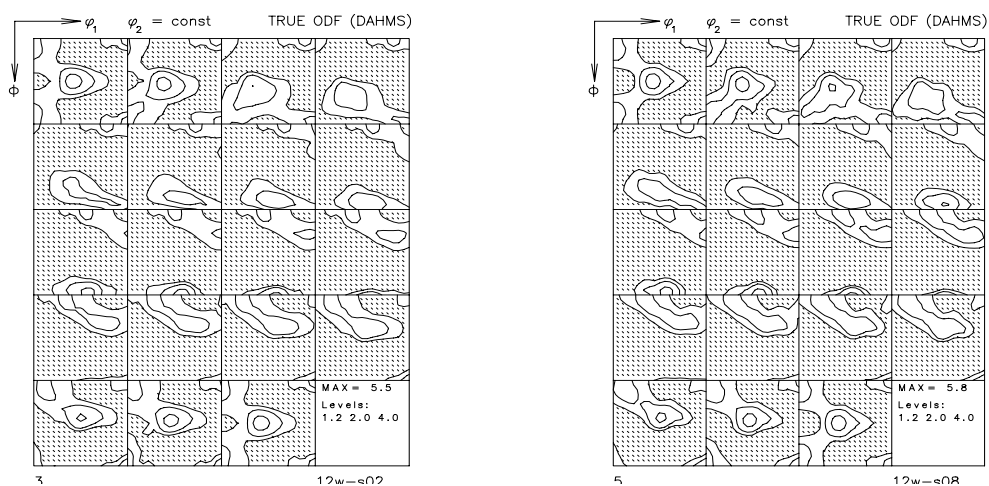
Fig. 86 a) The measured batch annealed texture near centre of the final gauge alloy, b) The measured batch annealed texture near surface of the final gauge alloy.
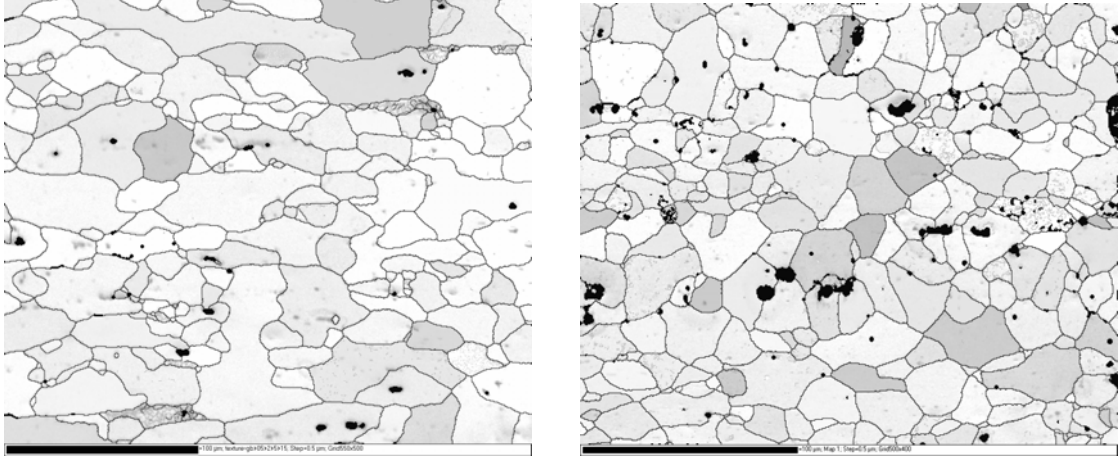
Fig. 87 a) The measured batch annealed microstructure near centre of the final gauge alloy, b) The measured salt bath annealed microstructure of the final gauge alloy.

6. Discussion.

6.1   Nuclei distribution: The basic knowledge of recrystallization nucleation obtained from several experimental studies is not sufficient enough to decide the relationship between identities of initial grains and the number of nuclei emerges from them. As discussed earlier the creation of nuclei depends on local variation in microstructure, which is very much frequent at higher deformation stages. Moreover, when different parts of a grain deformed and recovered differently, the identity of initial grain is lost in terms of its orientation. This makes the early stage of nucleation a very complex process to count and to relate the emerging nuclei to the identity of the initial grain. In our study we have established a correlation between deformation energy of a deformed grain and the frequency of nucleation considering uniform energy of each deformed grain. In practice different fragments of an initial grain may recovery differently because of their different dislocation densities and orientations and may lead to a situation where both low and high nuclei densities are probable for a particular deformed grain (including all of its fragments) with certain average deformation energy. Different types of nuclei distributions are included in this modelling approach to make the model more versatile.

The mechanism of nucleation discussed so far, depends on the dislocation density of the original grain orientation and on that of surroundings. This model identifies each deformed grain with its deformation energy. Grains with different orientations and deformation energies converge at regions of orientation change, leaving those regions as locations of sharp disorientations and deformation energy variation. As found earlier the rearrangement of dislocations occurs locally to create nuclei, which are in strict sense small volume entities with comparatively low dislocation densities and surrounded by the regions of high deformation energy and sharp orientation gradient, this microstructural change due to dislocation rearrangements can be attributed to the recovery process, which depends on the local deformation heterogeneity and chemistry of this alloy. A suitable orientation and local chemistry effect may lead to the creation of nuclei near accumulated disorientations, which belong to deformed grains with comparatively low dislocation density, where the recovery rate is influenced more by above mentioned orientation and microchemistry factors than the initial dislocation density. In order to capture the real picture of deformed grains, wherefrom new grains

emerge, different nuclei distribution functions based on the deformation energy of grains, were applied with constant nucleation kinetics for recrystallization simulation. The highest difference in nuclei number in the nuclei distribution 1 imparts a clustering effect in deformed grains. The deformed grains with higher dislocation densities than the mean value get the nucleation privilege factor more than one compared to the nucleation privilege factor less than one for those deformed grains having lower dislocation densities than the mean dislocation density. The resulting texture is defined by the nucleation privilege factor of deformed orientation but not as clearly as the recrystallization texture from nuclei distribution 2. A moderate intensity in recrystallization texture, obtained from nuclei distribution 1, improves a little bit in recrystallization texture, got from nuclei distribution 2. The rolling texture components become clear and the intensity of recrystallization texture component also improves because of less segregation and less congested surrounding which favours growth. The resulting grain distribution changes from a log normal to normal distribution due to the change in distribution from nuclei distribution 2 to 3. The recrystallization texture obtained from the nuclei distribution 3 favours deformed orientations with less dislocation density a near {100}<100> oriented texture is the result. Though the recrystallization texture intensity is low, the presence of a stronger {100}<100> texture component than other texture components is attributed to the orientation dependent lower dislocation density near {100}<100> orientation. The dislocation density based flow stress model in combination with the Taylor type grain interaction model is also capable of delivering the orientation dependent dislocation density which has lower value for near cube texture orientations. This is one important finding in favour of cube formation by orientation dependent nucleation. The texture intensity however is found very low. A similar type of texture and microstructure is found for decreasing nucleation rate. The texture intensities are improved in this case. The decrease in nucleation kinetics changes the microstructure distribution as well. The sharpening of the grain distribution peaks denotes the increase in frequency of the larger grains in microstructure. The dependency of recrystallized microstructure on the nucleation kinetics is discussed in details in the following section.

6.2 Time dependent nucleation: Two basic features, which promote nucleation, are

(i)   deformation energy,

(ii)   mobility of grain boundary.

From the thermodynamical point of view the deformation energy provides the driving force for nucleation. The local variation in deformation energy between a crystallite with low dislocation density and the surrounding with high dislocation density imparts the initial push for that crystallite in form of a subgrain or a cell for moving ahead to fulfil the nucleation condition in association with favourable disorientation. The variation in deformation energy can be an outcome of diverse factors like degree of deformation, texture, grain diameter and the presence of precipitates etc.

At a very early stage of deformation all grains are not deformed equally. A non-uniform deformation of different grains is expected after a small degree of deformation. Further deformation may make the deformation uniform taking more grains in account. In the a polycrystalline material where the deformation depend on the orientation of grains and a lot of other factors like grain diameter etc. an exact view on the uniformity/nonuniformity of deformation have been addressed by earlier mentioned simulations and experiments. It is now well understood that after a certain degree of deformation the developments of other substructural features like different microscopic and macroscopic bands make deformed microstructure more heterogeneous. For a pure material of certain stacking fault energy where recovery is not so pronounced the heterogeneity in substructure and that in deformation energy is described by imposed macroscopic strain, initial grain orientations and grain diameter of deformed material. The substructure developments in different texture components during hot deformation of a two-phase aluminium alloy are also available from different investigations referred earlier. The analysis shows that depending on the orientation of individual grain, the in grain disorientation profile varies which is a result of the presence of many microscopic features including different dislocation boundaries and variation in cell and cellblock sizes. This local variation in disorientation profile is responsible for another condition for nucleation i.e. the maturation of crystallites with low deformation energy to nuclei. This a time dependent phenomenon affected by the local availability of suitable disorientation with favourable mobility. The crystallites, which obtain a suitable surrounding spurt out as growing grain at first and other wait for a little longer time to have a favourable disorientation, created either by local arrangements of free dislocations and/or by low angle boundary movements through diffused dislocations. The local variation in deformation energy during early stage of deformation is a combination of macroscopic and microscopic strain accumulations. The effect of

individual grain kinematics, grain interaction can not dilute the macroscopic gradient formation as a result of deformation constraints like geometry of samples, macroscopic strain references and availability of easy and difficult paths in samples for deformation which are defined as frictional variation in plastic deformation. These macroscopic and microscopic inhomogeneities are very much susceptible to generate different dislocation densities in different grains and can be analysed in simulation from local grain shear and local von Mises strain. The contribution of grain boundary and the diameter of the initial grains in local substructure formation are also related. A significant effect on substructural variation can be observed from experiments on deformed samples with different cast grain diameter and with same starting textures. Moreover, evidences of characteristic change of boundary during deformation are also not rare. The presence of particles or precipitates makes substructure development more complex because it influences the dislocation movements and rearrangements. The spacing between particles may determine the localized microstructure developments through formation of a lot of geometrically needed dislocations apart form the statistically needed dislocations and through restriction on subsequent their movements. The experimental observation shows that the nucleation site saturation occurs in close vicinity to particles while nucleation is delayed in the bulk. The local variation of dislocation density, the presence of matured and premature cellblock or subgrains and diverse availability of suitable growth environments are potent enough to regulate nucleation in a time sequence during annealing.

A clear picture of the nucleation kinetics for aluminium alloy is very difficult to obtain from experiments. Moreover, the nucleation kinetics may not follow a particular law of mathematics. As the pre-recrystallized microstructure is heterogeneous, the nucleation kinetics should also have a similar characteristic as defined by the heterogeneity of the deformed structure and subsequent microscale pre-nucleation events. The basic aim of this nucleation kinetics study was to find out the effect of this kinetics on recrystallied microstructure so that the role played by the growth in heterogeneity development in recrystallied grains, can be determined. The accumulated results derived from different nucleation kinetics show that increasing nucleation kinetics increases the smaller grains and vice versa. A very slow kinetics of nucleation (increasing type two) can deliver grain distribution, which is very close to the observed one but for that nucleation should continue to the end of recrystallization, which is in contrary to the observations because

investigation shows that the nucleation time for 2 phase aluminium alloys is very short because of presence of precipitates.

With the knowledge of associated difficulties in determination of nucleation kinetics, this part of the recrystallization simulation is not generalized, which brings the possibilities of using certain nucleation kinetics for a particular alloy. Apart from this model can also change its different nucleation subroutine calling sequence to make any source amenable to be site saturation or to be time dependent nucleation. The deformation texture model (GIA) delivers distinguishable nuclei texture characteristics of their own. The nuclei sources namely grainboundary, transition band, stable orientation etc. can generate different recrystallization textures when they are called in various ways. The model performed a study on the resulting recrystallization textures obtained from above mention criterion. The potentiality of a nucleation source depends on the initial or deformed state of the material. In 2-phase aluminium alloy with small deformation the nucleation during recrystallization is activated first from near precipitate regions. The weak intensity of the recrystallization texture is observed. The experimental evidences prove that the contribution of particle-stimulated nuclei reduces while contributions of other sources mainly from deformation band and retained cube grains increase with prior recrystallization deformation. Two different mechanisms like a fast orientation dependent recovery and/or favourable growth kinetics because of suitable disorientation may be responsible for that. Whatever be the cause this model can take into account the variation in nucleation kinetics of different sources making them either site saturation or time dependent. An early nucleation of transition band and that of stable orientation nuclei increase the texture intensity and improve the strength of the cube, {100}<100> texture orientation. The early nucleation of particle-stimulated nuclei reduces the texture intensity while the fast nucleation of rolling textures retains its identity. A fast nucleation of particle stimulated nuclei during recrystallization after small pre-recrystallization deformation and an early nucleation of transition band to stable orientation nuclei after intense prior recrystallization deformation can be possible.

6.3   Effect of initial microstructure: The base of recrystallization is the deformed structure. The deformation energy of each orientation gives the rare opportunity to assess the nucleation frequency, nuclei distributions and the subsequent

developments of nuclei in deformed surroundings. The microstructure factors, which impart strong effects on this phenomenon, are

    (i)   grain diameter

    (ii)   texture

    (iii)   particles or precipitates

    (iv)   solute elements.

(i) Effect of grain diameter: The effect of grain diameter is rooted to its involvement in substructure developments during deformation. The substructures are defined in terms of in grain features like transition bands, stable regions and location discrete dislocation densities. The resulting mobile interfaces appear from the deformation induced geometrical changes of grains. The later factor directly affects the calculated nucleation density. The frequency of nucleation is a function of available mobile interfaces per unit volume. The mobile interfaces per unit volume and nucleation frequency decrease with the increase in initial grain diameter. Since the inhomogeneity in deformation or the different deformation bands depend on the initial grain diameter, the overall nucleation frequency is increased. The substructure developments during deformation of nearly similar oriented grains of different diameters reveal a stronger disorientation profile for smaller grains than that of larger grains in all directions. The disorientation profile is strongest along deformation direction while it is weakest along transverse direction. All these minute details of substructure developments should be added to the simulated initial deformed structure of this model. The effect of grain diameter is so far taken into consideration through input data of deformation texture and deformation energy. In the present state of the model the recrystallization kinetic variation because of the initial grain diameter can happen because of variation in nuclei density and variation in frequency of grain-to-grain deformation energy. The cell or subgrain diameter is calculated from the deformation energy. A sharp change in the nuclei probability and nuclei density are found with variable subgrain diameter. The effect of variable nuclei density arises from the variable deformed grain diameter and sub grain diameter on texture and kinetics is found to have moderate effect. The texture intensity decreases with the increase in nuclei density. The recrystallization exponent changes from 2.16 to 1.9 with the increase in nuclei density from 10^{15} to 6×10^{15} per cubic meter. The subsequent growth after nucleation also changes due to the effect of deformation energy change frequency with initial grain diameter. The recrystallization

texture, microstructure and kinetic study with constant number of randomly oriented and randomly located nuclei were performed. The kinetics becomes faster with large initial grains. The enhancement of recrystallization kinetics and formation of cube orientations are results of the increased grain diameter, which also improves the frequency of larger grains after recrystallization. The frequency of larger grains increases as well. The recrystallization kinetics is not very much varied. Approximately 12.5% increase in 50% recrystallization time is noted due to the grain diameter change from 25 micrometer to 60 micrometer. The properties of increasing initial grain are well reproduced in grain boundary nucleation as well. The model is capable of including both the random orientation of nuclei and nuclei of orientation of the original grain. In both studies a similar effect of initial grain diameter on recrystallization kinetics, grains distribution and in recrystallization microstructure is found. The recrystallization texture and kinetics obtained from these two types of nuclei orientations consideration are clearly different. The selection of grain orientations as the nuclei orientation slows down the kinetics because the grain oriented nuclei cannot grow inside the original grains. This growth restriction arises because of orientation effect. In the case of randomly selected grain boundary nuclei the growth constrains imparted by the orientation effect on mobility does not appear. The volume fraction of the near cube texture orientation is significantly improved in the case when the grain orientation is selected as nuclei orientation. The selection of grain orientation as nuclei orientation reduces the Cu orientation strongly. The overall texture intensity is increased except the Cu orientation. One example of hot rolled fully recrystallized aluminum alloy shows similar kind of recrystallization texture where the Cu orientation is considerably low compared to other rolling texture orientations. The basic aim of the earlier study was to find out the impact of the grain boundary nucleation after small and after high deformation levels. Since the severe deformation may randomize the near grain boundary orientations the random selection of nuclei orientation can be applicable to recrystallization after severe deformation, while the original grain oriented nuclei may suit recrystallization after small deformation degree.

(ii) Influence of texture: A strong dependency of the average dislocation density and local disorientation profile on degree of deformation affect the nucleation and subsequent growth. The total amount of slip for each orientation calculated from the Taylor type deformation texture model, GIA, was used in dislocation based flow stress

model to calculate the orientation dependent deformation energies. The orientation dependent deformation energies are found to have minor effect on the growth kinetics. It may control the nucleation frequency to a large extent but unable to reflect any significant change in recrystallization growth kinetics. Similar growth kinetics also can be obtained from the average deformation energy of all orientations. The major impact on growth comes from the influence of disorientation on grain boundary mobility.

a. The variation in deformation texture orientations with an average dislocation density, a constant number of nuclei and grain size can give diversified recrystallization texture because of oriented growth effect. The results obtained from this study show the effect of disorientation accumulations with different deformation stages and its effect on the grain boundary mobility to determine the recrystallization texture of an aluminum alloy. The simulations, mentioned in the result section, performed to reveal the effect of oriented growth. This model considers one reference orientation list, which consists of three Euler orientations, their Σ relation with a particular reference direction and the angular deviations defined by Brandon criterion. The Σ value assignment to disorientation between the microstructure and nucleus orientation is based on disorientation calculations between the microstructure orientation – reference orientation and nucleus orientation -reference orientation. All calculations were performed with orthorhombic crystal symmetry. Depending on the number of available Σ relations the mobility of the boundary is assigned. The $\Sigma7$ boundary was considered to have maximum mobility. The average mobility level can be defined to any level in between the maximum and the minimum mobility. The minimum mobility is given to low angle boundaries. The simulated recrystallization texture intensity is found to increase with prior recrystallization cold deformation. The result of the highest mobility of $\Sigma7$ boundary forms strong cube component of the texture. The intensity of cube texture in simulation results increases with the increase in the cube texture intensity in the initial microstructure. It shows that this strong oriented growth mainly affects the cube texture component.

b. Application of average dislocation density and orientation dependent dislocation density where all other factors are same. The discrete dislocation density variation is found to impart similar effect in recrystallization kinetics, as continuous average dislocation density obtained from them.

(iii) **Effects of precipitates:** The presence of particles or precipitates in most of the commercial aluminum alloys plays an important role because its dual effects mutually contradictory to each other. An enhancement in substructural heterogeneity because of high dislocation density around particles and local reorientations of crystallites in deformation zone increases the nuclei density, which favors the recrystallization while the increase in particle densities decreases spacing among them and makes low and high angle boundary pinning more frequent.

a. Effect of precipitate density on number of recrystallization nuclei: The particle or the precipitate stimulated nucleation model calculates the number of nuclei per unit volume from the deformation zone of the particle or the precipitate. Two different modules are available for this purpose. One module takes into account a predefined possibility of a particle to give recrystallization nuclei. It calculates the total deformation zone volume of potent precipitates. The number of nuclei per unit volume of the deformation zone is derived from the total deformation zone volume with the help of the above mentioned nucleation possibility per unit volume. The deformation zone radius is described in terms of the precipitate radius. The number of nuclei depends on the precipitate density because the total deformation zone volume is a function of precipitate number. The second module is based on the nucleation from the deformation zone surface of precipitates. The nuclei density in this case is dependent on the precipitate radius. Apart from the precipitate density the subgrain diameter inside the deformation zone also regulate the nuclei density. The average subgrain diameter inside deformation zone is smaller than the subgrain diameter outside of it. The geometrically necessary dislocation density factor makes the difference.

b. Effect of precipitate radius on number of recrystallization nuclei: The nuclei density is very much sensitive to the precipitate radius. Both the

calculations of deformation zone area and deformation zone volume include the precipitate radius. The number of nuclei is proportional to the 3/r where r is the radius of the particles, which are assumed to be spherical. The nominal values of the precipitate data were obtained from the CNG model. The nuclei density is more affected by the subgrain diameter than the particle radius.

c. Effect of back driving force on kinetics: The basic theory of back driving force on the recrystallization is a function of volume fraction and radius of precipitates. This model considers a normalized value of back driving pressure ($3F_v \gamma/ 2r$), which acts against the driving pressure, defined by the dislocation density. The volume fraction F_v of any spherical precipitate of radius r is given by $4N_p \pi r^3/3$ where N_p is the number of precipitates per unit volume. The back driving force per unit area or the Zener drag can be expressed by precipitate number (N_p), precipitate radius (r) and grain boundary energy (γ). The number of precipitates is obtained from precipitation kinetics model, which can deliver the time dependent precipitate number and radius. The temporal precipitation characteristics can also be included in the model. The number of precipitates obtained from the above source is increased to find the effect of precipitate density in recrystallization kinetics. Since the back driving force is proportional to the number of precipitate and square of the precipitate radius. The kinetic delay calculated by 100 times increase in precipitate number should be the same as that calculated by 10 times increase in precipitate radius. The results reflect exactly the same.

(iv) Influence of solute elements: It is well known that impurity elements may bring a drastic effect on the recrystallization kinetics and this effect might be much stronger than that produced by precipitates. The effect is caused by interaction between solutes and grain boundaries and this takes place because the stress field around the solutes and that along grain boundaries is reduced when solutes segregate along grain boundaries. The moving boundary is effectively held back at high concentration of solutes and at low temperature while it can make itself free at a very low concentration of solutes in combination of high temperature. The well discussed velocity term of recrystallization front consisting of driving force and the

mobility used in this model is affected by the variation in solute element concentration. The presence of variable solute concentration changes the mobility of the recrystallizing front continuously. The efficiency of the model is tested with a time dependent solute (Fe) concentration environment (Fig. 55 a, b). It is presumed that a long annealing at high temperature during recrystallization should vary the concentration of solutes of aluminium alloys. The time dependent concentration of iron which includes the concentration variation from the order of 10^{-06} to 10^{-03} with intermediate maxima and minima at 10^{-04} and 10^{-09} during heating of an aluminum alloy is obtained from precipitation kinetics model (ClaNG). The utility of the scalable sub grid is reflected in pursuing grain boundary mobility variation because of changing solute atmosphere. The resulting temporal velocity change is depicted in the kinetic curve of this alloy. The slope of the kinetic curve decreases with increase in solute concentration till 10^{-04} and then continuously increases with the descending solute concentration till 10^{-09}. The interaction offered by the maximum solute concentration is found to restrict fully the grain boundary movements. The precise growth law of this model eliminates any discontinuity in mobility of grain boundary in between.

6.4 The simulation of recrystallization of AA5182 alloy from transfer slab to final gauge:
The simulation of recrystallization of AA5182 aluminium alloy at different stages of strip production starting from the transfer slab to final sheet was done with this model. The starting deformation texture of transfer slab was random. The simulation work assumes a full recrystallization in between hot rolling passes. Though there is every possibility of not including all production and material parameter for all those calculations, the results show a fairly good agreement between modelled and experimental data.

The difference in batch annealed and salt bath annealed final cold rolled sheet can be attributed to the effect of heating profile (time vs. temperature) on the recrystallization. The presence of substructure in the batch annealed alloy shows that the alloy is not fully recrystallized.

The temperature dependency of recrystallization during batch annealing comes through the mobility and the static recovery during recrystallization. The model can also produce partially recovered microstructure finding a suitable external and internal

parameters defined by temperature profile, mobility of grain boundary, stacking fault energy, dislocation configuration etc. The recovery module of this model takes into account the three different possibilities like climb of perfect and extended dissociated and cross slip of screw dislocations. Here the climb of extended dissociated dislocations is considered to be the controlling mechanism. The consideration of partial dislocations introduces the effect of stacking fault energy on recovery kinetics. The effects are found to be very strong. A wise selection of jog energy, stacking fault energy and batch annealing temperature can give a similar partially recrystallized microstructure with same degree of recrystallized fraction. The fully recrystallized simulated microstructure of final sheet is compared with fully recrystallized salt bath annealed material here. The decrease in recrystallization texture intensity after full recrystallization is also found in simulation.

In the result section the possibility of formation of through thickness microstructure and that texture gradient are mentioned. The simulations on AA5182 alloy sheet production mentioned earlier delivers the macroscopic location discrete input data through out the thickness. The half of the thickness was divided into ten numbers of elementary blocks. The input microstructure variables like orientations and deformation energy were distinguishable. Out of these through thickness variables one near centre and another near surface were chosen to depict though thickness deformation microstructure gradient on lattice. The recrystallization simulations were performed with two different initial deformed microstructures and four type of nuclei orientations and locations. Since nucleation probability depends on the properties of the deformation microstructure, the number of nuclei varies between surface and the center. The final recrystallization microstructures from surface and from centre of the simulated sheet reveal that because of more strain location on surface of the sheet the recrystallized microstructure near surface of the sheet is consisting of finer grains than the centre of the sheet. The through thickness texture gradient brings the difference. It is worthy to mention here that an identical precipitate number and a precipitate radius are used for both input values. Through thickness variation of precipitate data may produce different results.

7.1. Summary.

1. Based on the modified cellular automata approach of Reher [60] a cellular operator model has been developed that is capable of accounting for spatial and temporal inhomogeneity on a finer scale. For this a scalable subgrid automaton is introduced that allows for a high spatial resolution on demand and still high computational efficiency. The scalable subgrid permits to track the minute changes of growth front during recrystallization owing to local variations of boundary mobility and net driving force. This approach substantially improves the prediction of grain morphology and grain statistics.

2. This new cellular operator model for recrystallization (CORe) has been connected to the grain cluster deformation texture model GIA to account for different nucleation mechanisms. The GIA model renders the deformation texture in terms of grain cluster that in sum properly reflects the deformation texture. Moreover, the GIA model is interfaced to a work hardening model 3IVM that provides information on the dislocation densities of the individual grains in a cluster, depending on the total amount of slip. The individual clusters are evaluated with regards to their behaviour during deformation. Divergence of grain orientation is taken as measure for nucleation in transition band, large stored energy differences (e.g. large difference in dislocation density) across grain boundaries are interpreted as nucleation along grain boundaries and stored energy differences across the deformation zone around the randomly distributed second phase particles are considered as particle stimulated nucleation. Each process contributes specific nucleus orientation.

3. The information on the property of grain to a specific nucleation mechanism is coupled with the information on the local dislocation density to predict the absolute number of nuclei of a specific orientation and location as needed for quantitative recrystallization texture prediction. For this purpose a statistical model for the probability of nucleation sites has been developed based on the imbalance of driving force at interfaces, i.e. grain boundaries or band like structures (transition band). The model renders information on the absolute number of nuclei without adjustable parameters and allows quantitative grain size and texture prediction.

4. Since the model has been mainly developed for Al alloys, recovery during annealing was taken into account to reduce the local driving force. Different kinds of recovery

mechanisms has been included in this model based on the dislocation climb and cross slip.

5. The CORe model has also been interfaced to a microchemistry model (ClaNG) that provides information on the temporal evolution of precipitates volume fraction, precipitate size distribution and solute content in solution. The information is available for any grid element at any time and can be utilized to determine the Zener drag and solute drag at the recrystallization growth front.

6. The developed advanced recrystallization model has been subjected to parameter studies to probe the influence of material chemistry and processing conditions on recrystallization kinetics, morphology and texture. In particular their effect on the evolution of cube texture has been investigated.

7. In particular, the model predicts a dependency of recrystallization kinetics, grain size and cube intensity on initial grain size. A strong cube texture in the deformed structure and strong growth competition produce a strong cube texture. An increase of the nucleation rate invariably tends to randomize the texture, irrespective of what growth law was used. Good agreement of the model predictions with experimental results has been ascertained.

7.2. Zusammenfassung.

1. Basierend auf einem Ansatz aus der Literatur (Reher [60]) wurde ein Modell für einen Zellulären Operator entwickelt. Es ist in der Lage, räumliche und zeitliche Inhomogenitäten mit höherer Auflösung zu berücksichtigen. Hierfür wird eine Automatik zur skalierbaren Erzeugung von Untergittern vorgestellt, das eine hohe räumliche Auflösung bei dennoch hoher Effizienz hinsichtlich des Rechenaufwandes zulässt. Das skalierbare Untergitter ermöglicht es, die genauen Änderungen der Wachstumsfront bei Rekristallisation zu verfolgen, die aus lokalen Variationen der Korngrenzbeweglichkeit und der gesamten Antriebskraft resultieren. Dieses Verfahren verbessert die Vorhersage von Kornmorphologie und Kornstatistik erheblich.

2. Dieses neue "Cellular Operator Modell für Rekristallisation" (CORe) wurde verknüpft mit dem Verformungstexturmodell GIA, um verschiedene Keimbildungsmechanismen zu berücksichtigen. Das GIA-Modell berechnet die Verformungstextur für ein Cluster von Körnern, das im ganzen die Verformungstextur korrekt wiedergibt. Obendrein ist das GIA-Modell verknüpft mit einem Verfestigungsmodell 3IVM, das Informationen liefert über die Versetzungsdichten in den einzelnen Körnern eines Clusters, abhängig von der Gesamtdehnung. Die einzelnen Cluster werden ausgewertet hinsichtlich ihres Verhaltens während der Verformung. Die Divergenz der Kornorientierung wird als Maß für die Keimbildung im Übergangsband verwendet, große gespeicherte Energiedifferenzen (z.B. große Unterschiede in Versetzungsdichten) über Korngrenzen hinweg werden interpretiert als Keimbildung an Korngrenzen, und gespeicherte Energiedifferenzen in Verformungszonen um die zufällig verteilten Partikel einer zweiten Phase werden als Partikel-unterstützte Keimbildung betrachtet. Jeder Prozess trägt zu spezifischen Keimorientierungen bei.

3. Die Information über den Beitrag eines Korns to einem bestimmten Keimbildungsmechanismus wird gekoppelt mit der Information über die lokale Versetzungsdichte, um die Anzahl von Keimen einer spezifischen Orientierung an einem Ort vorherzusagen, wie dies zur quantitativen Vorhersage einer Rekristallisationstextur benötigt wird. Zu diesem Zweck wurde ein statistisches Modell für die Wahrscheinlichkeit von Keimbildungsorten entwickelt, das auf dem

Ungleichgewicht der treibenden Kräfte an Grenzflächen, d.h. Korngrenzen oder Band-artigen Strukturen (Übergangsband). Das Modell liefert Information über die absolute Keimanzahl ohne anzupassende Parameter und ermöglicht eine quantitative Keimgrößen- und Texturvorhersage.

4. Da das Modell vor allem für Aluminiumlegierungen entwickelt worden ist, wurde Erholung während thermischen Auslagerungen berücksichtigt, um die lokalen Antriebskräfte zu verringern. Unterschiedliche Arten von Erholungsmechanismen basierend auf Klettern und Quergleiten von Versetzungen wurden in diesem Modell berücksichtigt

5. Das CORe-Modell wurde auch mit einem Mikrochemie-Modell (ClaNG) verknüpft, das Informationen liefert über die zeitliche Entwicklung von Volumenanteil und Größenverteilung von Ausscheidungen sowie den Lösungsanteil. Die Information steht zu jeder Zeit für jedes Gitterelement zur Verfügung und kann dazu genutzt werden, die Zener-Reibung und die Reibung durch gelöste Atome an der Rekristallisationswachstumsfront zu bestimmen.

6. Das entwickelte, verbesserte Rekristallisationsmodell wurde für Parameterstudien genutzt, um den Einfluss der Materialchemie und der Herstellungsbedingungen auf die Rekristallisationskinetik, die Morphologie und die Textur zu testen. Insbesondere wurde der Einfluss auf die Entstehung der Würfeltextur untersucht.

7. Insbesondere sagt das Modell eine Abhängigkeit der Rekristallisationskinetik, der Korngröße und der Würfelintensität von der Anfangskorngröße voraus. Eine ausgeprägte Würfeltextur in der verformten Struktur und starker Wachstumswettstreit führen zu einer ausgeprägten Würfeltextur. Ein Anwachsen der Keimbildungsrate führt unweigerlich zu einer zufälligeren Textur, unabhängig davon, welches Wachstumsgesetz verwendet wurde. Eine gute Übereinstimmung des Modells mit experimentellen Ergebnissen wurde festgestellt.

References.

1. Avrami M. J. Chem. Phys. 1939, 7:1103.

2. Kolmogorov AN. Izv. Akad. Nauk, USSR Ser. Metemat, 1937, 1:355.

3. Johnson WA, Mehl RF. Trans. Metall. Soc. A.I.M.E, 1939, 135:416.

4. Korbel A, Embury JD, Hatherly M, Martin PL, and Erbsloh HW. Acta. Met.1986; 34: 1999.

5. Doherty RD, Gottstein G, Hirsch J, Hutchinson WB, Lücke K, Nes E, and Wilbrandt. PJ. 8th Int. Conf. On Texture of Materials, Santa Fe (edited by J. S. Kallid and G. Gottstein), The Metallurgical Society of AIME. 1989; 189.

6. Lücke K and Engler O. Mater. Sci. Techno. 1990; 6:1113.

7. Embury JD, Poole WJ, and Koken E. Scripta Met. 1992; 27:1465.

8. Hatherly M. Proc. 6th Int. Conf. On Strength of Metals and Alloys (ed. R.C Gifkins), Pergamon, Oxford. 1982, 1181.

9. Mehl RF. ASM Metals Handbook, ASM, Metals Park, Ohio. 1948; 259.

10. Burke JE and Turnbull D. Prog. Metal Phys. 1952; 3:220.

11. Barto RL and Ebert LJ. Metall. Trans. 1971; 2:1643.

12. Duggan BJ, Lücke K, Köhlhoff G and Lee CS. Acta Metall. 1993; 41:1921.

13. Doherty RD and Cahn RW. J. Less Common Metals 1972; 28:279.

14. Iyer AS and Gordon P. Trans. Met. Soc. AIME. 1959; 215:729.

15. Hutchinson WB, Jonsson S and Ryde L. Scripta Metall 1989a; 23:671.

16. Hirsch J. Recrystallization 90 (ed. Chandra), TMS, Warrendale. 759.

17. Lücke K, Engler O. Proc. 3rd Int. Conf. on Aluminium Alloys, Trondheim. 1992; 439.

18. Vatne HE, Shahani R and Nes E. Acta Mater. 1996; 44: 4447.

19. Maurice C and Driver JH. Acta Metall. Mater. 1993; 41:1653.

20. Arai I, Koizumi M and Inagaki H. Proc. 6th Int. Conf. On Aluminium Alloys (ed. T. Sato, S. Kumai, T. Kobayashi and Y. Murakami) Toyohashi. 1269.

21. Dillamore IL and Katoh H. Met. Sci. 1974; 8:73.

22. Lee CS, Smallman RS and Duggan BJ. Script. Met. 1993; 29:43.

23. Inokuti Y, Doherty RD. Acta Metall. 1978; 26:61.

24. Ridha AA, Hutchinson WB. Acta Metall. 1982; 30:1929.

25. Hjelen J, Orsund R and Nes E. Acta Metall. 1991; 39:1377.

26. Raabe D, Zhao Z, Mao W. Acta Materialia. 2002; 50:4379.

27. Wert JA. Acta Materialia. 2002; 50:3125.

28. Standford N, Dunne D and Ferry M. Mater. Sc. and Eng. 2002; A00:1.

29. Delannay L, Mishin OV, Juul Jensen D and van Houtte P. Acta Mater. 2001; 49: 2441.

30. Huges D. Acta Metall. Mater. 1993; 41:1421.

31. Ibe G and Lücke K. Recrystallization, Grain Growth and Textures (ed. H. Margolin), ASM, Metal Park, 1966;434.

32. Lücke K. ICOTOM 7, (eds. Brakman et al), Noordwijkerhout, 1984; 195.

33. Humphreys FJ and Hatherly M. Recrystallization and Related Annealing Phenomena, Pergamon. 1995.

34. Sebald R, Zhu G and Gottstein G. Proc. 1st Int. Conf. on RX and GG (ed. G. Gottstein and D. Molodov), Springer-Verlag, Berlin, 2001; 1027.

35. Gottstein G, Murmann HC, Renner G, Simpson CJ and Lücke K. ICOTOM 5 (ed. G. Gottstein and K. Lücke), Aachen, 1978, 521.

36. Liebmann B, Lücke K and Masing G. Z. Metallk 1956; 47:57.

37. Gokhle AM and DeHoff RT. Metall. Trans. 1985; 16A:559.

38. Vandermeer RA and Rath BB. Metall. Trans. A. 1989a; 20A:391.

39. von Neumann J. Computing and Computer Theory, Charles Babbage Inst. Reprint Ser. History of Computing (ed. W. Aspray, A. Burks), Cambridge, MA, MIT Press, 1963; 12.

40. Kurzydlowski KJ and Ralph B. The Quantitative Description of the Microstructure of Metals, Boca Raton, FL, CRC 1995.

41. Gottstein G. Physikalische Grundlagen der Materialkunde, Springer Verlag, Berlin, 1998; Chapter 1.

42. Gottstein G. Physikalische Grundlagen der Materialkunde, Springer Verlag, Berlin, 1998; Chapter 7.

43. Vandermeer RA, Juul Jensen D. Met. Trans. 1995; 26A: 2227.

44. Malin KW, Hanson K and Morris jr JW. Nucl. Mat. 1976; 20:39.

45. Marthinsen K, Lohne O and Nes E. Acta Metall. 1989; 37 :135.

46. Furu T, Marthinsen K and Nes E; Mater. Sci. Techn. 1990; 6:1093.

47. Marthinsen K, Furu T, Nes, E and Ryum N; in 'Simulation and Theory of Evolving Microstructures', (ed. M. P. Anderson, A. D. Rollett), TMS, Warrendale 1990; 87.

48. Juul Jensen D. Scripta Met. Mat. 1992; 27:1551.

49. Frost HJ and Thompson CV. Acta Metall. 1987; 35:529.

50. Humphreys FJ. Mat. Sci. Tech. 1992; 8:135.

51. Humphreys J. Integral Materials Modeling (ed. G. Gottstein and R Sebald), Shaker Verlag, Aachen. 2000; 65.

52. Humphreys J, Acta Mater. 1997; 45:4231.

53. Maurice C, Recrystallization-Fundamental Aspects and Relations to Deformation Microstructure, (ed. N. Hansen et al.), Riso National Laboratory, Roskilde, Denmark. 2000; 431.

54. Anderson MP, Srolovitz DJ, Grest GS and Sahni PS; Acta Met. 1984; 32:783.

55. Srolovitz DJ, Grest GS and Anderson MP; Acta Met. 1986; 34:1833.

56. Hesselbarth HW and Göbel IR. Acta Met. Mat. 1991; 39:2135.

57. Holm EA, Glazier JA, Srolovitz DJ and Grest GS. Phys. Rev. 1991; A43:2662.

58. Glazier JA, Anderson MP, Grest GS. Phil. Mag. 1990; B62:615.

59. Rollett. AD, Srolovitz DJ, Anderson MP and Doherty RD. Acta Met. 1992; 40:3475.

60. Reher FR. Doctoral Dissertation, RWTH Aachen 1998.

61. Marx. V, Reher FR and Gottstein G. Acta Mater. 1999; 47:1219.

62. Raabe D. Phil. Mag. 1999; A 79:2339.

63. Turnbull D. Trans AIME. 1951; 191:661.

64. Raabe D. The Simulation of Materials Microstructure and Properties, Wiley VCH, Stuttgart (1998).

65. Rollett AD and Raabe D, Computational Material Science. 2001; 21:69.

66. Raabe D, Beckers B. Modelling and Simulation in Mat. Sci. Eng., 2000; 8:118.

67. Radhakrishnan B, Sarma G and Zacharia T. Proc. 4th Int. Conf. On Recrystallization and Related Phenomena (ReX'99), (ed. T. Sakai, H. G. Suzuki), The Japan Institute of Metals, Tokyo. 1999; 633.

68. Vatne HE, Furu T and Nes E. "Recrystallization and Related Phenomena", Proc. Of ReX'96 (ed. T. R. McNelley, Monterey Inst. of Advanced Studies, Monterey. 1996; 95.

69. Gottstein G, Sebald R. "Thermomechanical Processing of Steel", J. J. Jonas Symposium, Canadian Institute of Mining, Metallurgy and Petroleum, Quebec, 2000; 21.

70. Gottstein G, Marx V and Sebald R. Proc. 4th Int. Conf. Recrystallization and Related Phenomena (ed. T. Sakai, H. G. Suzuki), The Japan Inst. of Metals, Tokyo. 1999; 15.

71. Aretz H, Luce R, Wolske M, Kopp R, Goerdeler M, Marx V, Pomana G and Gottstein G. Integral Materials Modelling (ed. G. Gottstein and R. Sebald), Shaker Verlag, Aachen. 2000; 89.

72. Luce R, Wolske M, Kopp R, Roters F and Gottstein G. Comp. Mat. Sci. 2001; 21:1.

73. Jonas JJ, Toth LS and Urabe T. Mat. Sci. For. 1994; 157-162:1713.

74. Engler O. Textures and Microstructures. 1997; 28:187.

75. Engler O. Textures and Microstructures. 1999; 32:197.

76. Engler O and Vatne HE. JOM. 1998; 50:23.

77. Engler O, Vatne HE. Proc. 12th Int. Conf. on Texture of Materials. ICOTOM-12 (ed. J. A. Szpunar, NRC Research Press, Ottawa, Ontarion, Canada. 1999; 393.

78. Engler O. Proc. 21st Risϕ Int. Symp. On Material Science, Risϕ Nat. Lab., Roskilde, Denmark. 2000; 329.

79. Vatne HE, Furu T, Φrsund R and Nes E. Acta. Mat. 1996; 44:4463.

80. Sebald R. Doctoral Dissertation. RWTH Aachen. 2001.

81. Schmitter U. Diploma Thesis. RWTH Aachen. 1991.

82. Wagner P. Doctoral Dissertation. RWTH-Aachen.

83. Ashby MF. Phil. Mag. 1966; 14:1157.

84. Crumbach M, Pamona G, Wagner P and Gottstein G. Proc. 1st Int. Conf. on RX and GG (ed. G. Gottstein and D. Molodov), Springer-Verlag, Berlin, 2001; 1053.

85. Goerdeler M and Gottstein G. Proc. 1st Int. Conf. on RX and GG (ed. G. Gottstein and D. Molodov), Springer-Verlag, Berlin, 2001; 1053.

86. Schneider M, Gottstein G, Löchte L and Hirsch J. Proc. 8th Int. Conf. on Aluminium Alloys (ed. P. J. Gregson and S. J. Harris), Trans Tech Publication, Switzerland. 2002; 637.

87. Christian JW. The Theory of Transformations in Metals and Alloys. Pergamon, Oxford.

88. Seefeldt M, Delannay L, Peeters B, Aernoudt E and van Houtte. Acta Mater. 2001; 49:2129.

89. Liu WC, Juul Jensen D and Morris JG. Acta Mater. 2001; 49:3347.

90. Cizek P. Scripta Materialia. 2001; 45:815.

91. Liu Q, Wert J and Hansen N. Acta Mater. 2000; 48:4267.

92. Humphrey FJ and Kalu PN. Acta. Metall. 1990; 38:917.

93. Derby B and Ashby MF. Scripta Met. 1987; 21:897.

94. Benum S and Nes E. Acta. Mater. 1997; 45:4593.

95. Ashby MF. Phil. Mag. 1970; 21:399.

96. Crumbach M and Gottstein G. Materials Scinence and Engg. 2004; A387-389:282.

97. Carrard M and Martin JL. Phil. Mag. 1988; A58(3):491.

98. Godfrey A, Juul Jensen and Hansen N. Acta Mater. 1998; 46:823

99. Crumbach M, Goerdeler M, Gottstein G, Neumann L, Aretz H and Kopp R. Modelling Simulation Mater. Sci. Eng. 2004; 12 No 1: S1.

100. Humphreys FJ. Acta. Metall. 1977; 25:1323

101 Fridel J. Dislocations. Addison-Wesley, London. 1964.

102. Argon AS and Moffatt WC: Acta Metall. 1981, 29:293.

103. Cherns D, Hirsch PB, Saka H. Strength of Metals and Alloys, Pergamon Press (ed. P. Haasen, V. Gerold and G. Kostorz), 1979 1:295.

104.   Stroh AN. Proc. Roy Soc. 1954, A223:404.

105.   Gottstein G, Shvindlerman L. Grain Boundary Migration in Metals-Thermodynamics, Kinetics, Applications. Boca Raton, FL, CRC 1999; 198.

106.   Lücke K, Detert K. Acta Metall 1957; 5:628.

Lebenslauf

Name:	Prantik Mukhopadhyay
Geburtsdatum:	1st Jan, 1973
Geburtsort:	Bishnupur, West Bengal (Indien)
Staatsangehörigkeit:	Indisch
Familienstand:	Verheiratet

Schulbildung:

1978-1988   Secondary School Certificate, West Bengal, Indien.

1988-1990   Higher Secondary Certificate, West Bengal, Indien.

Studium:

07/1999-03/2001   Studium des Metallurgical and Materials Engineering.-
Studiengangs am Indian Institute of Technology, Kharagpur,
Indien (IIT- Kharagpur) mit dem Abschluß ``Master of
Technology (M. Tech)``.

07/1990-06/1994   ``Bachelor of Engineering`` in ``Metallurgical Engineering``
an der ``Calcutta University`` in Indien.

Berufserfahrung:

07/2001-09/2005   RWTH-Aachen
Institut für Metallkunde und Metallphysik
Tätigkeit als Wissenschaftlicher Angestellter.

11/1994-07/1999   In einem Eisen und Stahl Industry, als
``Assistant Metallurgist`` für ``Quality Assurance``
department